Single-bubble sonoluminescence

Michael P. Brenner

Division of Engineering and Applied Sciences, Harvard University, Cambridge, Massachusetts 02138

Sascha Hilgenfeldt and Detlef Lohse*

Department of Applied Physics and J. M. Burgers Centre for Fluid Dynamics, University of Twente, 7500 AE Enschede, The Netherlands

(Published 13 May 2002)

Single-bubble sonoluminescence occurs when an acoustically trapped and periodically driven gas bubble collapses so strongly that the energy focusing at collapse leads to light emission. Detailed experiments have demonstrated the unique properties of this system: the spectrum of the emitted light tends to peak in the ultraviolet and depends strongly on the type of gas dissolved in the liquid; small amounts of trace noble gases or other impurities can dramatically change the amount of light emission, which is also affected by small changes in other operating parameters (mainly forcing pressure, dissolved gas concentration, and liquid temperature). This article reviews experimental and theoretical efforts to understand this phenomenon. The currently available information favors a description of sonoluminescence caused by adiabatic heating of the bubble at collapse, leading to partial ionization of the gas inside the bubble and to thermal emission such as bremsstrahlung. After a brief historical review, the authors survey the major areas of research: Section II describes the classical theory of bubble dynamics, as developed by Rayleigh, Plesset, Prosperetti, and others, while Sec. III describes research on the gas dynamics inside the bubble. Shock waves inside the bubble do not seem to play a prominent role in the process. Section IV discusses the hydrodynamic and chemical stability of the bubble. Stable single-bubble sonoluminescence requires that the bubble be shape stable and diffusively stable, and, together with an energy focusing condition, this fixes the parameter space where light emission occurs. Section V describes experiments and models addressing the origin of the light emission. The final section presents an overview of what is known, and outlines some directions for future research.

CONTENTS

*Electronic address: lohse@tn.utwente.nl

I. INTRODUCTION

A. The discovery of single-bubble sonoluminescence

Single-bubble sonoluminescence was discovered in 1989 by Felipe Gaitan, then a graduate student at the University of Mississippi working with Larry Crum (Gaitan, 1990; Gaitan and Crum, 1990; Gaitan *et al.*, 1992). Crum had seen hints of light emission from a single bubble in 1985 (Crum and Reynolds, 1985), and Gaitan's objective for his thesis was to search systematically for it. Gaitan was carrying out a set of experiments on the oscillation and collapse of bubbles, using a flask of liquid lined with transducers tuned to set up an acoustic standing wave at the resonant frequency at the jar. When the pressure amplitude P_a of the sound waves is larger than the ambient pressure $P_0=1$ bar, the pressure in the flask becomes negative, putting the liquid under tension. At large enough tension, the liquid breaks apart (cavitation), creating unstable bubble clouds in which the bubbles often self-organize into dendritic structures (streamers; see Neppiras, 1980). These cavitation clouds collapse with enormous force, powerful enough to do serious damage to the surfaces of solid bodies in their vicinity.

In his search for single-bubble sonoluminescence, Gaitan at some point found a regime with a moderate forcing pressure $P_a/P_0 \approx 1.2-1.4$ and with the water degassed to around 20% of its saturated concentration of air. He then observed that "as the pressure was increased, the degassing action of the sound field was reducing the number of bubbles, causing the cavitation streamers to become very thin until only a single bubble remained. The remaining bubble was approximately 20 μm in radius and [...] was remarkably stable in position and shape, remained constant in size and seemed to be pulsating in a purely radial mode. With the room lights dimmed, a greenish luminous spot the size of a pinpoint could be seen with the unaided eye, near the bubble's position in the liquid" (Gaitan *et al.*, 1992). The experiment is shown in Fig. 1, a sketch of a typical experimental setup for single-bubble sonoluminescence in Fig. 2.

At the time of Gaitan's experiment, all previous work with light-emitting bubbles involved many unstable bubbles being simultaneously created and destroyed. Using Mie scattering to track the volumetric contractions and expansions of the bubbles (Gaitan, 1990; Gaitan and Crum, 1990; Gaitan *et al.*, 1992) Gaitan and co-workers demonstrated that their setup indeed generated a single bubble, undergoing its oscillations at a fixed, stable position at a pressure antinode of the ultrasound field in the flask. The oscillation frequency f is that of the sinusoidal driving sound (typically 20–40 kHz), but the dynamics of the bubble radius is strongly nonlinear. Once during each oscillation period, the bubble, whose undriven (ambient) radius R_0 is typically around 5 μm, collapses very rapidly from its maximum radius $R_{\max} \sim 50$ μm to a minimum radius of $R_{\min} \sim 0.5$ μm, changing its volume by a factor of 1×10^6 (Barber *et al.*, 1992). Figure 3 shows the radius, forcing pressure, and light intensity (top to bottom) during this

FIG. 1. A sonoluminescing bubble. The dot in the center of the jar is the bubble emitting light. From Crum, 1994.

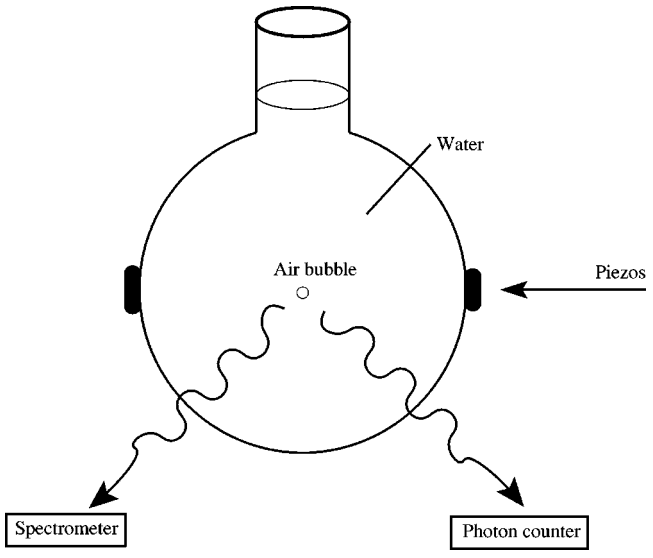

FIG. 2. Sketch of a typical setup for generating sonoluminescing bubbles.

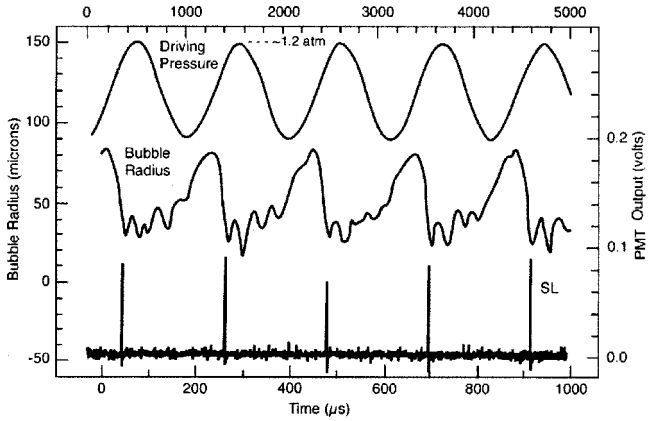

FIG. 3. Radius $R(t)$, driving pressure $P(t)$, and light intensity $I(t)$ from Crum (1994), as measured by Gaitan *et al.* (1992). A negative driving pressure causes the bubble to expand; when the driving pressure changes sign, the bubble collapses, resulting in a short pulse of light, marked SL.

process (Crum, 1994). The bubble expansion caused by the negative pressure is followed by a violent collapse, during which light is emitted. The process repeats itself with extraordinary precision, as demonstrated by measurements of the phase of the light emission relative to the driving.

Light emission from collapsing ultrasound-driven bubbles had long been dubbed sonoluminescence (SL). Researchers were familiar with the energy-focusing power of cavitation clouds, and it was therefore not surprising when Frenzel and Schultes (1934) demonstrated that these cavitation clouds emitted a low level of light [slightly earlier, Marinesco and Trillat (1933) had found indirect evidence when photographic plates fogged in an ultrasonic bath]. After all, if the cloud collapses violently enough to break the molecular bonds in a solid, causing cavitation damage (Leighton, 1994), there is no reason why photons should not also be emitted. The energy-focusing power of the cavitation cloud was understood to arise from a singularity occurring when a bubble collapses in an ambient liquid (Rayleigh, 1917): inertial forces combined with mass conservation lead to bubble-wall velocities that become supersonic during the collapse, causing rapid heating of the bubble interior. To the engineering community of the time, the fluid mechanics of this process were much more interesting than the character of the radiation produced. This was for a very practical reason: people wanted to understand how to prevent cavitation damage, or how to harness its energy-focusing power. Although historically the light emission has played a useful role in measuring properties of cavitation [Flint and Suslick (1991b) used the spectrum to measure the temperature in a cavitating bubble cloud], it was not considered of intrinsic importance until Gaitan's discovery of what is now known as single-bubble sonoluminescence (SBSL).

The brightness of Gaitan's single, isolated bubble caused great excitement in the scientific community; it is visible to the naked eye! Though the light emission from conventional cavitation clouds [now called *multibubble sonoluminescence* (MBSL); see Kuttruff, 1962; Walton and Reynolds, 1984; Brennen, 1995] is also visible as diffuse glowing, in that case no individual, stable bubbles can be identified. The excitement about single-bubble sonoluminescence was driven in large part by a set of experiments by Seth Putterman's group at UCLA from 1991 to 1997, which exposed further peculiarities, making single-bubble sonoluminescence seem very different from MBSL (the experiments of the UCLA group are reviewed by Barber *et al.*, 1997 and Putterman and Weninger, 2000). Was new physics (beyond that implied by the collapse mechanism of Lord Rayleigh in 1917) responsible for this difference? Many people were also excited by the fact that single-bubble sonoluminescence appeared to be much more controllable than its multibubble counterpart, bringing expectations of both good careful scientific studies and the possibility of new technologies, including the harnessing of the energy-focusing power of SBSL.

It is natural that the excitement at first caused speculation about very exotic conditions inside the bubble, such as extremely high temperatures and pressures. Even Hollywood caught on to the excitement, producing a movie in which the central character created a fusion reactor using a single sonoluminescing bubble. As the field matured over time and the models were refined, the results became more down to earth; for instance, the commonly believed maximum temperature at the bubble collapse has been revised downward during a decade of research from early estimates of 10^8 K to the more modest present-day estimates which cluster around 10^4 K.

In the years since SBSL was discovered, much has been learned about how and why it occurs. The goal of this review is to clarify the basic ideas that have proven necessary for a quantitative understanding of single-bubble sonoluminescence and to present an overview of the current state of the field, of what is known and what is yet to be fully understood.

B. Structure of the review

The structure of this review is as follows: The remainder of this Introduction presents an overview of the salient historical and experimental facts and qualitatively describes the ideas and issues that have been shown to be important for understanding the phenomenon. This overview will illustrate the enormous variety of physical processes taking place inside this simple experiment, ranging from fluid dynamics, to acoustics, to heat and mass transfer, to chemical reactions, and finally to the light emission itself. We shall then spend the next four sections following in detail the sequence of events that happen to a sonoluminescing bubble, beginning with the motion of the flask and liquid and proceeding to the dynamics of the bubble wall and interior. Figure 4 shows the radius $R(t)$ of the bubble as a function of time during a single cycle of the driving; the inset blows up the innermost ≈ 60 ns around the cavitation event, where

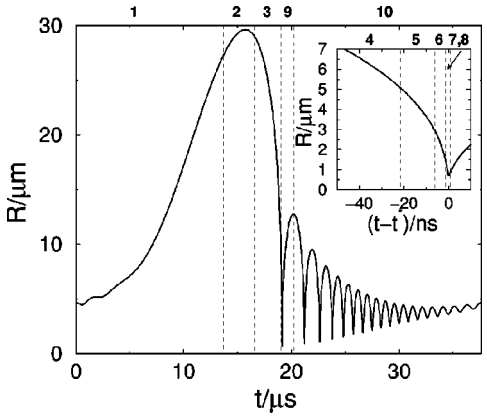

FIG. 4. Classical bubble dynamics calculation for a driving pressure amplitude $P_a=1.2$ atm, frequency $f=26.5$ kHz, and ambient bubble radius $R_0=4.5$ μm. One oscillation cycle of $R(t)$ is shown. The bubble expands to nearly ten times its ambient radius, then collapses extremely quickly, leading to adiabatic heating of the gas inside the bubble. The collapse is followed by afterbounces with roughly the eigenfrequency of the bubble. The vertical dashed lines and small-print numbers indicate the intervals 1–10 (summarized in Sec. VI) at which different physical processes are important, which are discussed throughout the review. The inset shows the innermost 60 ns around the time t^* of maximum compression and highlights the bubble radius during Rayleigh cavitation collapse, where the light is emitted.

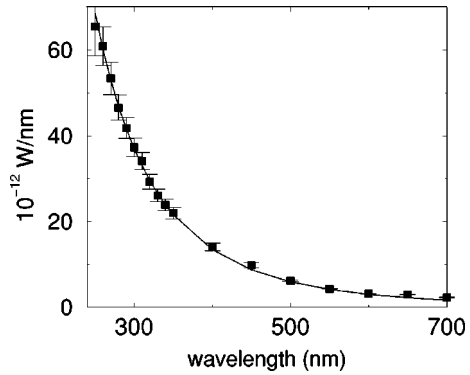

FIG. 5. Spectrum of single-bubble sonoluminescence, for water at 22 °C. The data points are redrawn from Fig. 1 of Hiller *et al.* (1992). Fits to a blackbody spectrum can be attempted for different temperatures, with best results for about 40 000 K (solid line), higher than the 25 000 K suggested by Hiller *et al.* (1992).

the bubble temperature rises rapidly due to adiabatic compression and light is emitted.

Section II reviews classical studies of the hydrodynamics of bubble motion, showing, for example, how to derive the equation for the bubble radius leading to Fig. 4, and also discussing the hydrodynamics of Lord Rayleigh's cavitation collapse (Fig. 4, inset). Section III describes the fluid dynamics of the bubble's interior, focusing mainly on what happens to the gas during the cavitation event, but also discussing water evaporation, heat transfer, and chemistry. Section IV discusses the physical processes that fix the ambient size R_0 of the bubble, including the diffusive and chemical processes of mass exchange between bubble and liquid as well as mechanical stability constraints. Finally, Sec. V discusses the light emission itself, which occurs when the bubble is in its maximally compressed state. The discussion will emphasize the mechanisms that are consistent with the current experimental data. In the final section, we give a brief summary and present our opinions on the current state of the field as well as the areas of activity with the brightest outlook for future work.

C. Historical overview

After Gaitan's discovery, the initial goal of research was to quantify how much more efficiently a single bubble focuses energy than a bubble cloud. To address this question, Barber and co-workers (Barber and Putterman, 1991; Barber *et al.*, 1992) measured the width of the light pulse, by studying the response of a single photomultiplier tube to the sonoluminescent flash. It was concluded that the width of the light pulse was less than 50 ps. The importance of the measurement was that this upper bound for the pulse width was much smaller than the time during which the bubble remained in its most compressed state. Roughly, the time scale of bubble compression is given by the time it takes a sound wave to travel across the minimum radius of the bubble. With a sound velocity of $c\sim1000$ m/s, one obtains a ballpark estimate of $R_{\min}/c\sim10^{-9}$ s, far in excess of the measured pulse-width limit. Lord Rayleigh's cavitation mechanism implies that the energy focusing is coupled to the bubble collapse: this discrepancy suggests that in SBSL the light emission is decoupled from the bubble dynamics.

The gauntlet was thus thrown, and a search for the correct mechanism began. An influential early idea [introduced independently by Greenspan and Nadim (1993), Wu and Roberts (1993), and Moss *et al.* (1994)] was that the energy focusing in the bubble was caused by a converging spherical shock. It had been known since the seminal work of Guderley (1942) (see also Landau and Lifshitz, 1987) that such shocks focus energy, and in the absence of dissipation the temperature of the gas diverges to infinity. In fact, Jarman (1960) had already suggested converging shocks as the source of multibubble sonoluminescence. This mechanism neatly solved the upper-bound problem for the width of the light pulse (since in this picture the light originates from a much smaller region in the center of the bubble) and proposed an elegant mechanism for energy focusing compounding Lord Rayleigh's bubble-collapse mechanism. Simulations by Wu and Roberts (1993) had the maximum temperature approaching 10^8 K, very hot indeed.

For several years, experimental information accumulated about the properties of sonoluminescing bubbles. Hiller *et al.* (1992, 1994, 1998) measured the spectrum of a sonoluminescing air bubble in water and demonstrated that it increases toward the ultraviolet (Fig. 5). The apparent peak in some spectra is due to the strong absorp-

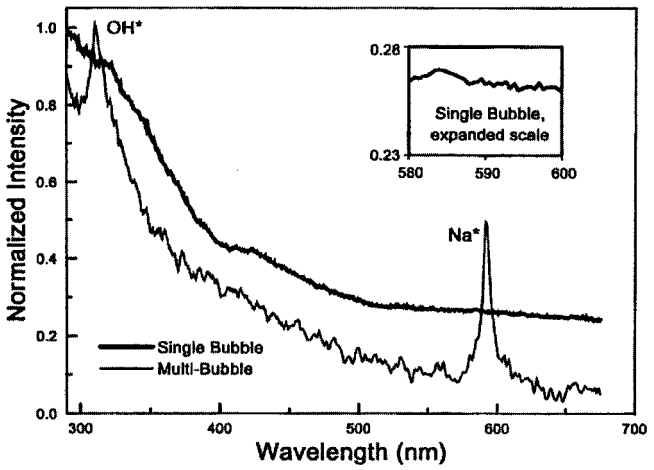

FIG. 6. MBSL (thin line) and SBSL (thick line) spectra in a 0.1M sodium chloride solution. Each spectrum was normalized to its highest intensity. Note the prominence (MBSL) and absence (SBSL, see the inset for an enlargement) of the sodium line near 589 nm. Figure reproduced from Matula *et al.* (1995).

tion of wavelengths below ≈200 nm by the water in the flask. In sharp contrast to the spectrum of MBSL, single-bubble sonoluminescence shows a smooth continuum, without spectral lines (see Fig. 6). The presence of spectral lines points to lower temperatures, since the atomic transitions leading to lines tend to be overwhelmed by continuous emission processes at high temperatures. By fitting the observed spectra to that of a blackbody emitter (Fig. 5), Hiller *et al.* (1992) concluded that the temperature of the gas was at least 25 000 K.

Barber *et al.* (1994) demonstrated that both the light intensity and amplitude of the oscillations of the bubble depend sensitively not only on the forcing pressure amplitude, but also on the concentration of the gas dissolved in the liquid, the temperature of the liquid, or small amounts of surface active impurities (Weninger *et al.*, 1995; Ashokkumar *et al.*, 2000; Toegel, Hilgenfeldt, and Lohse, 2000). As an example, Fig. 2 of Barber *et al.* (1994) shows the dependence of $R(t)$ and the total light intensity on the increasing drive level for an air bubble in water. As the forcing is increased, the bubble size abruptly decreases, and then the light turns on (see Fig 7). For some years, the precise reasons for this sensitivity (observed repeatedly in experiments) were difficult to understand, mostly because varying one of the experimental parameters, such as the water temperature, would tend to change others as well.

Perhaps most surprisingly, Hiller *et al.* (1994) found a sensitive dependence on the type of gas within the bubble: when the air dissolved in the liquid was replaced with pure nitrogen, the characteristically stable SBSL disappeared. With a gas composed of 80% nitrogen and 20% oxygen, there was still no sonoluminescence. Only when the inert gas argon was added did SBSL light emission return. Figure 8 shows a plot of the intensity of sonoluminescence as a function of the percentage of inert gas doped in nitrogen. For both argon and xenon, the intensity peaks around 1%, the concentration of argon in air.

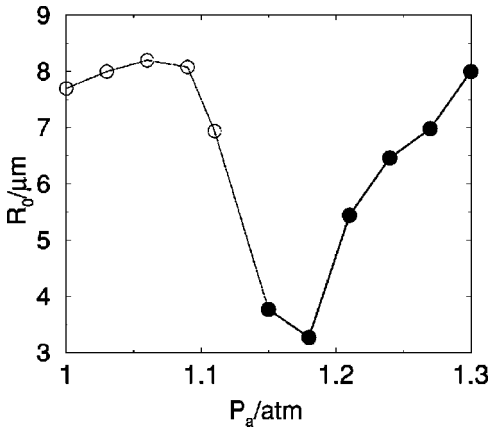

FIG. 7. The ambient bubble radius as a function of forcing pressure P_a for a gas mixture of 5% argon and 95% nitrogen at a pressure overhead of 150 mm. For sonoluminescing bubbles the symbols are filled; for nonglowing bubbles they are open. Note the abrupt decrease in bubble size right before the sonoluminescence threshold. The figure is a sketch from Fig. 38 of Barber *et al.* (1997). In that paper the ambient radius is obtained from a fit of the Rayleigh-Plesset equation to the $R(t)$ curve. In that fit heat losses are not considered explicitly, but material constants are considered as free parameters. Therefore the values for R_0 are only approximate; see the discussion in Sec. II.E.

SBSL can be achieved with a pure noble gas as well, but in a vastly different range of gas concentrations: In the original experiment with air, Gaitan (1990) observed stable light emission when degassing using a partial pressure of $p_\infty^{air}/P_0 \sim 0.2–0.4$; i.e., the water contained 20–40 % of the air it would contain if in saturation equilibrium with a pressure of $P_0 = 1$ bar. Barber *et al.* (1995) demonstrated that, when using pure argon gas, the degassing has to be 100 times stronger, requiring partial pressures as low as $p_\infty^{\mathrm{Ar}}/P_0 \sim 0.002–0.004$ to obtain stable SBSL. The pressures p_∞ are the partial gas pressures used in experiment when preparing the degassed liquid.

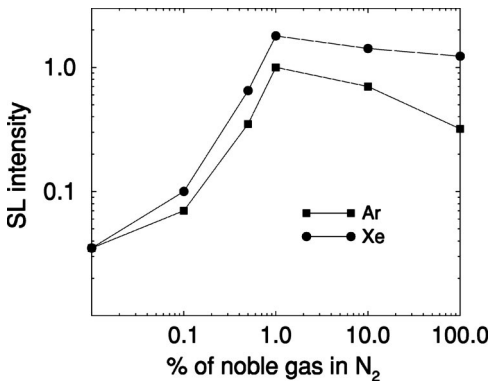

FIG. 8. Dependence of the sonoluminescence intensity (normalized to that of air) in water as a function of the percentage (mole fraction) of noble gas mixed with nitrogen. Two noble gases are shown: xenon (●) and argon (■). Both give maximum light intensity around 1% dissolution, as does helium (not shown). The figure is a sketch from Fig. 22 of Barber *et al.* (1997).

During this time the predominant belief in the field was that shocks (see, e.g., Barber *et al.*, 1994, 1997) were somehow important for the energy focusing and light emission of sonoluminescence. However, there was little agreement as to the details of how this worked, and many other physical mechanisms were suggested, including dielectric breakdown of the gas (Garcia and Levanyuk, 1996; Lepoint *et al.*, 1997; Garcia and Hasmy, 1998), fracture-induced light emission (Prosperetti, 1997), bremsstrahlung (Moss, 1997; Frommhold, 1998), collision-induced emission (Frommhold and Atchley, 1994; Frommhold, 1997; Frommhold and Meyer, 1997), and even the quantum-electrodynamical Casimir effect (Eberlein, 1996a, 1996b), an idea pioneered in this context by Schwinger (1992).

The difficulty in evaluating these ideas was that they required probing the bubble collapse in greater detail than was experimentally possible. This led Robert Apfel to pose a "challenge to theorists" in a session on sonoluminescence at the annual meeting of the Acoustical Society of America in Honolulu in 1996. The challenge was to make concrete, experimentally testable predictions. Many creative ideas were collected at this meeting, only a fraction of which still survive today. [One of the early casualties includes the acoustic-resonator theory developed by the present authors speculating on energy storage in the bubble (Brenner, Hilgenfeldt, *et al.*, 1996).]

Meanwhile, it was equally clear that at least some of the experimental facts of sonoluminescence were direct consequences of the classical theory of bubble dynamics, having nothing to do with light emission per se. The time scale of the light emission is so much shorter than a complete cycle of the acoustic driving that bubble dynamics goes a long way towards explaining issues of bubble stability and constraints for driving parameters. Since Lord Rayleigh's characterization of cavitation collapse (Rayleigh, 1917), bubble dynamics had become well understood,[1] but, although the theory was formally quite mature, it had never been put to work in the precise regime of single-bubble sonoluminescence.

The application of classical bubble dynamics to SBSL substantially clarified the experimental situation. The first contribution in this regard was made in the original paper of Gaitan *et al.* (1992), which demonstrated that the radius of the bubble as a function of time observed experimentally exhibits the same behavior as solutions to the Rayleigh-Plesset equation (to be derived in Sec. II); subsequently, studies by Löfstedt *et al.* (1993, 1995) confirmed and elaborated on this conclusion. The Rayleigh-Plesset theory is remarkably simple, and it captures many important features of single-bubble sonoluminescence. To practitioners of classical bubble dynamics, the excellent agreement was particularly surprising because this theory has long been known to show large quantitative discrepancies even for bubbles that are more weakly forced than in the case of SBSL (Prosperetti *et al.*, 1988). In the SBSL parameter regime, the periodic forcing of the pressure waves in the container leads to a periodic bubble response, with a cavitation collapse happening exactly once per cycle [chaotic motion as in Lauterborn (1976) and Lauterborn and Suchla (1984) is notably absent]. The qualitative and even most quantitative features of bubble oscillations agree with the experimental observations. The solution also has the courtesy to predict its own demise: at cavitation collapse the speed of the bubble wall approaches or surpasses the speed of sound in the liquid, contradicting one of the essential assumptions of the theory. The total time during which the bubble wall is supersonic is a tiny fraction of a cycle; the errors that accumulate in this regime do not substantially affect the rest of the cycle.

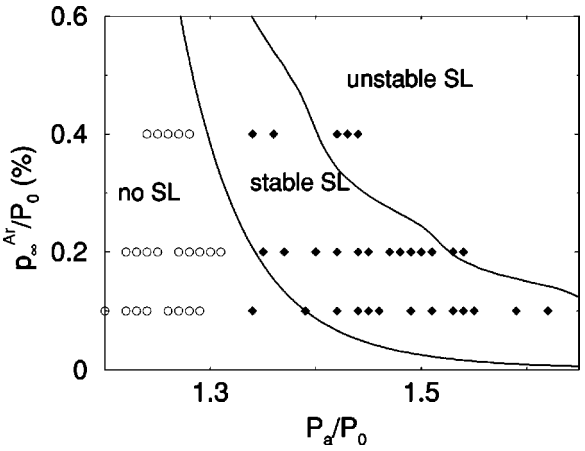

FIG. 9. Phase diagram in the $p_\infty^{\mathrm{Ar}}/P_0$ vs P_a/P_0 parameter space, according to the hydrodynamic/chemical theory of Hilgenfeldt *et al.* (1996) and Lohse *et al.* (1997). The driving frequency is $f=33.4$ kHz. The three phases represent stable SL, unstable SL, and no SL. The symbols represent measurements by Ketterling and Apfel (1998), either stable sonoluminescing bubbles (♦) or stable, nonsonoluminescing bubbles (○), showing good agreement with the earlier theoretical predictions.

If the solutions to the Rayleigh-Plesset equation explain the experimental measurements of the bubble radius, then their stability must constrain the parameter space where SBSL can occur (Brenner *et al.*, 1995; Brenner, Hilgenfeldt, *et al.*, 1996; Hilgenfeldt *et al.*, 1996). There are three major instabilities of the bubble that need to be avoided: (i) the bubble must not change shape (shape instabilities; Brenner *et al.*, 1995; Hilgenfeldt *et al.*, 1996); (ii) the average number of gas molecules in the bubble must not increase or decrease over time (diffusive instability; Brenner, Lohse, *et al.*, 1996; Hilgenfeldt *et al.*, 1996); (iii) the bubble must not be ejected from the acoustic trap where it is contained (Bjerknes instability; Cordry, 1995; Akhatov *et al.*, 1997; Matula *et al.*, 1997). All of these constraints must be satisfied in a parameter regime where the bubble oscilla-

[1]This was primarily due to the contributions of Plesset, 1949, 1954; Epstein and Plesset, 1950; Plesset and Zwick, 1952; Plesset, 1954; Plesset and Mitchell, 1956; Eller and Flynn, 1964; Eller, 1969; Eller and Crum, 1970; Prosperetti, 1974, 1975, 1977a, 1977d; Plesset and Prosperetti, 1977; Prosperetti and Lezzi, 1986; Prosperetti *et al.*, 1988.

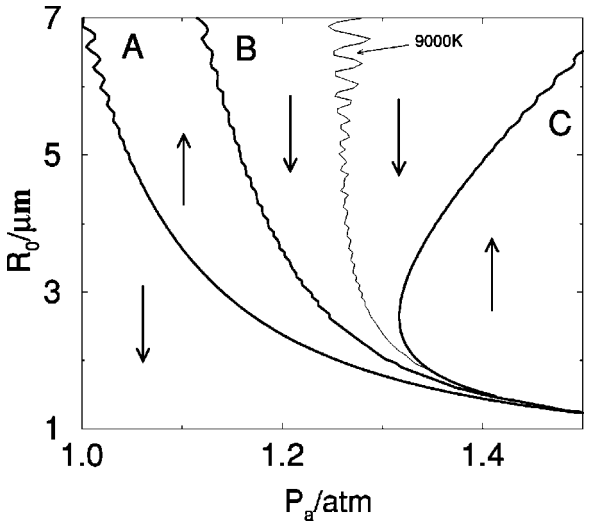

FIG. 10. Phase diagram for air at $p_\infty/P_0=0.20$ in the R_0-P_a space. The arrows denote whether the ambient radius grows or shrinks at this parameter value. Curve A denotes the equilibrium for an air bubble; on curve C the bubble contains only argon. The intermediate curve B necessarily exists because of the topology of the diagram and represents an additional stable equilibrium. The thin line indicates where the (approximate) threshold temperature of nitrogen dissociation (~9000 K) is reached. From Lohse *et al.* (1997).

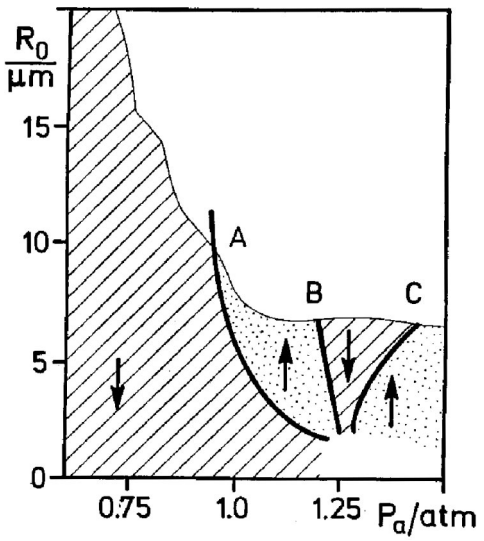

FIG. 11. Experimental phase diagram in the R_0-P_a parameter space for air at $p_\infty/P_0=0.20$. The driving frequency is 20.6 kHz. Arrows indicate whether the bubbles grow or shrink. Three equilibrium curves A, B, and C can be recognized. In between curves B and C there is a "dissolution island." The shaded area shows the shape-stable parameter domain (see Sec. IV.D). Figure adopted from Holt and Gaitan (1996).

tions become nonlinear enough for sonoluminescence to occur. The allowable parameter space of SBSL is thus severely limited to a narrow range of relative gas concentrations $c_\infty/c_0=p_\infty/P_0$ and forcing pressure amplitudes P_a (see Fig. 9).

While the regime of stable sonoluminescence in argon gas is in good agreement with that predicted by the hydrodynamic stability calculations of Hilgenfeldt *et al.* (1996), Barber *et al.* (1995) found that the ranges of dissolved gas concentrations for stable SBSL were lower by a factor of 100 in pure argon gas than in air. Löfstedt *et al.* (1995) pointed out that a sonoluminescing bubble cannot possibly be in diffusive equilibrium for these parameters and postulated another "anomalous mass flow," whose mechanism would be "the key to SL in a single bubble."

To account for these discrepancies to classical bubble dynamics, Lohse *et al.* (1997) proposed that the extra mass-ejection mechanism of Löfstedt *et al.* (1995) is of a chemical nature. The gas in the bubble is hot enough upon collapse to allow for significant dissociation of N_2 and O_2. The dissociated nitrogen and oxygen, as well as some radicals from dissociated water vapor, will undergo chemical reactions, whose products are very soluble in water and are expelled from the bubble. Only inert, nonreactive gases (such as argon) remain inside according to this "argon rectification hypothesis." This idea immediately resolves the apparent discrepancy between the measured and predicted parameter regimes for stable SBSL in air: if the bubble ends up filled with argon gas only, then only the argon dissolved in the liquid has to be in diffusive equilibrium with the bubble. As air contains 1% of argon, the effective dissolved gas concentration for diffusive stability of argon is 100 times smaller, and explains the hundredfold difference between observed concentrations for air and argon bubbles. The phase diagram in the R_0-P_a space resulting from that

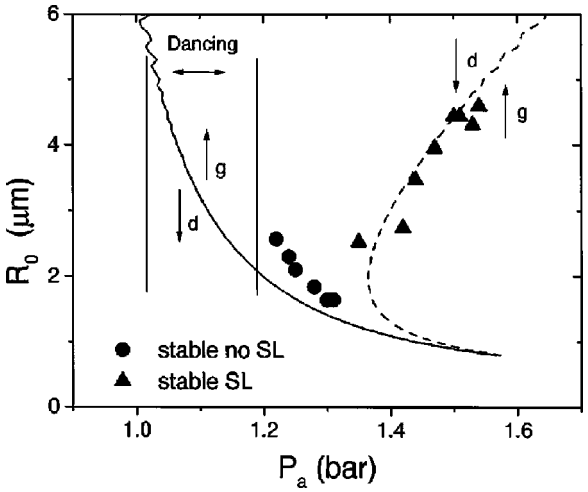

FIG. 12. Experimental phase diagram for air saturated in water to 20%. Each data point represents the P_a and R_0 found from a single $R(t)$ curve and is indicated to be luminescing and/or stable. The curves in the plot are lines of diffusive equilibrium for a given gas concentration $c_\infty/c_0=0.2$ (solid line) and $c_\infty/c_0=0.002$ (dashed line). The range of P_a where dancing bubbles were observed is indicated, as are regions of bubble growth (g) and dissolution (d) relative to each equilibrium curve. The stable no-SL points (●) correspond to a stable chemical equilibrium which would lie above the $c_\infty/c_0=0.2$ curve if plotted. From Ketterling and Apfel (1998).

theory is shown in Fig. 10. In particular, the theory predicts a new stable branch (called "B" in Fig. 10) on which mass losses from chemical reactions and growth from rectified diffusion just balance.

Experiments by Holt and Gaitan (1996) on bubble stability published contemporaneously with the theoretical work indeed showed this extra regime of bubble stability predicted from the argon rectification hypothesis (see Fig. 11). Ketterling and Apfel (1998, 2000a, 2000b) later showed the stability predictions to be quantitatively correct. Figure 12 shows experimental measurements of a phase diagram in comparison with theoretical predictions. One consequence of the interplay of diffusive and shape instabilities is indicated in this figure: bubbles can "dance" due to the recoil when they undergo fragmentation (see Sec. IV.E).

Phase diagrams such as Figs. 9–12 help us to understand the limitations of the parameter space for sonoluminescence, and in particular the crucial role of noble gases for SBSL stability. The same theoretical concepts could be applied to explain the pronounced increase in the intensity of emitted light with decreasing water temperature (Hilgenfeldt, Lohse, *et al.*, 1998), and the quenching of light due to small concentrations of surfactants, both of which were shown to be in agreement with experiments (Ashokkumar *et al.*, 2000; Matula, 2000; Toegel, Hilgenfeldt, *et al.*, 2000).

There was, however, still the nagging problem of the light emission itself. In contrast to the bubble dynamics, the available experimental information was insufficient to constrain the theories. The breakthrough contribution was made by Gompf *et al.* (1997), who measured the width of the light pulse using time-correlated single-photon counting (TC-SPC). This technique has a much higher resolution for measuring flash widths than a single photomultiplier tube, because it measures time delays in arrivals of single photons. The measurement of the delay time between the two photons reaching the two different photomultiplier tubes is repeated many times so that the width of the flash can be reconstructed. Gompf *et al.* (1997) discovered that the width of the light pulse is actually of the order of a few hundred picoseconds (see Fig. 13), much longer than the previous 50-ps upper bound measured by Barber and Putterman (1991). Moreover, since Gompf *et al.* (1997) could now resolve the shape of the light pulse, it was possible to study the dependence of the width on external parameters (the forcing pressure and dissolved gas concentration; see Fig. 14).

After this paper was published, at a meeting on sonoluminescence at the University of Chicago, two other groups announced that they had confirmed its findings: Moran and Sweider (1998) and Hiller *et al.* (1998) also used TC-SPC. At the same time, Gompf's group succeeded in obtaining an independent confirmation of the much longer duration of the light pulse using a streak camera for direct measurement of the pulse width (Pecha *et al.*, 1998). A previous attempt by Moran *et al.* (1995) employing a streak camera had yielded only a tentative upper bound for pulse width, which again proved too small.

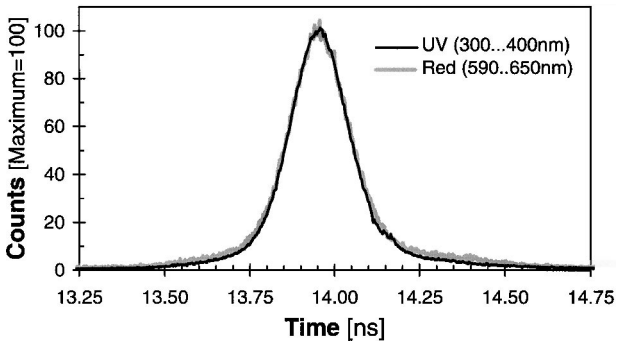

FIG. 13. First measurement of SBSL pulse widths. The parameters were $P_a = 1.2$ bars, $f = 20$ kHz, and the gas concentration was 1.8-mg/l O_2. Both the width in the red and the ultraviolet spectral range were measured. The indistinguishable widths rule out blackbody radiation, but not a thermal emission process in general. From Gompf *et al.* (1997).

The increased experimental resolution of TC-SPC and the subsequent discovery of a long flash width put all of the theories of light emission and energy focusing, which required ultrashort flash widths, out of business. Moreover, as was emphasized by Gompf *et al.* (1997) in their seminal paper, the measurement restored hope that a variant of the simplest possible theory for the light emission might be correct: the cavitation collapse of the bubble is so rapid that heat cannot escape from the bubble. Therefore, the bubble heats up, leading to light emission. Figure 15 shows the heating as calculated by Gompf *et al.* (1997), by solving a variant of the Rayleigh-Plesset equation for the bubble radius and assuming adiabatic heating (ratio of specific heats $\Gamma = 5/3$) near the collapse. Although the calculation contains some severe approximations, the agreement is quite reasonable.

This idea was buttressed by an earlier numerical simulation of Vuong and Szeri (1996), which, when reinterpreted with the new experiments in mind, questioned the notion that strong shocks are important for single-bubble sonoluminescence. Vuong and Szeri included dis-

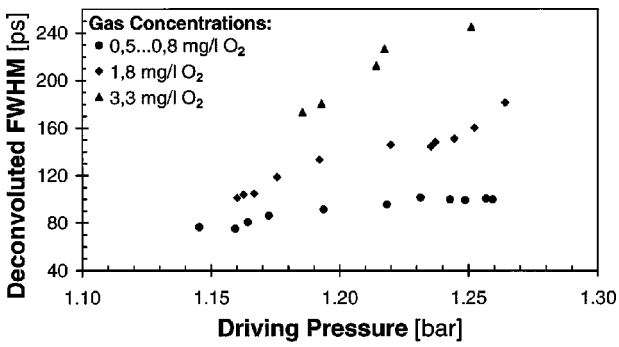

FIG. 14. Dependence of the full width at half maximum of the SBSL pulse on the driving pressure and the gas concentration at room temperature. $f = 20$ kHz. From Gompf *et al.* (1997).

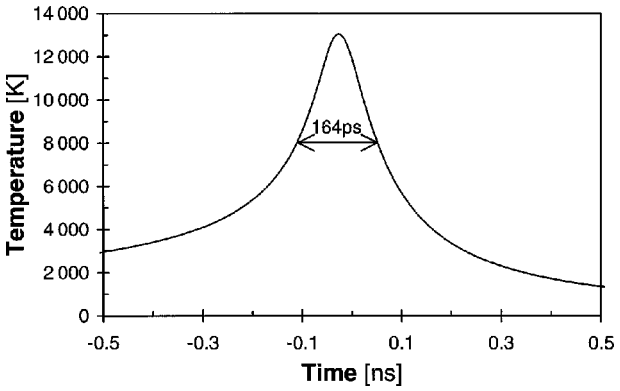

FIG. 15. Calculated shape of temperature pulse using a simple model based on the Rayleigh-Plesset equation, assuming the gas temperature and density are uniform throughout the collapse. Figure reproduced from Gompf *et al.* (1997).

sipative effects and showed that the strong shocks predicted by Wu and Roberts (1993) and Moss *et al.* (1994, 1996, 1997) were absent in noble gas bubbles, and were replaced by gentler inhomogeneities. The predicted maximum temperatures in the bubble were therefore much lower, several 10^4 K, compared with the 10^8 K previously announced by Wu and Roberts (1994). Moreover, the hot spot was not highly localized in the bubble center. These arguments were elaborated upon by Vuong *et al.* (1999); these models are much closer to the simple picture of adiabatic heating and thermal light emission than the shock-wave scenario. The temperature profiles and motions of Lagrangian points as computed by Vuong and Szeri (1996) are shown in Fig. 16: The characteristic scale over which temperature varies is of the order of the bubble radius.

Since the experimental resolution of the flash, researchers have focused on trying to determine which variant of the thermal light-emission model is correct. Is the interior of the bubble uniform? Is the radiation blackbody, bremsstrahlung, or some other process? Is the bubble optically thin or thick? What physical mechanism is suppressing spectral lines? Since experiments are now able to measure both the shape of the light pulse and the spectrum independently and accurately, it is possible to determine how these quantities depend on experimental parameters like forcing pressure, gas concentration, etc. The power of these measurements is that they provide severe constraints for theories of SBSL light emission that did not exist when the pulse width was believed to be very short. Moreover, since the bubble dynamics itself is well understood, closer examination of these parameter dependencies makes it possible to focus attention on subtle details of the light-emitting process. Single-bubble sonoluminescence has thus become a rather sophisticated testing ground for the ability of mathematical models and numerical simulations to explain detailed experimental data from a complicated physical process.

Although there are still open questions about the details of the light emission, considerable progress has been made. When Gompf *et al.* (1997) resolved the light

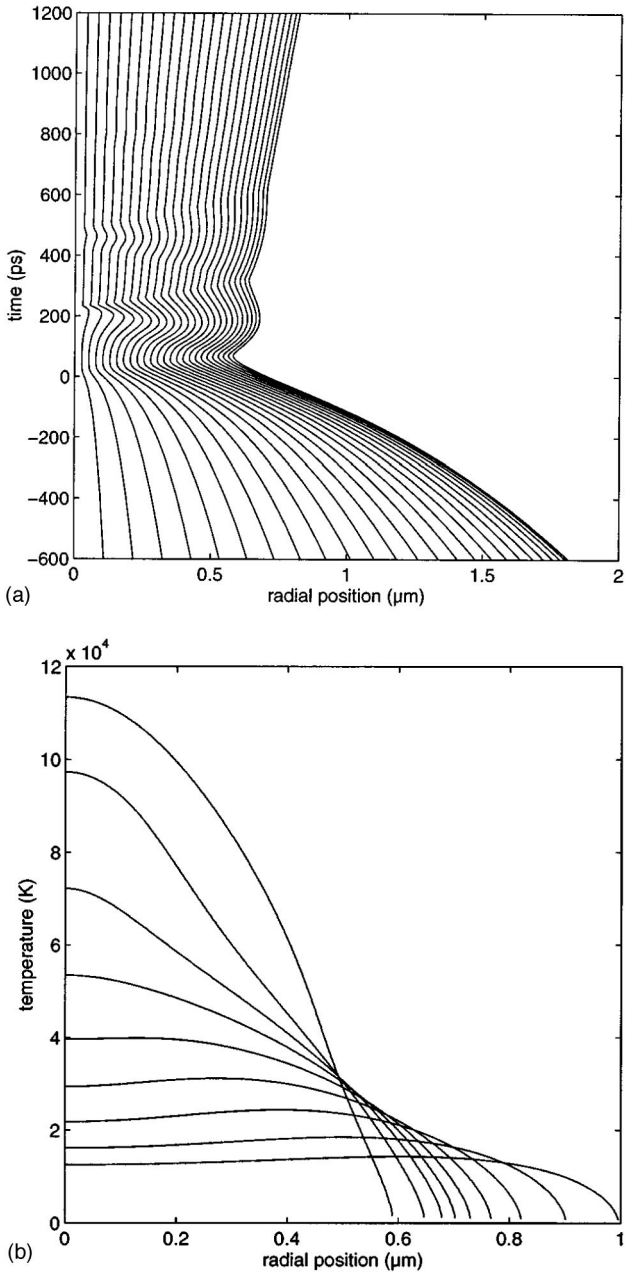

FIG. 16. Motion and temperature in a bubble shortly before collapse: (a) motion history of 20 Lagrangian points inside a $R_0=4.5$ μm bubble driven at $P_a=1.3$ atm and $f=26.5$ kHz. Strong wavy motion occurs inside the bubble, but no shock waves develop. (b) Temperature profiles in the bubble for various times around the bubble collapse. The profiles span a time interval of $\approx$170 ps near the collapse. The temperature at the center increases monotonically, until the maximum temperature is reached at the last snapshot. Note that the temperature profile is smooth, without any discontinuity that would be present with a shock. From Vuong and Szeri (1996).

pulses, they also made measurements of the dependence of the width on optical wavelength. Strikingly, such a dependence was found to be absent, contradicting a simple blackbody emission model, which demands that the width increase with the wavelength.

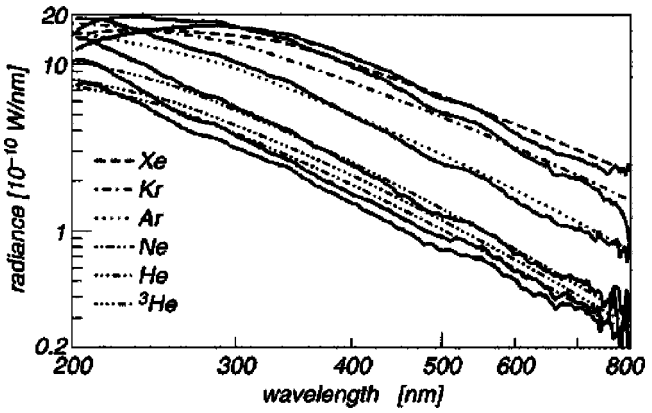

FIG. 17. Emission spectra from rare gases at room temperature. The dotted lines are calculations based on the theoretical model of Hammer and Frommhold (2000a). The only adjustable parameters in the comparison are the ambient radii and forcing pressures of the bubbles. From Hammer and Frommhold (2001).

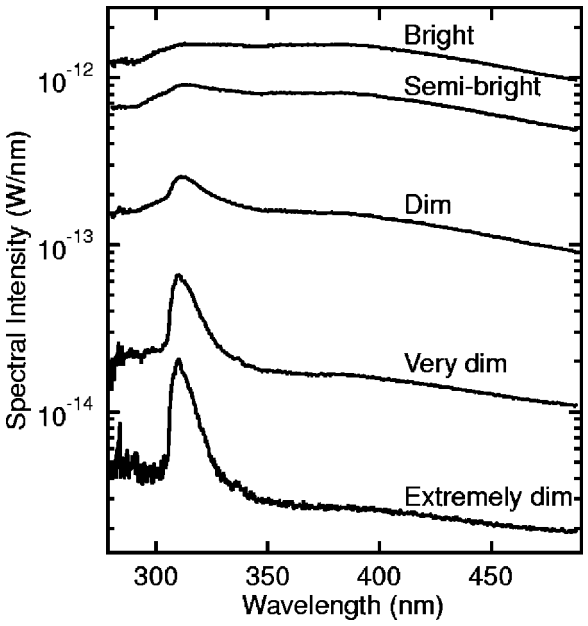

FIG. 18. Dependence of the spectra of argon SBSL (for a partial pressure of ≈150 torr at 25 °C) on the forcing pressure. Spectra are shown for five levels of overall brightness. The OH line is vanishing in the thermal bremsstrahlung spectrum with increasing forcing pressure P_a. From Young *et al.* (2001).

A resolution for this conundrum was hinted at in numerical simulations by Moss *et al.* (1994, 1997, 1999), who realized that the temperature-dependent photon absorption coefficients of the gas must be taken into account. The size of the bubble and thus the size of the light-emitting region are so small that the bubble is nearly transparent for its own photons: the bubble is a volume emitter, not a surface emitter like an ideal blackbody. Among other things, Moss *et al.* (1999) used this idea to rationalize the qualitative shape of the emission spectrum in noble gases.

Hilgenfeldt *et al.* (1999a, 1999b) used varying absorption coefficients to explain the wavelength-independent pulse widths: Both the absorptivity and emissivity of the bubble drop precipitously directly after collapse for all wavelengths, since they depend exponentially on temperature, but only weakly on wavelength. Combining this model of thermal radiation with the parameter dependencies predicted by the stability constraints on the bubble, they also found agreement with the observed parameter dependencies of the pulse width, number of photons per burst, and spectral shape. Hammer and Frommhold (2000a, 2000b) demonstrated that this model could be refined with *ab initio* quantum-mechanical calculations of electron-neutral bremsstrahlung, further improving the agreement with experiments. Examples of their spectra are shown in Fig. 17.

An important aspect of bubble thermodynamics, which has been pointed out by Kamath *et al.* (1993), Yasui (1997b), Colussi and Hoffmann (1999), Moss *et al.* (1999), Storey and Szeri (2000, 2001); Toegel, Gompf, *et al.* (2000), Hilgenfeldt *et al.* (2001), and Putterman *et al.* (2001), is the presence of water vapor inside the bubble. Upon bubble expansion, vapor invades the bubble. At collapse, it cannot completely escape (condense at the bubble wall) because the diffusion time scale is much slower than the time scale of the collapse. Therefore water vapor is trapped inside the bubble (Storey and Szeri, 2000). It limits the maximum temperature in the bubble due to its lower polytropic exponent (compared to inert gases) and above all because of the endothermic chemical reaction $H_2O \rightarrow OH + H$, which eats up the focused energy. Within the model of Storey and Szeri (2000), taking water vapor and its chemical reactions into account leads to calculated maximum temperatures in the bubble of only around 6000 K. This seems to contradict experiments, in that thermal light emission would be strongly suppressed below the mea-

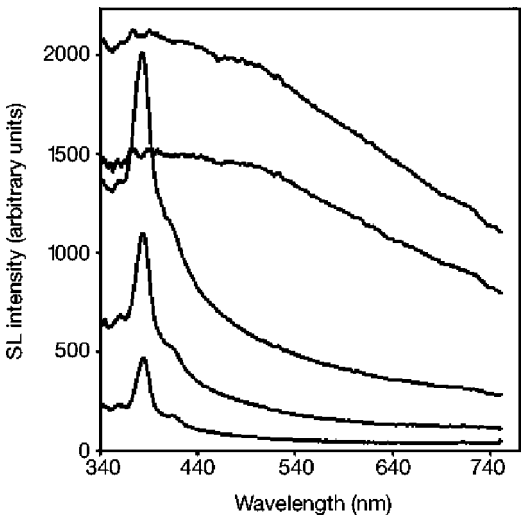

FIG. 19. Light-emission spectra from moving SBSL bubbles in adiponitrile. The driving pressure amplitude increases from bottom to top, between 1.7 bars and 1.9 bars. The spectral line at ≈400 nm corresponds to an excitation of CN. From Didenko *et al.* (2000b).

sured values, and is an indication that the modeling overestimates the amount of water vapor in the bubble.

In two very recent experiments, the signatures (characteristic lines) of the liquid or liquid vapor were detected in the spectrum, finally closing the gap between MBSL and SBSL. In both cases the lines belong to constituents of vapor molecules.

Young *et al.* (2001) discovered spectral lines for SBSL in water by decreasing the driving pressure very close to the threshold for SBSL. In this regime, the light pulse is so weak that Young *et al.* (2001) had to collect photons over several days. Figure 18 shows how, as the forcing pressure is increased, the OH line vanishes behind the enhanced continuum contribution to the spectrum.

Didenko *et al.* (2000b) found spectral lines of SBSL in organic fluids (see Fig. 19). These tend to require larger driving to show SBSL, because the vapor molecules have more rotational and vibrational degrees of freedom, leading to a weaker temperature increase at bubble collapse.

We believe that the observation of spectral lines heralds a new era of research on single-bubble sonoluminescence, one in which it will be possible to use SBSL to study chemical reactions. Such studies have long been conducted for multibubble cavitation, and indeed Suslick and collaborators (Suslick *et al.*, 1986; Flint and Suslick, 1991b; Didenko *et al.*, 1999) have used the widths and intensities of spectral lines in multibubble sonoluminescence to deduce the temperature of cavitation. The great advantage of using single-bubble sonoluminescence in these studies is that, in contrast to MBSL, the mechanics of SBSL is well understood and characterized. It thus seems possible that one will be able to use SBSL to carefully study chemical reactions under exotic conditions of high temperatures and extreme densities.

II. FLUID DYNAMICS OF THE FLASK

The very existence of a sonoluminescing bubble depends critically on a subtle balance of hydrodynamic and acoustic forces inside the flask. During sonoluminescence, a diverse array of physical effects influences this balance: the pressure becomes low enough that the liquid-air interface vaporizes, and temperatures rise so high that the gas inside the bubble emits light. Gas is continually exchanged between the bubble and the surrounding liquid, causing the number of molecules in the bubble to vary. In a small part of the cycle, the bubble-wall velocity may become supersonic. During all of these processes there is no *a priori* reason for the shape of the bubble to remain spherical, so this must be accounted for as well.

Although the equations of motion governing these effects were written in the nineteenth century, it is a triumph of twentieth-century applied mathematics that all of them can be accounted for simultaneously in a precise and controlled way. This is the theory of classical bubble dynamics, started by Lord Rayleigh (1917) during his work for the Royal Navy investigating cavitation damage of ship propellers. The formalism was substantially refined and developed by Plesset, Prosperetti, and others over a span of several decades. A review of early work is presented by Plesset and Prosperetti (1997); a later overview is given by Prosperetti (1998). The present section summarizes this theory with a view towards its application to experiments on single-bubble sonoluminescence. Our discussion will highlight the validity of the approximations made when the theory is applied to SBSL, and will also underscore how and why the theory works when it does. The presentation of this section was greatly influenced by the excellent recent review by Prosperetti (1998).

A. Derivation of the Rayleigh-Plesset equation

The ultrasonic forces in the liquid are caused by the oscillating transducers on the container walls, which are tuned to excite an acoustic resonance mode of the container, often the lowest. The Q factor of a typical flask is $\approx 10^3$, so the resonance is quite sharp. Its frequency is about 20 kHz for a container a few centimeters across, mercifully above the range of human hearing.[2] The driving pressure amplitude at the center of the flask is around $P_a \approx 1.2$–1.4 bars when SBSL occurs.

The equations governing the sound waves in the liquid are the compressible Navier-Stokes equations

$$\rho(\partial_t u + u \cdot \nabla u) = -\nabla p + \eta \nabla^2 u + \zeta \nabla \nabla \cdot u, \tag{1}$$

$$\partial_t \rho + \nabla \cdot (\rho u) = 0, \tag{2}$$

where u is the fluid velocity, ρ the density, p the pressure (as specified by an equation of state), η the shear viscosity, and ζ the bulk viscosity of the liquid. In writing these equations, we have assumed that the liquid is isothermal and so have neglected the equation for the fluid temperature. As an approximation, the bubble's extension compared to that of the flask and that of the sound wave is neglected, as it is orders of magnitude smaller.

The forces on the bubble depend on where it is located in the flask. In general there will be both an isotropic oscillatory pressure (causing volumetric oscillations) and, in addition, pressure gradients, quadrupole components, etc. In practice, for small bubbles, all that matters are the isotropic volumetric oscillations and the pressure gradients, which can create a net translational force on the bubble. The translation can vanish only at pressure maxima or minima. We shall see below that these forces cause sonoluminescing bubbles to be trapped at a pressure antinode of the sound field.

To compute the magnitude of the forces it is necessary first to characterize the volumetric oscillations, for which the sound field around the bubble is purely radial. The velocity can then be represented by a potential, with $u = \nabla \phi$. Equations (1) and (2) then become

$$\rho[\partial_t \phi + \tfrac{1}{2}(\partial_r \phi)^2] = -p, \tag{3}$$

[2]Efforts to scale up sonoluminescence have ventured into the lower-frequency regime of audible sound. Bad luck for the experimentalist.

$$\partial_t \rho + \partial_r \phi \partial_r \rho + \rho \nabla^2 \phi = 0. \tag{4}$$

Note the assumption that the flow field is purely radial and therefore viscous stresses are not important.

To proceed we need to combine Eqs. (3) and (4) into a single equation for ϕ. Defining the enthalpy $dH = dp/\rho$, and using $dp = (dp/d\rho)d\rho = c^2 d\rho$ (with c the speed of sound in the liquid) implies

$$\nabla^2 \phi = \left[\frac{u}{c^2} (\partial_t u - \partial_r H) \right] + \frac{1}{c^2} \partial_t^2 \phi, \tag{5}$$

where $u = \partial_r \phi$ is the radial velocity field. As long as the fluid velocity is much smaller than c, the square-bracketed terms are negligible. The linear $c^{-2}\partial_t^2 \phi$ term is only negligible close to the bubble: at distances on the order of the sound wavelength away from the bubble, this term will become important.

We would like to solve Eq. (5) for the velocity of the bubble wall dR/dt, caused by the resonant oscillation of the container. We proceed in two steps: near the bubble the velocity potential obeys the Laplace equation, $\nabla^2 \phi = 0$. The solution satisfying the boundary condition at the bubble wall $\partial_r \phi(r = R) = \dot{R}$ is

$$\phi = -\frac{\dot{R} R^2}{r} + A(t), \tag{6}$$

where $A(t)$ is a free constant. This free constant is determined by matching the solution (6) onto the pressure field far from the bubble. Neglecting the sound radiated by the bubble itself, the velocity potential far from the bubble is a standing wave—the acoustic mode that is excited by the transducer. For our present purposes, we do not require the entire spatial structure of this mode, but only the field close to the bubble. Since the bubble is much smaller than the sound wavelength, this sound field will be independent of r, so that $\phi = \phi_\infty(t)$. Matching the near field and the far field implies $A = \phi_\infty$. The pressure in the neighborhood of the bubble is then $p = -\rho \partial_t \phi_\infty = P_0 + P(t)$, i.e., the sum of the background static pressure $P_0 = 1$ bar and the sinusoidal driving pressure $P(t) = -P_a \sin \omega t$.

The velocity field in the liquid around the bubble then follows as

$$u = \frac{\dot{R} R^2}{r^2}. \tag{7}$$

We now use this to solve for the dynamics of the bubble wall. To this end, we use the force balance on the bubble surface, which gives

$$\begin{aligned} p_g(t) + \Sigma_{rr}[r = R(t)] &= p_g(t) - p[R(t)] + 2\eta \partial_r u(r = R) \\ &= p_g(t) - p[R(t)] - 4\eta \frac{\dot{R}}{R} = 2\frac{\sigma}{R}, \end{aligned} \tag{8}$$

where Σ_{rr} is the radial component of the stress tensor in the liquid, σ is the surface tension of the gas-liquid interface, and p_g is the pressure in the gas, assumed to be spatially uniform. Evaluating this formula using Eq. (3) for the pressure in the liquid gives

$$R\ddot{R} + \frac{3}{2}\dot{R}^2 = \frac{1}{\rho}\left(p_g - P_0 - P(t) - 4\eta \frac{\dot{R}}{R} - \frac{2\sigma}{R} \right). \tag{9}$$

Equation (9) is the celebrated Rayleigh-Plesset equation. The left-hand side of the equation was known to Lord Rayleigh (though never written). A historical review of the development of this equation is given by Plesset and Prosperetti (1977).

Closing the equation requires knowing the pressure in the gas. Roughly speaking, when the bubble wall moves slowly with respect to the sound velocity in the gas, the pressure in the gas is uniform throughout the bubble. In this regime, how strongly the pressure depends on the bubble volume depends on the heat transfer across the bubble wall (Prosperetti *et al.*, 1988). The pressure-volume relation is given by

$$p_g(t) = \left(P_0 + \frac{2\sigma}{R_0} \right) \frac{(R_0^3 - h^3)^\gamma}{[R(t)^3 - h^3]^\gamma}. \tag{10}$$

Here R_0 is the ambient radius of the bubble (i.e., the radius at which an unforced bubble would be in equilibrium), and h is the van der Waals hard-core radius determined by the excluded volume of the gas molecules.

If the heat transfer is fast (relative to the time scale of the bubble motion), then the gas in the bubble is maintained at the temperature of the liquid, and the pressure is determined by an isothermal equation of state with $\gamma = 1$. On the other hand, if the bubble wall moves very quickly relative to the time scale of heat transfer, then heat will not be able to escape from the bubble, and the bubble will heat (cool) adiabatically on collapse (expansion). For a monatomic (noble) gas, this implies that $\gamma = \Gamma = 5/3$. The dimensionless parameter that distinguishes between these two regimes is the Péclet number,

$$\mathrm{Pe} = \frac{|\dot{R}| R}{\chi_g}, \tag{11}$$

where χ_g is the thermal diffusivity of the gas.

This idea about heat transfer is based on a more careful version of this argument by Kamath *et al.* (1993) and Prosperetti *et al.* (1998). They showed that the temperature T_s at the bubble surface is basically the water temperature: Conservation of energy at the bubble interface requires continuity of the heat flux,

$$K_g \partial_r T = K_l \partial_r T_l, \tag{12}$$

with the thermal conductivities K_g and K_l of gas and liquid. The gradients are estimated via the thermal boundary layer thicknesses δ_g and δ_l in and around the bubble,

$$\partial_r T = \frac{T_g - T_s}{\delta_g}, \quad \partial_r T_l = \frac{T_s - T_l}{\delta_l}, \tag{13}$$

where T_g is the temperature at the bubble center. The diffusion lengths can be estimated with the relevant time scale Δt of the bubble oscillation and the respective thermal diffusivity χ, namely, $\delta \sim \sqrt{\chi \Delta t}$. With the con-

nection between thermal conductivity and diffusivity, $K = \chi \rho C_p$, where C_p is the specific heat per unit mass, one obtains the final result,

$$\frac{T_s - T_l}{T_g - T_s} = \sqrt{\frac{\chi_g \rho_g C_{p,g}}{\chi_l \rho C_{p,l}}}. \tag{14}$$

Since the density and the specific heat of water are so much larger than the respective values for gas, the right-hand side of Eq. (14) is typically of the order of 10^{-3}–10^{-2}. Therefore the temperature drop basically occurs inside the bubble, and the temperature at the surface basically equals the water temperature.

If the rate of heat transfer is intermediate between adiabatic and isothermal, the situation is more complicated. Here, a correct calculation requires solving the heat conduction problem throughout the bubble cycle and using the computed temperature in the bubble to evaluate the pressure in the gas (through its equation of state). This is quite a difficult task. Over the years, several methods have been proposed that amount to varying γ continuously between the isothermal value and the adiabatic value (Plesset and Prosperetti, 1977; Prosperetti *et al.*, 1988; Kamath *et al.*, 1993) depending on the Péclet number. This approach can yield quantitatively incorrect results, as shown by Prosperetti and Hao (1999), in large part because energy dissipation from thermal processes is neglected.

B. Extensions of the Rayleigh-Plesset equation

So far we have not considered damping of the bubble dynamics by the sound radiated by the bubble itself. The most complete and elegant derivation of this effect is due to Lezzi and Prosperetti (1987; Prosperetti and Lezzi, 1986).

In arriving at Eq. (9), we asserted that the velocity potential of the sound field in the liquid far from the bubble is the same as in the absence of the bubble, $\phi = \phi_\infty(t)$. The radial sound wave emitted from the bubble introduces a modification,

$$\phi = \phi_\infty(t) - \frac{1}{r} F(t - r/c) \approx \phi_\infty(t) - \frac{1}{r} F(t) + \frac{\dot{F}(t)}{c}, \tag{15}$$

where we have estimated the velocity potential at small r. As above, this now must be matched to the near-field velocity potential Eq. (6). The matching yields $F(t) = R^2 \dot{R}$ and $A(t) = \phi_\infty + \dot{F}/c$. Substituting this into the pressure jump condition one obtains

$$\rho(R\ddot{R} + \tfrac{3}{2}\dot{R}^2) = [p_g - P_0 - P(t)] - 4\eta \frac{\dot{R}}{R} - 2\sigma \frac{1}{R} + \frac{\rho}{c} \frac{d^2}{dt^2}(R^2 \dot{R}). \tag{16}$$

The sound radiation term is of order $\dot{R}/c$ times the other terms in the equation. When the bubble-wall motion is slow it is therefore negligible.

When $|\dot{R}|/c \sim 1$, sound radiation is important. Formally, sound radiation raises the order of the Rayleigh-Plesset equation from second order to third order. At first glance, this seems strange, because physically initial conditions are given for both R and $\dot{R}$, but not $\ddot{R}$. The discrepancy arises because Eq. (16) has a spurious unstable solution which grows exponentially in time. This is unphysical; the initial condition on $\ddot{R}$ must be chosen to suppress this solution.

As emphasized by Prosperetti *et al.* (1988; Prosperetti and Hao, 1999), this procedure is inherently impractical, as numerical errors will always excite the spurious solution. A better way to take care of this is to calculate the $d^2/dt^2\,(R^2\dot{R})$ term using the Rayleigh-Plesset equation itself. A standard way of doing this was invented by Keller and co-workers (Keller and Kolodner, 1956; Keller and Miksis, 1980) and leads to the Keller equation (Prosperetti and Lezzi, 1986; Brennen, 1995)

$$\left(1 - \frac{\dot{R}}{c}\right)\rho R\ddot{R} + \frac{3}{2}\dot{R}^2\rho\left(1 - \frac{\dot{R}}{3c}\right) = \left(1 + \frac{\dot{R}}{c}\right)[p_g - P_0 - P(t)] + \frac{R}{c}\dot{p}_g - 4\eta\frac{\dot{R}}{R} - \frac{2\sigma}{R}. \tag{17}$$

As discussed by Prosperetti *et al.* (1988; Prosperetti and Lezzi, 1986), the precise form of this equation is not unique: There is a one-parameter family of equations that can be consistently derived from Eq. (16), namely,

$$\left(1 - (\lambda+1)\frac{\dot{R}}{c}\right)\rho R\ddot{R} + \frac{3}{2}\dot{R}^2\rho\left(1 - (\lambda + \tfrac{1}{3})\frac{\dot{R}}{c}\right) = \left(1 + (1-\lambda)\frac{\dot{R}}{c}\right)[p_g - P_0 - P(t)] + \frac{R}{c}\dot{p}_g - 4\eta\frac{\dot{R}}{R} - \frac{2\sigma}{R}, \tag{18}$$

where the parameter value $\lambda = 0$ recovers the Keller equation, and $\lambda = 1$ results in the formula used by Herring (1941) and Trilling (1952). Introducing higher-order terms leads to variations like the form derived by Flynn (1975a, 1975b), but Prosperetti and Lezzi (1986) have shown that the higher order does not, in general, guarantee higher accuracy of the formula. Other well-known forms of Rayleigh-Plesset derivatives are compared by Lastman and Wentzell (1981, 1982). Prosperetti and Lezzi (1986) demonstrate that, for a number of relevant examples, the Keller equation yields results in closest agreement with full partial differential equation numerical simulations.

An "odd cousin" of Eq. (18) is the Gilmore equation (Gilmore, 1952; Brennen, 1995),

$$\left(1-\frac{\dot{R}}{C}\right)R\ddot{R}+\frac{3}{2}\dot{R}^2\left(1-\frac{\dot{R}}{3c}\right)=\left(1+\frac{\dot{R}}{C}\right)\frac{H}{\rho}+\left(1-\frac{\dot{R}}{C}\right)\frac{R}{C}\frac{\dot{H}}{\rho}, \tag{19}$$

whose derivation relies on the Kirkwood-Bethe approximation (Kirkwood and Bethe, 1942). In Gilmore's equation, the key quantity is the enthalpy H, and not the pressure. In this approach, the speed of sound C is not a constant, but depends on H. According to Gompf and Pecha (2000; Pecha and Gompf, 2000), this allows one to model the increase of the speed of sound with increasing pressure around the bubble, which leads to significantly reduced Mach numbers at bubble collapse.

The breakdown of the Rayleigh-Plesset variants when $|\dot{R}|/c$ approaches unity is reflected in unphysical singularities when $|\dot{R}|/c\sim 1$ in the major terms of the equations. Since equations with different λ lead to similar results, one solution to this problem is to delete all the prefactors in parentheses containing $\dot{R}/c$. We thus arrive at a popular form in the context of sonoluminescence (see, for example, Löfstedt *et al.*, 1995; Barber *et al.*, 1997),

$$\rho(R\ddot{R}+\tfrac{3}{2}\dot{R}^2)=[p_g-P_0-P(t)]-4\eta\frac{\dot{R}}{R}-2\sigma\frac{1}{R}+\frac{R}{c}\frac{d}{dt}(p_g). \tag{20}$$

For very strong forcing, these different equations deviate in the small time interval of bubble collapse, though they are in near-perfect accord for the rest of the driving cycle. Therefore they can be expected to produce quantitative discrepancies for the properties of the collapsed bubble (e.g., the minimum radius, maximum gas pressure, etc.). These discrepancies are a principal source of modeling error for theories of SBSL. Another is the treatment of heat exchange via an effective polytropic exponent in Eq. (10). Simple refinements for heat exchange have been employed by Yasui (1995), though the only infallible solution is a direct calculation of the heat transfer. This was first carried out in numerical simulations by Vuong and Szeri (1996) and more recently by Moss *et al.* (1999).

Given these difficulties, it is surprising that solutions to Rayleigh-Plesset-type equations still provide a quantitatively accurate representation of the mechanics of a sonoluminescing bubble and of many of its accompanying effects. Recently, Lin *et al.* (2001) achieved a better understanding of why finite Mach number corrections to Rayleigh-Plesset-type equations are relatively unimportant. They showed that the Rayleigh-Plesset equation is quite accurate even with significant spatial inhomogeneities in the pressure field inside the bubble. This extends the utility of the Rayleigh-Plesset equation into the regime where the Mach number for the gas $M_g=\dot{R}/c_g$ (where c_g is the speed of sound in the gas) is no longer small. Lin *et al.* (2001) show that the relevant condition is not $|M_g|<1$, but $|\epsilon_p|<1$, where

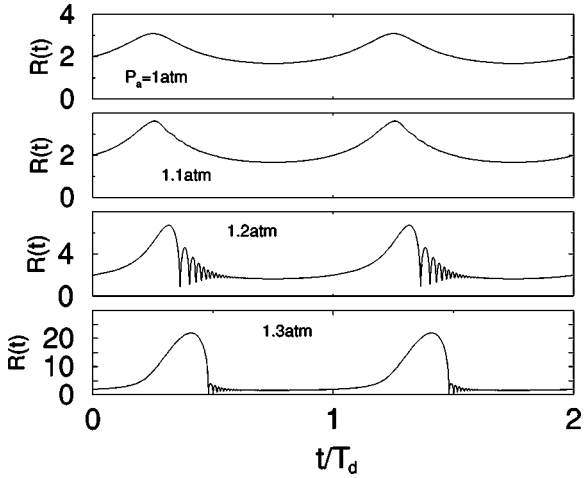

FIG. 20. Solutions to the modified Rayleigh-Plesset Eq. (20) at forcing pressures $P_a=1.0$, 1.1, 1.2, and 1.3 atm. The ambient bubble radius is $R_0=2$ μm, the frequency $f=1/T_d=26.5$ kHz.

$$\epsilon_p\equiv\frac{R\ddot{R}\rho_{gas}}{\Gamma p(r=0,t)}, \tag{21}$$

i.e., what is relevant is the bubble-wall *acceleration*. So even in the sonoluminescence regime, Lin *et al.* (2001) find excellent agreement when comparing their full gas-dynamical partial differential equation simulations with the solutions to the Rayleigh-Plesset ordinary differential equation with the assumption of a uniform pressure inside. They also developed an approximation for the internal pressure field, taking into consideration first-order corrections from pressure inhomogeneity.

In the remainder of this section, we present calculations and experiments on bubble dynamics during a cycle of the driving, discussing the various physical effects that are important away from the bubble collapse. Later sections will describe our present knowledge of the collapse itself.

C. The bubble's response to weak and strong driving

First, to give some feeling for solutions to the Rayleigh-Plesset equation, we study small oscillations of the bubble about its ambient radius R_0. A straightforward calculation (Brennen, 1995) shows that such a bubble oscillates at the resonant frequency

$$2\pi f_0=\sqrt{\frac{1}{\rho R_0^2}\left(3\gamma P_0+(3\gamma-1)\frac{2\sigma}{R_0}\right)}. \tag{22}$$

A typical sonoluminescing bubble has $R_0\approx 5$ μm, corresponding to a resonant frequency of $f_0\approx 0.5$ MHz, much higher than the frequency of the driving $f\approx 20$ kHz.

Figure 20 shows solutions to the modified Rayleigh-Plesset Eq. (20) for a bubble at different forcing pressures. At low forcing, the bubble undergoes almost sinusoidal oscillations of relatively small amplitude, with a period equal to that of the external forcing f. Here, the oscillations are essentially "quasistatic," because the resonant frequency is so much larger than f: the oscilla-

tory pressure forcing is balanced by the gas pressure (Löfstedt *et al.*, 1993; Hilgenfeldt, Brenner, *et al.*, 1998), with inertia, surface tension, and viscosity playing a negligible role. At a critical pressure around $P_a \approx P_0$, such quasistatic oscillations are no longer possible, resulting in a nonlinear response of the bubble. The critical P_a depends slightly on R_0, and is referred to as the (dynamical) Blake threshold (Blake, 1949; see also Hilgenfeldt, Brenner, *et al.*, 1998). Beyond this threshold, sonoluminescence can occur.

In the SBSL regime, the solution to Eq. (20) in this regime can be divided into several different stages.

- *Expansion*: During the negative half-cycle of the driving, the applied tension makes the bubble expand. Since $f \ll f_0$, the expansion continues until the applied pressure becomes positive. The time scale of this regime is thus set by the period of the driving pressure wave and is typically $\approx 20\ \mu$s for sonoluminescence experiments. This is sufficient to increase the bubble radius by as much as a factor of 10.
- *Collapse*: When the driving changes sign, the expanded bubble is "released" and collapses inertially over a very short time (~ 1 ns for SBSL bubbles). The solution during collapse is well described by the classical solution of Lord Rayleigh. SBSL light emission occurs at the end of the collapse.
- *Afterbounces*: After the collapse, the bubble spends the remaining half of the cycle oscillating about its ambient radius at roughly its resonant frequency $f_0 \gg f$, giving rise to characteristic "afterbounces."

It is worthwhile at this point to comment on the roles of surface tension and viscosity. The surface tension term is dynamically important when it is as large as the external forcing pressure, implying that $\sigma/R \sim P_a$. This occurs when the bubble radius is smaller than $R_\sigma = \sigma/P_a$. For water, this corresponds to a radius of $\approx 0.7\ \mu\text{m}/(P_a/\text{bar})$. We shall see below that this length scale plays an important role in determining the stability of the solutions to the Rayleigh-Plesset equation with respect to both dissolution and breakup.

Viscous effects are important when the viscous damping time scale is of the order of the time scale of bubble motion, roughly $\nu/R_0^2 \sim f_0$, with the kinematic viscosity $\nu = \eta/\rho$. For water, this does not occur; for more viscous fluids it can be important (Hilgenfeldt, Brenner, *et al.*, 1998).

D. The Rayleigh collapse

Now we turn to the behavior of the bubble radius near the collapse. As emphasized above, this is the regime in which the Rayleigh-Plesset description is in danger of breaking down. The approach to the collapsed state, however, can be captured very well by the equation, and is given by a classical solution of Lord Rayleigh.

Lord Rayleigh (1917) imagined a bubble dynamics for which only liquid inertia mattered, with gas pressure, surface tension, and viscosity all negligible—in other words, the collapse of a void. The equation for the wall motion of the bubble/void is then $R\ddot{R} + 3/2\dot{R}^2 = 0$ and can be directly integrated. The solution is of the form $R(t) = R_0[(t_* - t)/t_*]^{2/5}$, with the remarkable feature of a divergent bubble-wall velocity as t approaches the time t_* of total collapse. Lord Rayleigh pointed out that this singularity is responsible for cavitation damage, and it is also the central hydrodynamic feature responsible for the rapid and strong energy focusing that leads to sonoluminescence.

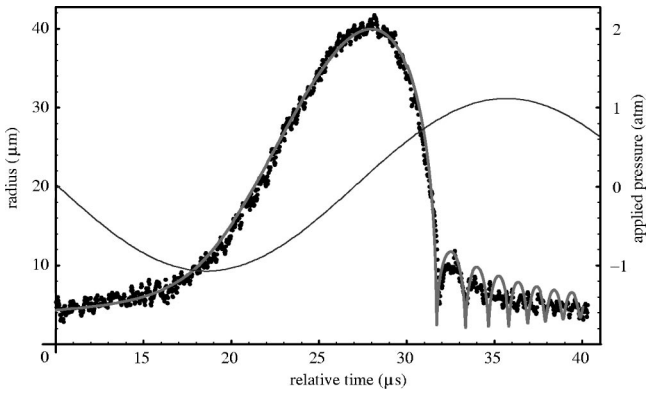

FIG. 21. Measured $R(t)$ (with Mie scattering, dots) and a fit to these data based on the Keller equation (solid curve). The thin curve shows the driving pressure $P(t)$. From Matula (1999).

Clearly, something must stop the velocity from diverging. For the Rayleigh-Plesset Eq. (9) to capture sonoluminescence, it must contain the physical effect that does this. Viscous stresses $4\eta\dot{R}/R \propto (t_* - t)^{-1}$ and surface tension forces $\sigma/R \propto (t_* - t)^{-2/5}$ diverge at slower rates than the inertial terms $[\propto (t_* - t)^{-6/5}]$ and are therefore too weak. What about the gas pressure? The collapse rate is eventually so fast that the heat does not have time to escape the bubble. The pressure in the gas then obeys the adiabatic equation of state, which diverges as $p_g \propto R^{-3\Gamma} \propto (t_* - t)^{-2}$ (for a monatomic ideal gas with $\Gamma = 5/3$), which is stronger than the inertial acceleration. This effect is therefore capable of stopping the collapse. Modifications from the ideal gas law, e.g., van der Waals forces [see Eq. (10)], do not affect this conclusion.

Although the gas pressure can halt Rayleigh collapse, it turns out that the most strongly divergent term in Eq. (20) is the last one, associated with sound radiation into the liquid during the last stages of collapse; it diverges as $(t_* - t)^{-13/5}$ (Hilgenfeldt, Brenner, *et al.*, 1998), and overwhelms the other terms. Up to 50% of the kinetic energy in the collapse may end up as a radiated pressure wave (Gompf and Pecha, 2000).

E. Comparison to experiments

Of course, it is crucial to compare solutions of Rayleigh-Plesset equations to experimental data on the bubble radius as a function of time. However, neither the ambient bubble radius R_0 nor the driving pressure P_a is known *a priori*. R_0 changes through gas diffusion

as well as evaporation/condensation of water vapor (see Sec. III), and the (local) driving pressure P_a is very sensitive to perturbations of the flask geometry, such as might be caused by a small hydrophone attempting to measure P_a. In addition, the precision of such a hydrophone is limited to roughly 0.05 bar.

The standard procedure has been to measure $R(t)$ with Mie scattering[3] and then to fit the data to Rayleigh-Plesset-type dynamics by adjusting R_0 and P_a. A typical trace for a sonoluminescing bubble's radius during a cycle of the drive is shown in Fig. 21. The filled circles represent experimental measurements, and the solid line is a solution to the Keller equation under the assumption of isothermal heating ($\gamma=1$). Superimposed as a thin line is the applied forcing pressure.

The problem with these fits is that R_0 and P_a sensitively depend on model details. In particular, if one adjusts R_0 and P_a such that the bubble's maximum is well fitted, the afterbounces are always overestimated (see Fig. 21). Better fits can be achieved by allowing more parameters, e.g., by allowing the material constants such as the viscosity or the surface tension to vary. Barber *et al.* (1992), for example, used seven times the usual value of the viscosity of water to achieve a fit to the afterbounces. As clarified by Prosperetti and Hao (1999), the larger viscosity effectively parametrizes other damping mechanisms not captured in simple Rayleigh-Plesset-type models. In particular, Prosperetti and Hao (1999) included thermal losses, following Prosperetti (1991), reducing the size of the afterbounces. Yasui (1995) had some success by introducing thermal boundary layers as well.

Another effect that must be considered when fitting experimental $R(t)$ curves to Rayleigh-Plesset models is the invasion of water vapor at bubble maximum. This leads to a varying ambient radius R_0 over the bubble cycle, being largest at maximum radius. Since many early fits of $R(t)$ curves (summarized by Barber *et al.*, 1997) did not consider these effects, the resulting values for R_0 and P_a are only approximate.

Mie scattering data near the collapse are also notoriously difficult to interpret because of the unknown index of refraction inside the compressed bubble and because the bubble radius R becomes of the order of the light wavelength. The simple proportionality of Mie intensity and R^2, valid for larger R, gets lost and the relation even becomes nonmonotonic (Gompf and Pecha, 2000). Moreover, at collapse, the light is reflected not only from the bubble wall, but also from the shock wave emitted from the bubble at collapse. This subject will be treated in the next subsection.

Another light-scattering technique based on differential measurement and polarization (differential light scattering) has been developed by Vacca *et al.* (1999) in order to measure the dynamics of the bubble radius. With this technique a time resolution of up to 0.5 ns around the Rayleigh collapse has been achieved.

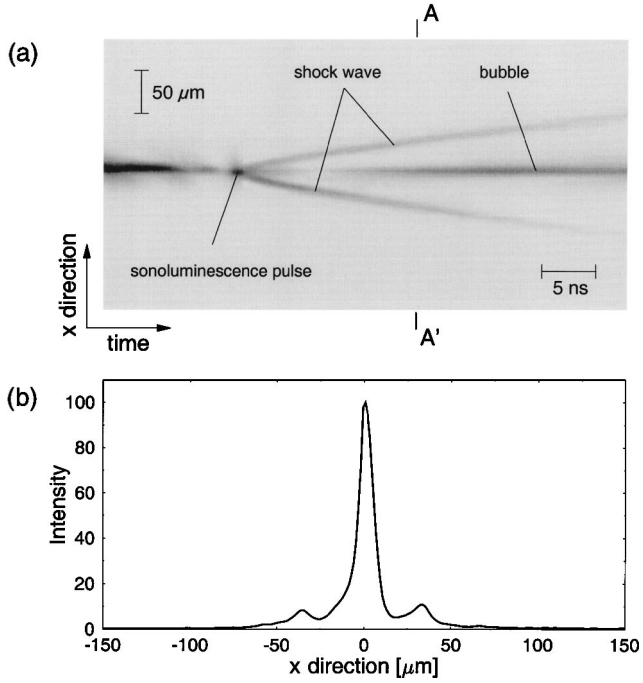

FIG. 22. Outgoing shock wave from a collapsing bubble: (a) Streak image of the emitted outgoing shock wave from the collapsing bubble and (b) an intensity cross section along the line AA'. From Pecha and Gompf (2000).

F. Sound emission from the bubble

The Rayleigh-Plesset equation predicts the response not only of the bubble radius, but also of the surrounding liquid. This has been detected by Cordry (1995), Holzfuss, Rüggeberg, and Billo (1998), Matula *et al.* (1998), Wang *et al.* (1999), Gompf and Pecha (2000), Pecha and Gompf (2000), and Weninger *et al.* (2000). Matula *et al.* (1998) used a piezoelectric hydrophone to measure a pressure pulse with fast rise time (5.2 ns) and high amplitude (1.7 bars) at a transducer at 1-mm distance from the bubble. Wang *et al.* (1999) carried out a systematic study of the strength and duration of the pressure pulses as a function of gas concentration, driving pressure, and liquid temperature. They demonstrated that a probe 2.5 mm from the bubble observes pressure pulses with rise times varying from 5 to 30 ns as the driving pressure and dissolved gas concentration vary. The amplitude of the pressure pulses varies between 1 and 3 bars.

Another study of this type was carried out by Pecha and Gompf (2000; Gompf and Pecha, 2000). They measured pressure amplitudes and rise times consistent with the other measurements, and were able to measure the pressure pulse much closer (within 50 μm) to the bubble. In addition, using a streak camera and shadowgraph technique, they visualized the shock wave leaving the bubble (see Fig. 22). Pecha and Gompf (2000) found

[3]See, for instance, the work of Gaitan, 1990; Barber *et al.*, 1992, 1997; Gaitan *et al.*, 1992; Lentz *et al.*, 1995; Weninger, Barber, and Putterman, 1997; Matula, 1999; Gompf and Pecha, 2000; Pecha and Gompf, 2000; Weninger *et al.*, 2000.

that the shock velocity in the immediate vicinity of the bubble is as fast as 4000 m/s, much faster than the speed of sound $c=1430$ m/s in water under normal conditions, but in good agreement with the results of Holzfuss, Rüggeberg, and Billo (1998). This high shock speed originates from the strong compression of the fluid around the bubble at collapse. From the nonlinear propagation the pressure in the vicinity of the bubble can be estimated to be in the range 40–60 kbar.

For large enough P_a the presence of shocks in the liquid results from the Rayleigh-Plesset dynamics for the bubble wall, independent of the state of motion of the gas inside the bubble. Comparisons by Wang *et al.* (1999) between the strength of the measured pulse and that predicted by the Rayleigh-Plesset equation show that the strength of the wave in the liquid can be accounted for without including the effects of possible shocks in the gas.

Another interesting effect of the emitted sound radiation is that it influences measurements of the bubble radius by Mie scattering. Gompf and Pecha (2000; Pecha and Gompf, 2000) showed that in the last nanoseconds around the minimum radius most of the Mie scattering is by the highly compressed water around the bubble (see Fig. 22), not by the bubble surface itself. Neglecting this effect leads to an overestimate of the bubble-wall velocity. Taking this effect into account, Gompf and Pecha (2000) found the bubble wall accelerates to about 950 m/s, revising previously reported values of 1200–1600 m/s by Weninger, Barber, and Putterman (1997; Putterman and Weninger, 2000).

G. Bjerknes forces

All of the calculations above assume that the center of the bubble is stationary in space. When neglecting viscous effects, the instantaneous force on the bubble is given by

$$\mathbf{F}_{bubble}=-\int p\,\mathbf{n}\,dS, \tag{23}$$

where $\mathbf{n}$ is the outward normal vector to the bubble surface, and $p=-\rho\partial_t\phi$ is the pressure in the fluid. Multiplication of Eq. (23) by $\hat{\mathbf{b}}$, the unit vector in the direction from the origin to the bubble position, gives the force component in that direction. Using Gauss's theorem and time averaging over a driving period, we obtain the (primary) *Bjerknes force*, first described by Bjerknes (1909),

$$F_{Bj}=\langle\hat{\mathbf{b}}\cdot\mathbf{F}_{bubble}\rangle=\langle-\tfrac{4}{3}\pi R^3|\nabla p|\rangle. \tag{24}$$

To leading order, we can replace ∇p by $\nabla p(r=0,t)$ here. While both p and R are periodic, the product occurring in Eq. (24) does not, in general, average to zero. For the center of the bubble to be stationary, this force must vanish. For bubbles at a pressure minimum or maximum, such as in the center of a flask in an SBSL experiment, $\nabla p=0$, and indeed $F_{Bj}=0$. When the bubble is slightly off center, it depends on the relative phase of the pressure at the center and the bubble-radius dynamics if the net effect of F_{Bj} is to drive the bubble back to the center (stabilizing it), or to drive it further away. For linearly oscillating bubbles, it is easy to verify that bubbles whose resonance frequency f_0 is greater than the driving frequency f are attracted by pressure maxima (antinodes) and repelled by pressure minima (nodes). Bubbles with a smaller resonance than driving frequency show the opposite behavior. Indeed, for SBSL bubbles $f_0\gg f$, and they are driven toward the pressure antinode at the center of the flask, where they are driven maximally.

A subtle correction to these results originates in the small buoyancy force,

$$F_{buo}=\frac{\rho g}{T}\int_0^{T_d}V(t)dt, \tag{25}$$

which also acts on the bubble (here g is the gravitational acceleration, $T_d=1/f$ the period of the driving, and V the bubble volume). This upward force must balance the downward component of the Bjerknes force so that the resulting equilibrium position is not in the center of the flask ($z=0$), but at (Matula *et al.*, 1997)

$$z_{equi}\approx\frac{\rho g}{k_z^2P_a}\frac{\int V(t)dt}{\int V(t)\sin(\omega t)dt}, \tag{26}$$

where k_z is the wave number of the standing pressure field along the direction of gravity. Experiments by Matula *et al.* (1997) on z_{equi} qualitatively agree with equation Eq. (26). However, the theoretical prediction seems too small by a factor of about 10. Matula (1999) gives evidence that the discrepancy could be connected with the back reaction of the bubble on the sound field.

Note that both the acoustic and the buoyancy forces are fluctuating over one period, leading to small fluctuations of the equilibrium position as well. Aspherical, weaker bubble collapses and fainter light emission could be a consequence. Matula (2000) presented evidence that in microgravity, SBSL is somewhat stronger than for normal gravity, because the bubble collapse is more spherical.

For small driving pressures, the position of an SBSL bubble is stabilized by the Bjerknes forces (see above). But sonoluminescing bubbles are strongly driven, which leads to variations in the phase shift between driving and bubble dynamics. As pointed out by Cordry (1995), Akhatov *et al.* (1997), Matula *et al.* (1997), and Matula (1999), for very large forcing pressure, F_{Bj} can become repulsive, driving the bubble away from the center of the flask, rendering SBSL impossible. The calculations of Akhatov *et al.* (1997), Matula *et al.* (1997), and Matula (1999) demonstrate that this Bjerknes instability occurs above pressure amplitudes of $P_a\approx1.8$ bars, already above the upper threshold where single-bubble sonoluminescence usually occurs. Current experimental data appear to indicate that shape instabilities limit the upper threshold of sonoluminescence, which is discussed

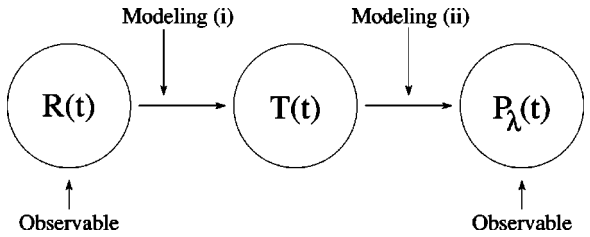

FIG. 23. The difficulty in modeling SBSL. The bubble temperature $T(t)$ is obtained from the radius dynamics $R(t)$ (left), and the spectral radiance $P_\lambda(t)$ is in turn deduced from the temperature. In contrast to $R(t)$ and $P_\lambda(t)$, the temperature cannot be measured directly.

in detail below. It should be remarked, however, that those calculations neglect the back reaction of the bubble's pressure field on the bubble, as well as the effect of water vapor, and so might overestimate the Bjerknes threshold in some situations.

III. THE BUBBLE INTERIOR

One of the key problems in sonoluminescence research is that direct measurements of the state of matter inside the bubble are extremely difficult to perform. Practically all information about the conditions inside the bubble is obtained indirectly. One can measure and model the bubble dynamics and then use this as a basis for inferring the temperatures, pressures, etc. inside the bubble. Or, alternatively, one starts with observations of the light emission and uses the spectral information, the intensity, and the widths of the light pulses to deduce the conditions inside. These two approaches to modeling SBSL are sketched in Fig. 23.

The information obtained in these two ways should obviously be consistent in a viable theory of sonoluminescence. If this consistency condition is fulfilled, however, it is still not clear whether both the hydrodynamic model for the interior of the bubble and the model of the light emission are correct, as modeling errors could compensate each other.

The most crucial variable of the bubble interior for which direct measurement is not possible is temperature. As will be discussed in Sec. V, light emission is expected to depend sensitively on this quantity. In addition, the contents of the bubble are a complicated function of time. Even when starting out with a certain well-defined gas or gas mixture inside the bubble, processes of gas diffusion (Fyrillas and Szeri, 1994), gas rectification (Lohse *et al.*, 1997), water-vapor condensation and evaporation (Moss *et al.*, 1999), and chemical reactions (Yasui, 1997a; Storey and Szeri, 2000) lead to variations in composition, both within a cycle (time scales of microseconds) and over many cycles (time scales of seconds). All properties of the matter inside the bubble (the equations of state, thermal diffusivity, viscosity, etc.) in turn depend on both gas composition and temperature. Unfortunately, there are few solid data for these important dependencies under the extreme conditions of sonoluminescence, conditions not approached in any other lab experiment, with the possible exception of shock tubes (Zel'dovich and Raizer, 1966).

A quantitative understanding of single-bubble sonoluminescence requires that each of these difficulties be addressed step by step. To the present authors, one of the exciting features of modern research on single-bubble sonoluminescence is that it is a testing ground for how well mathematical models can deal with such a complicated situation.

We shall organize our discussion of the state of matter in the bubble's interior into two parts: in this section, we shall describe the fluid mechanics of the bubble's interior and the various attempts to use it to infer bubble temperatures at collapse. The goal of this section is to understand both the maximum temperature and the composition of the bubble. These pieces of information can then be fed directly into a model of the light emission, a discussion of which will be deferred to Sec. V. Although we have chosen for reasons of presentation to break up our discussion into these two parts, it should be emphasized that the research is not at all independent: Models of the light emission critically depend on the temperatures predicted from hydrodynamic calculations, while more sophisticated models of gas dynamics have in turn been developed in order to explain properties of the light emission.

In Sec. III.A, we shall summarize work in which the full compressible gas-dynamical equations inside the bubble are solved. Over the years (spurred on by more detailed information about the light emission) the models have incorporated more and more physical effects. The most important modifications of the earliest models concern the inclusion of dissipative and transport processes, in particular those involving water vapor inside the bubble.

An alternative approach assumes a (nearly) uniform bubble interior and thus avoids the solution of the Navier-Stokes equations. While less accurate, such modeling is computationally inexpensive and allows for the calculation of temperatures for many more parameter combinations. Several variants of this simpler approach are treated in Sec. III.B.

We briefly mention here that molecular dynamics is a third possibility for modeling the bubble interior. Following the motion of the $\sim 10^{10}$ molecules or atoms in a SBSL bubble is beyond the capability of present-day computers, so that simulations have had to be conducted with a far smaller number of quasiparticles (Matsumoto *et al.*, 2000; Metten and Lauterborn, 2000), limiting the prospect for quantitative comparison with experiment. One of the main problems of this type of approach is that, due to the reduced number of particles, the number of particle *collisions* is drastically lower than in reality, and therefore it is hard to achieve thermal equilibrium.

A. Full gas dynamics in the bubble

Assuming local equilibrium, the motion of the gas inside the bubble can be described by the Navier-Stokes

equations and the equations of energy and mass conservation (Landau and Lifshitz, 1987),

$$\partial_t \rho_g + \partial_i(\rho_g v_i) = 0, \tag{27}$$

$$\partial_t(\rho_g v_i) + \partial_j(p_g \delta_{ij} + \rho_g v_i v_j - \tau_{ij}) = 0, \tag{28}$$

$$\partial_t E + \partial_i[(E + p_g)v_i] - \partial_i(v_j \tau_{ij}) - \partial_i(K_g \partial_i T) = 0. \tag{29}$$

Velocity components inside the gas are denoted v_i; ρ_g and p_g are the gas density and pressure, while $E = \rho_g e + \rho_g v^2/2$ is the total energy density, with e the internal energy per unit mass. T is the gas temperature and K_g its thermal conductivity. The viscous stress tensor is given by

$$\tau_{ij} = \eta_g(\partial_j v_i + \partial_i v_j - \tfrac{2}{3}\,\delta_{ij}\partial_k v_k), \tag{30}$$

where η_g is the gas viscosity and the effects of the second viscosity have been neglected. These equations have to be completed with an equation of state, connecting density, pressure, and temperature. Depending on the degree of sophistication, it might also be necessary to include the effects of vibrational excitation, dissociation, ionization, and intermolecular potentials. In addition, the material parameters K_g, η_g themselves depend on temperature and pressure.

Finally, one must impose boundary conditions at the moving bubble wall $r = R(t)$. These can be dealt with in two ways: either the velocity at the bubble wall is taken to be that predicted by the Rayleigh-Plesset equation $v_r(r,t) = \dot{R}(t)$, or alternatively one could solve the full fluid-dynamical equations also in the surrounding water. For completeness, boundary conditions for both mass and heat exchange must also be formulated.

This problem has been attacked with an increasing level of detail, motivated by advances in experiments. We review these efforts in roughly chronological order, grouping them into

- inviscid models (Wu and Roberts, 1993; Moss *et al.*, 1994; Kondic *et al.*, 1995; Chu and Leung, 1997);
- dissipative models (Vuong and Szeri, 1996; Moss *et al.*, 1997; Cheng *et al.*, 1998);
- dissipative models including phase change, in particular that of water vapor (Storey and Szeri, 2000).

All of these approaches treat the bubble as spherically symmetric.

1. Inviscid models

Motivated by the measurements of Barber *et al.* (1992) indicating that the width of the SBSL light pulse was shorter than 50 ps, early theories focused on the idea that shocks were important for single-bubble sonoluminescence (Greenspan and Nadim, 1993; Wu and Roberts, 1993; Moss *et al.*, 1994). Shock focusing provides a natural mechanism for producing both extremely high temperatures and a pulse width that is much smaller than the time the bubble stays fully collapsed.

One of the first numerical solutions of the (spherical) gas-dynamical equations driven by the Rayleigh-Plesset dynamics was done by Wu and Roberts (1993). The most important approximations of this work were (i) viscosity and thermal diffusion are assumed negligible, (ii) no heat or mass exchange takes place between the bubble and the surrounding water, and (iii) a van der Waals equation of state with a polytropic exponent $\Gamma = 7/5$ is assumed throughout the collapse. For a $R_0 = 4.5\ \mu$m bubble driven at $P_a = 1.275$ atm and $f = 26.5$ kHz, Wu and Roberts (1993, 1994) found a spherical shock wave launching from the wall, focusing to the center, and reflecting outward again. Temperatures in excess of 10^8 K and light pulses of 1.2-ps duration were predicted.

The high temperatures and short pulse widths can be understood from the classical analytical solution of the equations of gas dynamics in an imploding sphere by Guderley (1942; see also Landau and Lifshitz, 1987). Guderley neglected viscosity and thermal diffusion, and assumed an ideal gas equation of state. His result shows that a converging shock wave focuses to the center of the sphere with a radius

$$R_s(t) \sim (t^* - t)^{\alpha}, \tag{31}$$

with an exponent $\alpha \approx 0.6884$ for $\Gamma = 5/3$ and $\alpha \approx 0.7172$ for $\Gamma = 7/5$. Here t^* represents the time at which the shock reaches the bubble center. In the case of $\Gamma = 5/3$, the temperature at the center of the shock diverges as $R_s^{-\beta}$, with $\beta \approx 0.9053$. When the shock reaches the bubble center, the temperature is mathematically infinite. With a van der Waals equation of state the same singularity (31) with a slightly different exponent occurs; Wu and Roberts (1994) show that their simulations converge onto this solution. Similar calculations were performed by Moss *et al.* (1994) and Kondic *et al.* (1995). Moss *et al.* (1994) used a more sophisticated equation of state for air inside the bubble, limiting the maximum temperature through the energy-consuming processes of dissociation and ionization. They also solved the full equations for the motion of the water around the bubble.

The unphysical divergence of temperature from Guderley's solution must, of course, be avoided in reality. Evans (1996) noted that the converging spherical shock wave will be susceptible to instabilities in its shape (much like the bubble shape instabilities discussed in detail in Sec. IV). Evans calculated a relatively slow divergence of the relative size of the perturbations, approximately scaling as $\delta R_s / R_s \propto r^{-\chi_0}$ with $\chi_0 < 1$. He concluded that very high temperatures would still be possible inside the bubble, but that the shape instability does set a limit to the degree of energy focusing.

Dissipative processes also are capable of stopping the temperature divergence of Guderley's solution. Both heat and temperature diffusion potentially disrupt the formation of a shock wave because they counteract the steepening gradients at the shock front. The question here is primarily one of time scales: when a converging pressure wave travels towards the bubble center, can it

steepen sufficiently quickly to develop into a (strong) shock? Or is dissipation so strong that a front never develops before the center is reached? These ideas were first touched upon by Vuong and Szeri (1996, described in some detail below), who demonstrated the difficulty of generating shocks in a model where the transport coefficients depend on gas density.

In the years since the shock picture was proposed, there has been direct experimental evidence arguing against the likelihood of shock formation. Following the work of Ohl *et al.* (1998; Ohl, 2000) on laser-induced cavitating bubbles, which also emit light ("single-cavitation bubble luminescence," SCBL), Baghdassarian *et al.* (1999, 2001) found that highly shape-distorted bubbles are still able to give off considerable luminescence. In such bubbles a spherical shock wave cannot exist. Evans (1996) showed that an asphericity of only 5% in the bubble wall is sufficient to disrupt the energy-focusing power of a shock.

2. Dissipative models

Kondic *et al.* (1995) realized the necessity of including dissipation in the gas dynamics, giving some estimates for heat conduction and pointing out radiative transfer as an energy-loss mechanism (the latter process turns out to have a negligible effect on the total-energy balance of the bubble). Going beyond estimates, Vuong and Szeri (1996) included thermal and viscous dissipation in solving the equations of motion of the gas.[4] To do this properly, it is essential to understand how the material properties (thermal conductivity and viscosity) depend on the temperature and on the pressure. At the extreme conditions achieved in the bubble, those dependencies are not known, and one has to try either to derive them from first principles or to extrapolate approximate relationships known from measurements at lower pressures and temperatures. Vuong and Szeri (1996) and also Cheng *et al.* (1998) do the latter and assume the linear relation

$$K_g = K_g(T_0)\frac{T}{T_0} \tag{32}$$

between heat conductivity and temperature; the pressure dependence is neglected (see also Kamath *et al.*, 1993; Yasui, 1995).

Vuong and Szeri (1996) and Cheng *et al.* (1998) also included the heat flux in the water by coupling to the equation

$$\partial_t T_w + u\,\partial_r T_w = \chi_l \frac{1}{r^2}\partial_r(r^2 \partial_r T_w) \tag{33}$$

[4]We remark that viscous effects had been previously considered in bubble dynamics, primarily by Prosperetti (1991) and Kamath *et al.* (1993). As described in Sec. II, these authors also drew the important conclusion that the heat transport between the interior of the bubble and the liquid results in a bubble with an isothermal boundary for most of the forcing cycle.

TABLE I. Maximum temperatures achieved in a $R_0 = 4.5\ \mu$m pure argon bubble driven at $f = 26.5$ kHz. A dissipative gas dynamics model was used in five runs using different driving pressure amplitudes P_a and gas species. From Vuong and Szeri (1996).

Run	Gas	P_a (atm)	$T_{\max}$ (K)
I	Ar	1.1	20 000
II	Ar	1.2	52 000
III	Ar	1.3	118 000
IV	He	1.3	43 000
V	Xe	1.3	202 000

for $r > R(t)$; $T_w(r,t)$ and $u(r,t)$ are the temperature and the spherical velocity field in the water, and χ_l the thermal diffusivity. The radius $R(t)$ is given by the Rayleigh-Plesset equation. At the boundary $r = R(t)$, the heat flux out of the bubble and into the fluid must match, and the same is generally assumed for the temperatures of liquid and gas.

The main result of Vuong and Szeri's paper shows that no shocks occur in argon bubbles. Though some wavy structures can be seen, they do not steepen to a shock, as can be seen in Fig. 16. The temperature profile in the collapsing bubble is not dramatically peaked near the center, but rather shows slow variations for most of the radius, with a strong decline to the ambient water temperature near the wall. Nevertheless, through the nearly adiabatic compression of the gas in the bubble, very high temperatures above 10^5 K are achieved in the simulations. The precise values depend on the type of gas employed and on the control parameters, as seen in Table I. However, all values are dramatically lower than in the calculations without viscosity and thermal conductivity carried out by Wu and Roberts (1993), Moss *et al.* (1994), and Kondic *et al.* (1995).

Cheng *et al.* (1998) confirmed the results of Vuong and Szeri (1996) for argon and in addition repeated the calculation for pure nitrogen gas. They found that, for nitrogen with its smaller polytropic exponent $\Gamma = 7/5$, shocks can develop for strong enough forcing, but they are limited to a tiny region around the center of the bubble, and the peak power (assuming blackbody radiation) is much less than that of argon. In particular, the width of the power pulse is in the range $\leqslant 5$ ps, much smaller than observed by Gompf *et al.* (1997). Earlier, Moss *et al.* (1997) had arrived at similar conclusions about shock occurrence when neglecting viscosity and normal heat conduction, but including heat conduction of the ionic and electronic constituents of the ionized gas generated in the bubble. Their finding that "it is more difficult to generate a shock in Ar than in N_2" thus seems to be true no matter what the dissipation process involved.

One of the main reasons that shocks are suppressed in argon bubbles is that the strong heating already supplied through adiabatic compression (with $\Gamma = 5/3$) results [via Eq. (32)] in an enormous thermal conduction, which levels temperature gradients in the bubble (Vuong and

Szeri, 1996), preventing the steepening of the wavy disturbances into a shock. In nitrogen ($\Gamma = 7/5$) this effect is less pronounced and shocks can develop for strong collapses (Moss *et al.*, 1997; Cheng *et al.*, 1998).

A more general statement on shock suppression is made by Lin and Szeri (2001), who attribute the difficulty of observing any sign of spherically converging shocks to the presence of adverse entropy gradients. In the case of sonoluminescing bubbles, the sound speed in the gas increases towards the center of the bubble, delaying and weakening shock formation.

Vuong and Szeri (1996) also analyzed the dependence of the peak temperature on the type of inert gas employed. Both MBSL and SBSL intensity increase with increasing atomic weight of the noble gas, from He to Xe. Often, the lower thermal conductivity of xenon compared to helium has been favored as the main reason for higher temperatures and more light emission in Xe (Verral and Sehgal, 1988; Greenspan and Nadim, 1993; Hickling, 1993, 1994). However, the inert gases also vary in diffusivity, ionization potential, and many other physical properties, and it is important to determine which are crucial in the context of sonoluminescence. Vuong and Szeri find that contributing to the higher peak central temperatures in their numerical simulations with xenon bubbles (see Table I) are not only the effect of lower thermal conductivity of Xe, but in addition another mechanism also due to the larger mass of this inert gas: waves in heavier gases carry more momentum and travel more slowly, leading to stronger compression lasting for a longer time.

A further noteworthy complication of the gas dynamics inside the bubble originates from a weak mass segregation effect inside an oscillating bubble. Storey and Szeri (1999) have shown that for a mixture of two gases with different masses the heavier one has a slightly higher concentration at the bubble's edge, whereas the lighter one is concentrated towards the bubble's center. This segregation is caused by the mass dependence of the diffusion coefficients. If the bubble's interior were a mixture of inert gases (the example analyzed by Storey and Szeri, 1999), this effect would have little relevance. But when water vapor is considered (see Sec. III. A. 3), mass segregation can have important effects when comparing helium bubbles with xenon bubbles (Storey and Szeri, 1999; Yasui, 2001): The water-vapor concentration in helium bubbles is smaller than that in xenon, since in helium the mass diffusivity is higher. Such a distribution of vapor tends to diminish the differences in peak temperatures between Xe and He (see also Sec. V. F. 3).

3. Dissipative models including water vapor

Over time, dissipative models for the bubble's interior have become more and more complex. An important step was the realization that the water vapor inside the SBSL bubble plays a crucial role in regulating the heat transfer to and from the bubble (Kamath *et al.*, 1993; Yasui, 1997a; Colussi and Hoffmann, 1999; Moss *et al.*, 1999; Storey and Szeri, 2000; Toegel, Gompf, *et al.*, 2000). This effect of liquid vapor has been well known in multibubble sonoluminescence for decades (Jarman, 1959; Flint and Suslick, 1989, 1991a, 1991b). In addition, the water vapor invading a collapsing bubble will undergo chemical reactions that also change the temperature (Kamath *et al.*, 1993; Yasui, 1997a; Gong and Hart, 1998; Storey and Szeri, 2000).

Initially, attempts to incorporate water vapor were restricted to simplified models (e.g., Yasui, 1997a). To our knowledge, the first full numerical simulation of a sonoluminescing bubble with water vapor was performed by Moss *et al.* (1999), building on their earlier work (Moss *et al.*, 1997), which will be discussed in detail in Sec. V. Moss *et al.* (1999) kept the amount of water vapor fixed and uniform during the cycle and did not take chemical reactions into consideration. Thermal conduction is included for the neutral gas inside the bubble, for ions, for electrons, and for the water around the bubble. Due to the high pressures and densities inside the collapsed bubble, ions, electrons, and neutral particles equilibrate on a time scale much shorter than the other relevant time scales, so that a single temperature field $T(r,t)$ is sufficient (rather than having different temperatures for the ions, electrons, etc., as in Moss *et al.*, 1997). The equation of state was obtained from a combination of data and theoretical work by Young and Corey (1995).

The fixed water-vapor content was fit to one data set of Gaitan and Holt (1999) on the light intensity for known forcing pressure, frequency, and compression ratio (R_{max}/R_0), and then extrapolated to other forcing pressures, frequencies, and compression ratios. For standard conditions at $T_w = 20\,^{\circ}\mathrm{C}$ and $f \approx 20$ kHz, the fixed water-vapor concentration was found to be 30–40 %. At collapse, the transfer of vapor out of the bubble is too slow to keep up with the bubble-wall motion, so that vapor becomes trapped inside the bubble (Moss *et al.*, 1999). This point of view was later confirmed and investigated further by Storey and Szeri (2000; see below). For the extreme conditions achieved at collapse, fixing the amount of water inside the bubble is not as crude an approximation as it may sound.

The main result of Moss *et al.* (1999) was that the inclusion of a sufficient quantity of water vapor leads to a smaller (effective) adiabatic exponent γ. Heating is thus reduced and shock waves can occur close to the center, in agreement with earlier work by Cheng *et al.* (1998) for nitrogen bubbles. The shock-wave heating, however, is very inhomogeneous. Although the center of the bubble can be very hot (up to 130 000 K in the examples given), the total radiating volume within the shock front is so small that there is far less optical emission than for adiabatic heating with a larger Γ which does not lead to shock waves (Vuong and Szeri, 1996; Cheng *et al.*, 1998). A large part of the compressional energy of the collapse is found to go into internal degrees of freedom rather than into heating of the bubble. Moss *et al.* (1999) argue that this is one reason why sonoluminescing bubbles are brighter at low water temperature (Barber *et al.*, 1994), where the water vapor pressure is less.

The model of Moss *et al.* (1999) does rather well in explaining the trends in the experimental data of Gaitan and Holt (1999). Moss *et al.* in particular stress that a pure argon bubble leads to very different heating characteristics (and thus light emission) when compared to an argon bubble with some water vapor in it; only the latter is consistent with the data. Calculations without water vapor would predict that a strongly driven bubble in the Gaitan-Holt measurements ($R_0=6.0\ \mu$m, $R_{max}=64\ \mu$m) should emit 100 times as much light as a weakly driven bubble ($R_0=2.1\ \mu$m, $R_{max}=30\ \mu$m). The experiments actually show an intensity ratio of only ~ 10, in agreement with simulations including water vapor. The calculated results are extremely sensitively dependent on the experimental conditions and parameters—or, likewise, the modeling assumptions. A particularly striking example is the dependence on the ambient pressure P_0. Reducing it from $P_0=1$ bar to 0.99 bar can lead to 1.6 times more light, according to the model. The reason for the sensitivity lies not so much in the hydrodynamics, but in the extremely strong dependence of the light intensity on the temperature achieved in the bubble, as we shall discuss in detail in Sec. V. In the above example the temperature of the light-emitting region in the bubble increases by just 5%.

The restriction of Moss *et al.* to constant water-vapor content is relaxed in a remarkable paper by Storey and Szeri (2000), who build on their earlier work on mass segregation in gas bubbles containing a mixture of different inert gases (Storey and Szeri, 1999). The transport parameters (thermal diffusion, mass diffusion, and viscosity) are calculated from equations based on Chapman-Enskog theory (Hirschfelder *et al.*, 1954); thermal dependencies are considered as far as they are known. The equations of state are of the Soave-Redlich-Kwong type (Gardiner, 1984; Reid *et al.*, 1987). Storey and Szeri (2000) argue that although the basic physical mechanisms they uncover are robust, the exact numbers do depend on (unknown) details of the equation of state.

Evaporation and condensation are modeled using a kinetic theory (Carey, 1992). The rate of mass transport (per unit area) at which water molecules pervade the interface is $\propto(p_{\mathrm{H_2O}}-p_{sat})$, where $p_{\mathrm{H_2O}}$ is the partial pressure of water and p_{sat} the saturation pressure at the temperature of the interface. Not all water molecules that hit the wall actually stick to it, only a fraction σ_a thereof. This accommodation coefficient is chosen to be 0.4, following Yasui (1997a) and Eames *et al.* (1997).

As an example, Storey and Szeri (2000) study a bubble initially consisting of argon, with $R_0=4.5\ \mu$m and driven at $P_a=1.2$ bars and $f=26.5$ kHz: Including water vapor, the maximum temperature is reduced from 20 900 K (cf. Vuong and Szeri, 1996) to 9700 K, due to the lower Γ. No shock waves are observed under these conditions. The amount of water in the bubble is not constant at all, as can be seen from Fig. 24: A large amount of water evaporates into the bubble during the main expansion when the pressure is low; at this stage vapor is in equilibrium with the vapor pressure. At

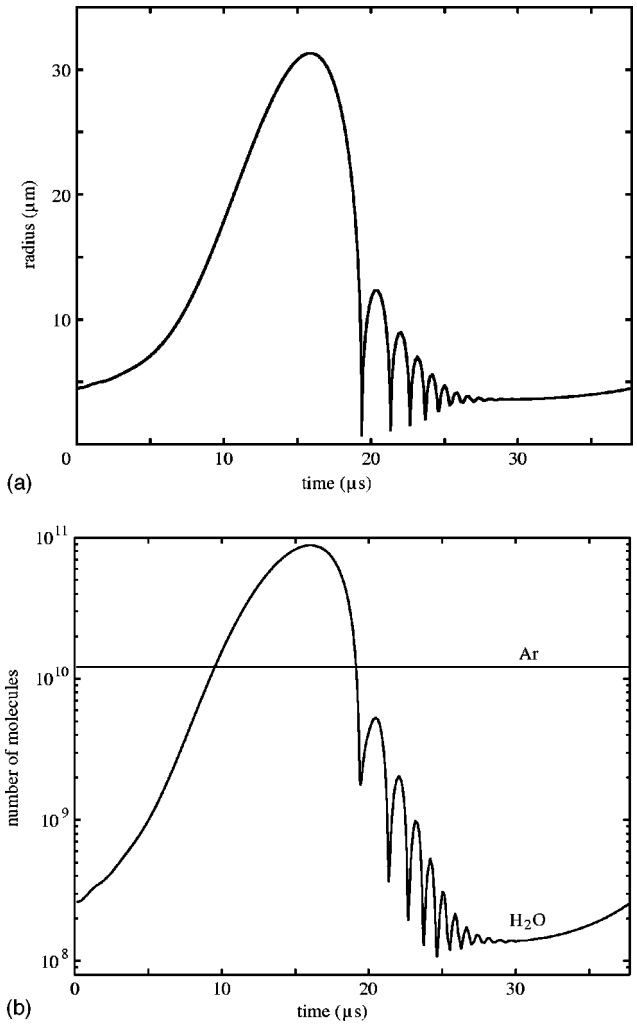

FIG. 24. Importance of water vapor exchange between bubble and fluid: (a) Bubble dynamics and (b) number of water molecules in the bubble as a function of time for an (initially) $R_0=4.5\ \mu$m argon bubble driven at $P_a=1.2$ atm and $f=26.5$ kHz. Note the comparison in (b) to the constant number of argon atoms. From Storey and Szeri (2000).

bubble maximum, about 90% of the bubble contents is water. Vapor condenses out of the bubble again at collapse, but not completely, since the time scale of the collapse $\tau_{dyn}=R/|\dot{R}|$ becomes much smaller than the time scale for the transport of water vapor out of the bubble. The vapor transport is a two-step process, consisting of diffusion to the wall and condensation, so that it involves two time scales, one for vapor diffusion in the bubble,

$$\tau_{dif}=\frac{R^2}{D_{\mathrm{H_2O}}(R,T)}\approx\frac{1}{D_{\mathrm{H_2O}}(R_0,T_0)}\frac{R_0^3T_0^{1/2}}{RT^{1/2}}, \tag{34}$$

and one for condensation at the wall,

$$\tau_{con}=\frac{R}{c_g}\sqrt{\frac{2\pi\Gamma M_{\mathrm{H_2O}}T_0}{9\sigma_a^2M_0T_{int}}}, \tag{35}$$

where $c_g=\sqrt{\Gamma p_{g0}/\rho_{g0}}$ is the sound velocity of the gas in the initial state, and $M_{\mathrm{H_2O}}$ and M_0 are the molecular masses of water and the initial bubble content, respec-

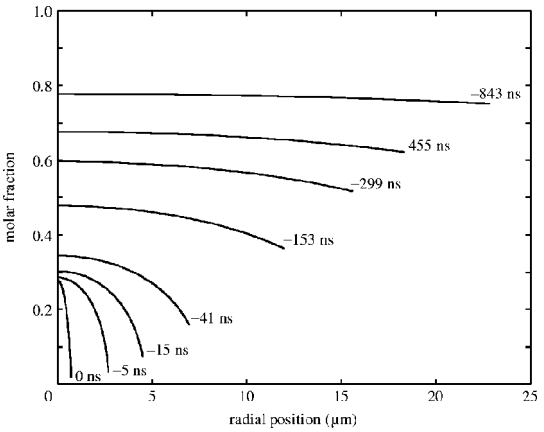

FIG. 25. Profiles of the molar fraction of water vapor vs radius for several times prior to the moment of minimum radius (time=0, leftmost profile). In order of increasing radius, the other curves correspond to times prior to collapse of $t=-5$, 15, -14, -153, -299, -455, and -843 ns. Calculation for a $R_0=4.5$ μm argon bubble driven at $P_a=1.2$ atm and $f=26.5$ kHz. From Storey and Szeri (2000).

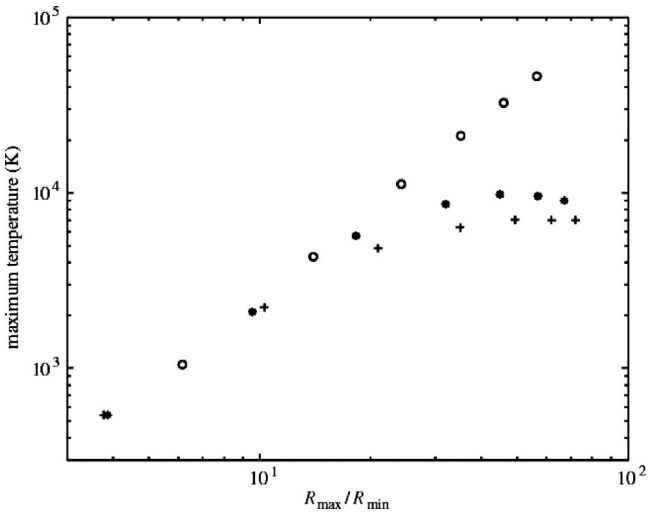

FIG. 26. Dependence of the bubble center temperature on the compression ratio R_{max}/R_{min}. ○, calculations without water vapor; *, with water vapor, but no reactions; +, with water vapor, including reactions. Note the logarithmic scale on the axes. From Storey and Szeri (2000).

tively. Figure 25 shows the profiles of the water-vapor molar fraction inside the bubble for various times: In the early part of the collapse, $\tau_{dyn} \gg \tau_{dif}, \tau_{con}$, so that the profiles are uniform. The vapor concentration is decreasing, as water has sufficient time to escape. Later, when $\tau_{dyn} \ll \tau_{dif}, \tau_{con}$ (the three lowest profiles of Fig. 25, starting from 15 ns before the collapse), the water-vapor profile is essentially "frozen" within the bubble. Therefore, the bubble consists of $\approx 14\%$ water vapor (on a molar basis) through the collapse; the vapor is trapped in the bubble's interior.

Comparing the time scales τ_{dif} and τ_{con}, Storey and Szeri (2000) found that the vapor transport was always diffusion limited ($\tau_{dif} > \tau_{con}$). Models with unrealistically low accommodation coefficients $\sigma_a \sim 0.001$, like that of Colussi *et al.* (1998), on the other hand, could well be condensation limited.

Rather remarkably, when applying their numerical model to the more strongly forced bubbles of Moss *et al.* (1999; see above), Storey and Szeri (2000) find average water-vapor concentrations close to what Moss *et al.* obtained from fitting their numerical results to the Gaitan and Holt (1999) data mentioned above, a strong indication that these numbers are in the right ballpark.

In the second part of their paper, Storey and Szeri (2000) consider chemical reactions of the water vapor. The reaction scheme employed originates from Maas and Warnatz (1988) and includes 19 forward and reverse elementary reactions of the nine species Ar, H, H_2, O, O_2, OH, HO_2, H_2O, and H_2O_2 (argon only enters the reactions as a third body). The reaction rates were taken from Gardiner (1984) and in the high-pressure limit, for which there is "considerable uncertainty," from Bowman *et al.* (1999).

With the chemical reactions included, the maximum temperature for the standard case (a $R_0=4.5$ μm argon bubble driven at $P_a=1.2$ bars and $f=26.5$ kHz) decreases from 9700 K (with water vapor, but without reactions) to 7000 K. Most of the reactions are endothermic and therefore eat up the collapse energy, which otherwise would be used for heating. The reaction pathways can also be interpreted as additional degrees of freedom, further lowering the effective polytropic exponent. Note that the time scales of the chemical reactions are so fast (because of the high densities) that thermochemical equilibrium should prevail in the collapse up to the point of minimum radius.

How does the bubble temperature depend on the forcing pressure? Figure 26 shows results by Storey and Szeri (2000) for the temperature at the center as a function of the compression ratio R_{max}/R_{min}. No shocks occurred in these calculations, so that the center temperature is a fairly good indication of the overall bubble temperature. For other parameter combinations (not shown in Fig. 26), Storey and Szeri (2000) do find shocks and very high maximum temperatures, but only right at the center, corresponding to $\sim 0.1\%$ of the total bubble volume. A suitably averaged temperature, representative of the actual energy content of the bubble, will be very similar to those shown in Fig. 26. It is noteworthy that for these shocks the presence of water vapor is necessary, as expected from the work of Cheng *et al.* (1998) and Moss *et al.* (1999). For a low compression ratio, hardly any vapor invades the bubbles of Fig. 26 and the three cases (without water vapor, with nonreacting water vapor, and with reacting water vapor) give roughly the same maximum temperature. The remarkable feature, however, is that the temperature *levels off* for large compression ratios when water vapor is taken into account, asymptoting to $\approx 10\,000$ K without chemical reactions and ≈ 7000 K with chemical reactions included. Thus the initial power-law increase of the maximum temperature with expansion ratio does not extend into the regime of SBSL temperatures: the effect of the larger expansion ratio of stronger forced bubbles is compensated by the

presence of more water vapor, thus limiting the heating at collapse.

This finding has important implications for the quest for "upscaled" sonoluminescence: To learn the limits of energy focusing and light emission, researchers have tried to induce more violent bubble collapses by, for example, applying nonsinusoidal driving pressures (Holzfuss, Rüggeberg, and Mettin, 1998) or reduced driving frequencies as suggested by Hilgenfeldt and Lohse (1999) and Toegel, Gompf, *et al.* (2000). But the larger expansion ratios achieved with these techniques lead to a larger water-vapor content of the bubble, which again limits the heating at collapse. A theoretical study by Toegel, Gompf, *et al.* (2000) shows that these two effects roughly cancel each other, essentially leading to the same temperature and the same amount of light at lower driving frequencies for otherwise identical bubble parameters. A residual upscaling effect may still be observed (as in Barber and Putterman, 1991) due to the possibility of stabilizing bubbles with larger R_0 at lower driving frequencies (see Sec. IV.D).

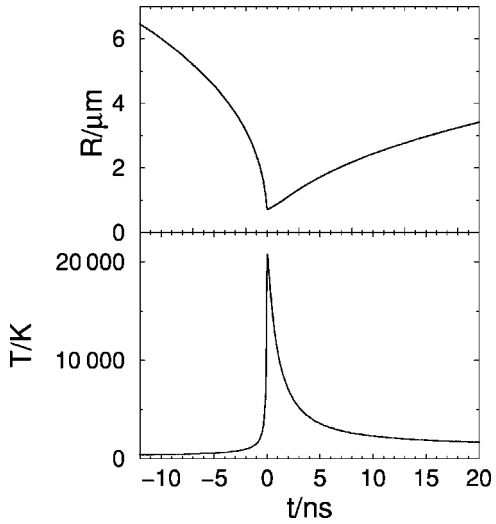

FIG. 27. Temperature inside the SBSL bubble within the simplified model of Hilgenfeldt *et al.* (1999a, 1999b). (a) Bubble dynamics and (b) temperature dynamics of $R_0=5$ μm bubble driven at 1.3-atm pressure amplitude at $f=20$ kHz. The temperature is calculated via Eq. (38); the full width at half maximum of the asymmetric peak is ≈ 1 ns.

B. Simple models

The previous section has shown that when the complex interplay of physical effects inside a sonoluminescing bubble is meticulously included, spatial inhomogeneities inside the bubble are not very pronounced. Therefore it seems reasonable to try to approximate the bubble's interior by spatially constant, time-dependent pressure $p_g(t)$ and temperature $T(t)$. Clearly, such an approximation is too crude to capture some of the aforementioned effects such as mass segregation (Storey and Szeri, 1999). However, such modeling simplifications are extremely useful tools in exploring the phase space of sonoluminescence (see Sec. IV). Such a scanning of phase space is at present not possible for the complete models discussed in the previous section.

Simple models assuming a uniform bubble interior have been developed with increasing detail; here, we shall discuss two types. Just as in the more elaborate models, one can either completely neglect heat and mass transfer to and from the bubble's exterior (Sec. III.B.1) or try to embody these effects (Sec. III.B.2).

1. Homogeneous van der Waals gas without heat and mass exchange

The simplest model is to assume an adiabatic equation of state for the bubble interior (Löfstedt *et al.*, 1993; Barber *et al.*, 1997),

$$p_{gas}(t)=\left(P_0+\frac{2\sigma}{R_0}\right)\frac{(R_0^3-h^3)^\Gamma}{\{R(t)^3-h^3\}^\Gamma}, \tag{36}$$

and the corresponding temperature equation

$$T(t)=T_0\frac{(R_0^3-h^3)^{\Gamma-1}}{[R(t)^3-h^3]^{\Gamma-1}}, \tag{37}$$

equivalent to Eq. (10) when replacing γ by $\Gamma=C_p/C_v$, the ratio of the specific heats. Equation (36) supplements the Rayleigh-Plesset equation and permits its solution.

One obvious problem with Eqs. (36) and (37) is that an adiabatic bubble motion is assumed with no heat exchanged between the bubble and the exterior. As pointed out in Sec. II, Péclet number estimates via Eq. (11) show that there is almost unrestricted heat exchange for most of the oscillation cycle, and the motion is isothermal. Only at bubble collapse is the Péclet number Pe larger than 1. This means that most of the time the ratio of the specific heat Γ has to be replaced by an isothermal exponent $\gamma=1$. Near the cavitation collapse there is a change in the adiabatic value $\gamma\to\Gamma$. Roughly speaking, this transition will occur when the Péclet number is of order unity.

In linear approximation, Prosperetti (1977c) derived a transition function $\gamma(\mathrm{Pe}(t))$ from the isothermal behavior $\gamma=1$ to the adiabatic behavior $\gamma=\Gamma$. Hilgenfeldt *et al.* (1999a, 1999b) have employed this approach to calculate approximately the temperatures and pressures in SBSL bubbles. The Rayleigh-Plesset equation is then supplemented by a differential version of Eq. (37) with variable $\gamma(\mathrm{Pe}(t))$,

$$\dot{T}=-[\gamma(\mathrm{Pe}(t))-1]\frac{3R^2\dot{R}}{R^3-h^3}T-(T-T_{w0})\chi_g/R^2. \tag{38}$$

The last term contains the ambient water temperature T_{w0} and the thermal diffusivity of the gas χ_g, which at high densities is assumed to follow Chapman-Enskog theory (Hirschfelder *et al.*, 1954). Equation (38), together with the Rayleigh-Plesset equation, gives a simple model for bubble radius and bubble temperature. The peak temperatures obtained—see Fig. 27—are com-

parable to bubble temperatures resulting from the more sophisticated model by Storey and Szeri (2000). The latter publication reports somewhat lower temperatures, though, because of the inclusion of heat loss and mass exchange in the model, to which we turn in the following section.

2. Homogeneous van der Waals gas with heat and mass exchange

In more sophisticated variants of the model, the heat and mass exchange between the bubble and its exterior are explicitly taken into account. One of the first models of this type was conceived by Yasui (1997a). The ingredients of his approach are (i) a Rayleigh-Plesset-type equation for the bubble radius with a van der Waals gas inside; (ii) a spatially homogeneous bubble interior with time-dependent pressure and temperature (the material constants inside the bubble such as the thermal conductivity are modeled as a function of the temperature); (iii) water-vapor exchange with the bubble's exterior due to condensation and evaporation; (iv) heat exchange with the bubble's exterior modeled by an energy flux depending on the compression, the temperature gradient, and condensation/evaporation; (v) a thin layer of water around the bubble that can be heated; (vi) 25 chemical reactions of the water vapor, following Kamath *et al.* (1993) and using data from Baulch *et al.* (1972–1976). It is crucial that the net effect of these reactions be consumption of thermal energy, i.e., they must be endothermic.

The central result of Yasui (1997a) is displayed in Fig. 28: At bubble maximum, the bubble consists nearly exclusively of water vapor. Even at collapse, the bubble still retains some of the water ($\sim 1\%$ of the total bubble contents). Because of the invading water vapor and the endothermic chemical reactions, the maximum temperature inside the bubble at typical control parameters is only around 10 000 K, in agreement with the complete model of Storey and Szeri (2000).

Models like that of Yasui (1997a) are useful for examining the energy balance at collapse. For standard parameters of single-bubble sonoluminescence (see Fig. 28), one finds in the last 120 ps before collapse a reduction of the thermal energy by 1.4 nJ through chemical reactions and by 0.6 nJ through thermal conduction. The loss through photon emission is negligible, only about 0.2 pJ.

Yasui (1997a) assumed that the transport of mass through the boundary layer was condensation limited, rather than diffusion limited (mass diffusion was not explicitly modeled, and thus assumed instantaneous). However, Storey and Szeri (2000) later showed that transport under SBSL conditions is diffusion limited (see Sec. III.A.3). Therefore Toegel, Gompf, *et al.* (2000; Toegel *et al.*, 2002) took the opposite approach and developed a simple diffusion-limited model for water-vapor exchange between bubble and liquid, using a boundary layer approximation. The diffusive change in the number of water molecules over time is then

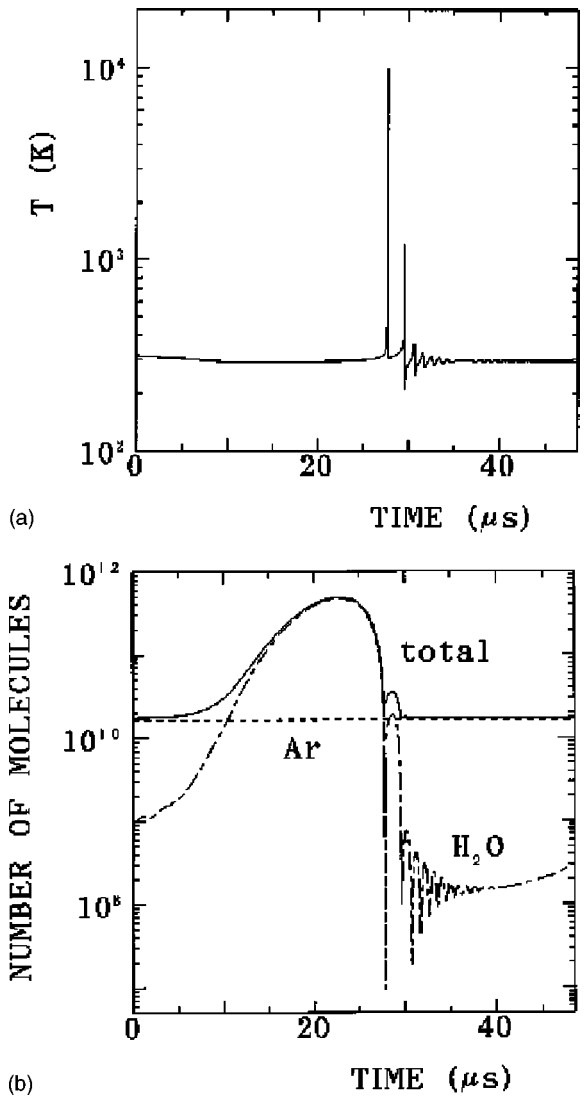

FIG. 28. Bubble temperature and number of molecules with the model of Yasui (1997a). The parameters are $R_0=5\ \mu$m, $P_a=1.35$ bars, $f=20.6$ kHz, $P_0=1$ atm, and a water temperature of $T_w=20\,^\circ$C. From Yasui (1997a).

$$\dot{N}^d_{\mathrm{H_2O}} = 4\pi R^2 D\,\partial_r n|_{r=R} \approx 4\pi R^2 D\,\frac{n_0 - n}{l_{diff}}, \tag{39}$$

where n_0 corresponds to the equilibrium density of vapor molecules at the wall and n is their actual concentration. The diffusion length is obtained through dimensional analysis as $l_{diff}=\min[(RD/\dot{R})^{1/2}, R/\pi]$, where D is the gas diffusion constant. The cutoff prevents the boundary layer from becoming unphysically large.

The heat flux is treated in complete analogy to the flux of water vapor by Toegel, Gompf, *et al.* (2000; Toegel *et al.*, 2002), i.e.,

$$\dot{Q} = 4\pi R^2 \chi_{mix}\,\frac{T_{w0} - T}{l_{th}}, \tag{40}$$

where Q is the heat content of the bubble, T_{w0} the equilibrium (ambient) temperature, and the thermal diffusion length is $l_{th}=\min[(R\chi_{mix}/\dot{R})^{1/2}, R/\pi]$ with the thermal diffusivity χ_{mix} of the gas mixture. Yasui (1997a)

uses a boundary layer as well, but in addition assumes a temperature jump between the outer edge of this boundary layer and the liquid. This temperature slip is more usually associated with low-density systems and does not appear in other work like that of Toegel, Gompf, *et al.* (2000) or Storey and Szeri (2000).

Chemical reactions can also be included in a boundary layer model (Toegel *et al.*, 2002). The most important endothermic process is

$$H_2O + 5.1\ \text{eV} \leftrightarrow OH + H, \tag{41}$$

whose inclusion already shows the essential effects of more sophisticated reaction schemes. Within the ordinary differential equations (ODE) formalism of Toegel *et al.* (2002), Eq. (41) yields reaction rates in good accord with those of Storey and Szeri (2000).

Together with the first law of thermodynamics and a van der Waals equation of state, the above formalism yields another ODE for the temperature inside the bubble,

$$C_v \dot{T} = \dot{Q} - p_g \dot{V} + h_w \dot{N}^d_{H_2O} - \sum_X \frac{\partial E}{\partial N_X} \dot{N}_X, \tag{42}$$

where the sum is over all species $X = \text{Ar}, H_2O, OH$, and H. The derivatives $\partial E/\partial N_X$ as well as the heat capacity C_v take into account rotational and vibrational degrees of freedom in the various molecules and are thus dependent on temperature. Therefore Eq. (42) is an implicite-quation for T. Finally, h_w is the enthalpy of water molecules near the (cold) bubble wall.

Equation (42) provides closure of the model together with a Rayleigh-Plesset equation variant. Similar equations were discussed by Yasui (1997a), though the explicit form of the terms differs as indicated above, and the diffusion-limited character of the transport was not taken into account. Such a set of four first-order equations for $R(t)$, $\dot{R}(t)$, $N_{H_2O}(t)$, and $T(t)$ can be solved for various physical parameters, such as forcing pressure P_a, ambient radius (without water vapor) R_0, water temperature T_{w0}, and driving frequency f, without much numerical effort. The scheme can also be easily extended to more reactions. The results of Toegel, Gompf, *et al.* (2000) agree well with the full simulations of Storey and Szeri (2000).

Most models that include chemical reactions inside the bubble—whether based on partial differential equations like that of Storey and Szeri (2000) or on ODE like those of Kamath *et al.* (1993) and Storey and Szeri (2001)—seem to underestimate the temperature inside the bubble. With the exception of the Yasui (1997a) model (in which water vapor is not prominent because its transport is very fast), all of these models seem to imply temperatures substantially below 10 000 K in the SBSL regime. Assuming a thermal light-emission mechanism (see Sec. V), these temperatures do not produce enough photons to comply with experimental results. Toegel *et al.* (2002) address this paradox and suggest that according to the Le Chatelier–Brown principle, the high densities inside the bubble favor the back reaction $H + OH \rightarrow H_2O$, in particular because of the finite excluded volume of the particles. The energy-consuming water dissociation is thus reduced, and higher temperatures in the bubble are possible (see also Sec. V). A result like this suggests that one cannot extrapolate the reaction rates at temperatures and pressures achieved in other laboratory experiments to the unusual regime of sonoluminescence particle densities. Thus it is advisable to revert to a first-principles statistical physics approach in order to deduce reaction rates under SBSL conditions, deriving the laws of mass action directly from the partition function (Toegel *et al.*, 2002).

Another similar, simple model with both heat and water-vapor exchange was developed by Storey and Szeri (2001). Here the authors even drop the assumption of boundary layers for heat and mass transport and rely on the ratios of the relevant time scales for bubble dynamics, particle diffusion, and heat diffusion. This approach still contains the same essential physics as the models of Yasui and Toegel *et al.* Storey and Szeri (2001) quantitatively tested the simple model against their full simulations (Storey and Szeri, 2000). In both approaches, they find the same trends (and similar values) for the peak temperature in the bubble, the mass percentage of argon in the bubble, and the number of reaction products, which again lends credibility to the simple ODE approach.

C. How accurate are the bubble temperatures?

It was mentioned in the introductory remarks that an understanding of the bubble interior and SBSL light emission hinges on a good understanding of the bubble temperature. The many models developed so far, with different degrees of sophistication, result in predictions for the peak temperature (suitably averaged over the bubble) ranging from 6000 K to slightly above 20 000 K, given the same (typical) driving parameters for an SBSL bubble. While this factor of uncertainty of about 3 is significant (and leads to widely different results for the ensuing light emission), it is reassuring that these models share a number of common traits: (i) They agree that the interior of the bubble heats up and becomes at least as hot as that measured for MBSL bubbles; (ii) water vapor is a major temperature-limiting factor, forming a substantial part of the bubble contents at collapse; and (iii) the temperature, when averaged over the bubble, is not likely to rise much above 10^4 K, ruling out the much too high predictions of earlier attempts at modeling SBSL. We shall see in Sec. V that a thermal origin of SBSL is deemed very likely today, and that the temperature range presented here does support light emission in the experimentally observed range of intensities. Indeed, any nonthermal theory of SBSL has to explain first why thermal emission, which explains the experimental results, is suppressed.

The uncertainties in bubble temperature and the resulting predictions for light emission do not allow for a direct comparison between experiment and theory for a specific combination of parameters (e.g., a bubble with

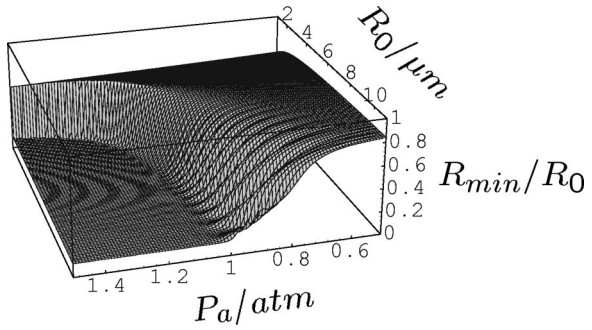

FIG. 29. Minimal bubble radius $R_{\min}/R_0$ as a function of R_0 and P_a. The frequency is $f=26.5$ kHz.

$R_0=5\ \mu$m, $P_a=1.3$ bars, and $f=20$ kHz). On top of the modeling uncertainties, the sensitive dependence of light emission on parameters severely limits the reproducibility of measurements. A comparison to experiment over a whole *range* of parameter values is much more promising, focusing on the experimentally robust dependence of bubble dynamics and light emission on various external parameters. The following section takes this step from single-parameter combinations to an overview of the parameter space of SBSL—starting with the question of under what conditions sonoluminescence can be observed at all.

IV. THE PARAMETER RANGE OF SINGLE-BUBBLE SONOLUMINESCENCE

In the previous section we studied the dynamics of a bubble under the action of a driving pressure of amplitude P_a, frequency $f=\omega/2\pi$, and with an ambient bubble radius R_0, all fixed to appropriate values for sonoluminescence to occur. The key question now is what happens if these and other experimental parameters are changed—will SBSL still be observed, and if so, will it be brighter or dimmer? What are the physical processes that determine the limits of the parameter regime of sonoluminescence? Experiments have shown that, apart from the parameters implicit in the Rayleigh-Plesset equation, other quantities of crucial importance to SBSL are the concentration of gas c_∞ dissolved in the liquid, the temperature of the liquid, the type of liquid, and the type of gas. The goal of this section is to under stand these parameter dependencies quantitatively.

Various physical constraints limit the parameter range in which sonoluminescence can be observed: to emit light, the bubble must be forced strongly enough for a cavitation event to occur during each cycle of the drive; the bubble must not break into pieces, which roughly translates into the requirement that viscous processes and surface tension be strong enough to limit the growth of bubble shape instabilities. For the consistent, stable light emission of SBSL, the number of gas molecules inside the bubble, averaged over one cycle of oscillation, must neither increase nor decrease. This requirement is what sets the ambient radius R_0 of the bubble; it involves a subtle interplay between diffusive processes exchanging gas between the bubble interior and the outside liquid, and chemical reactions. And finally, it is necessary that the Bjerknes forces holding the bubble trapped in the flask (see Sec. II.G) be strong enough to ensure that the center of the bubble does not move appreciably. This section presents the current understanding of each of these effects and assesses the extent to which the theoretical predictions agree with experiments.

A. The Blake threshold

Regardless of the exact mechanism of sonoluminescence, it is abundantly clear that the light results from energy focusing during a rapid bubble collapse. Therefore the bubble must be forced strongly enough to induce a cavitation event of sufficient violence—in essence, the Rayleigh collapse solution of Sec. II.D must be fully established. Whether this happens depends on both the ambient bubble size (mass of gas inside the bubble) and the forcing pressure. Figure 29 shows the minimal radius during a cycle of the drive as a function of forcing pressure P_a and ambient radius R_0. There is an abrupt transition $R_0(P_a)$ where the onset of Rayleigh collapse occurs and the gas inside the bubble gets strongly compressed, leading to heating. Therefore sonoluminescence can only occur above this threshold.

The functional form of this threshold curve can be deduced from dimensional considerations: other than the ambient radius R_0, the parameters in the Rayleigh-Plesset equation are P_a, P_0, σ, ρ, η, and ω. Since we are dealing with the transition from gentle oscillation to inertial collapse, we do not expect dissipative effects to be important and exclude the viscosity η from our considerations. From the remaining parameters, two independent length scales can be derived: the resonant bubble size $R_0^{res}=\sqrt{3P_0\rho^{-1}\omega^{-2}}$ [cf. Eq. (22)] and the capillary length scale σ/P_0. As we have seen in previous sections, SBSL bubbles are driven far from resonance, so R_0^{res} is too large to be important here.

The relationship between the critical ambient size and the pressure must therefore have the form

$$R_0^c=\frac{\sigma}{P_a}f\left(\frac{P_a}{P_0}\right) \tag{43}$$

with a dimensionless function f. A closer look at the Rayleigh-Plesset equation allows for the specialization

$$R_0^c=C\frac{\sigma}{P_a-P_0}, \tag{44}$$

where C is a scalar constant. A calculation like this was first performed by Blake (1949) for bubbles under static pressure. He found $C=2/3$ for isothermal bubble movement (cf. Brennen, 1995). The threshold in R_0-P_a space separating gently oscillating from violently collapsing bubbles is therefore known as the Blake threshold. More detailed studies for driven bubbles arrive at $C=4\sqrt{3}/9\approx 0.77$ (Leighton, 1994; Hilgenfeldt, Brenner, *et al.*, 1998).

Only bubbles larger than R_0^c in Eq. (44) can show SBSL, so that the Blake threshold criterion cuts down the available parameter space considerably. When shock waves inside the bubble were considered crucial for the light emission, Hilgenfeldt *et al.* (1996) suggested replacing this criterion with the threshold for strong shock formation, expected when the maximum bubble speed during collapse exceeds the speed of sound in the gas (although shocks can and will form at lower speeds as well). Because of the abruptness of the Blake threshold, supersonic velocities are reached already at parameter combinations very close to the threshold. Thus this shock threshold, like any other dynamical criterion for strongly collapsing bubbles, will effectively yield the same result as the Blake threshold calculations.

Further constraints set an upper limit to the bubble size, in order to ensure the bubble's stability. Let us first consider diffusive stability.

B. Diffusive stability

Since bubble dynamics and energy focusing during collapse are sensitively dependent on R_0, it is crucial for a stable SBSL bubble to maintain the same ambient radius, i.e., not to exchange any net mass with its surroundings. The gas exchange between the bubble and the liquid is affected by diffusion of gas through the liquid and by advection of this gas with the fluid velocity.

The typical model that is used for this process starts with the transport equation for the mass concentration $c(r,t)$ (mass/volume) of gas around a spherical bubble:

$$\partial_t c + u\,\partial_r c = D\,\frac{1}{r^2}\,\partial_r(r^2\partial_r c), \tag{45}$$

where D is the gas diffusion coefficient in water. The velocity $u(r,t)=R^2\dot{R}/r^2$ of the fluid a distance r from the center of the bubble is given by Eq. (6), with $R(t)$ entering through solution of the Rayleigh-Plesset equation. The gas in the bubble is assumed to remain in equilibrium with that in the liquid at the boundary of the bubble wall; hence the gas concentration at the bubble wall is given by Henry's law,

$$c(R,t)=c_0 p_g(R,t)/P_0. \tag{46}$$

Finally, the gas concentration far from the bubble is given by the ambient concentration c_∞,

$$c(\infty,t)=c_\infty. \tag{47}$$

The mass loss/gain of the bubble is then proportional to the concentration gradient at the bubble wall,

$$\dot{m}=4\pi R^2 D\,\partial_r c|_{R(t)}. \tag{48}$$

This model for the gas exchange is accurate as long as the Rayleigh-Plesset solution is valid. As was emphasized above, this may not be generally true very close to the point of bubble collapse. At collapse, many other effects could also play an important role and affect the gas transfer, including (a) sound waves in the liquid, (b) breakdown of Henry's law at the interface because of its fast motion, (c) chemical reactions inside the collapsed bubble, and (d) phase transformation (boiling) of the liquid surrounding the bubble.

First, we shall examine the consequences of mass diffusion alone and see what they imply about the sonoluminescence experiments. The advection of the solute in Eq. (45) reflects the conservation of fluid volume: a spherical shell of fluid around the oscillating bubble is pushed in or out when the bubble contracts or expands. For this reason, it is useful to think about the solutions to the equation in Lagrangian coordinates tracking the volume changes according to (Plesset and Zwick, 1952)

$$h(r,t)=\tfrac{1}{3}[r^3-R^3(t)]. \tag{49}$$

This transformation trick has often been used (e.g., Eller, 1969 or Brennen, 1995). If one was to neglect diffusion, the concentration field outside the bubble would be just $c=c(h)$. However, even in the limit where the mass diffusion coefficient is very small, it has important consequences (for example, an undriven bubble eventually dissolves by diffusion). The Henry's law boundary condition at the bubble wall implies that the gas concentration at the bubble wall is time dependent and in general different from the concentration c_∞ in the bulk. There is therefore a boundary layer near the bubble wall, where the gas concentration relaxes from the value dictated by Henry's law to c_∞. The numerical profile is shown in the paper by Hilgenfeldt *et al.* (1996).

The concentration gradient in the boundary layer dictates the mass flux into the bubble. There are two time scales over which mass transfer occurs: (i) during a single cycle of driving, gas is pushed into and out of the bubble when the bubble expands and contracts; (ii) over many cycles of driving, small net gains or losses of mass potentially accumulate to produce significant changes in the number of molecules in the bubble.

With the coordinate (49), we obtain from Eq. (45)

$$\partial_t c = D\,\partial_h(r^4\partial_h c). \tag{50}$$

Focusing on the boundary layer region close to the bubble ($r\approx R$) and redefining the time $\tau\equiv\int R^4 dt$ yields

$$\partial_\tau c = D\,\partial_{hh} c, \tag{51}$$

which is a pure diffusion equation. Following Fyrillas and Szeri (1994), the solution to this equation can be written $c(h,\tau)=c_\infty+c_{osc}(h,\tau)+c_{sm}(h,\tau)$. Here, c_{osc} is an oscillatory solution, transporting gas back and forth at the frequency of the bubble oscillations, but effecting negligible net gas transport. The smooth part of the profile c_{sm}, however, determines the gas exchange over time scales much longer than the oscillation period. For the number of molecules in the bubble to maintain equilibrium over long periods of time, it is necessary that $\langle c(h,\tau)\rangle=c_\infty$, where $\langle\cdot\rangle$ denotes averaging over τ. Specializing to the surface of the bubble, this implies (because of Henry's law)

$$\langle c\rangle_4 = c_0\frac{\int R^4 p_g(R,t)\,dt}{P_0\int R^4 dt}\equiv c_0\frac{\langle p_g\rangle_4}{P_0}=c_\infty. \tag{52}$$

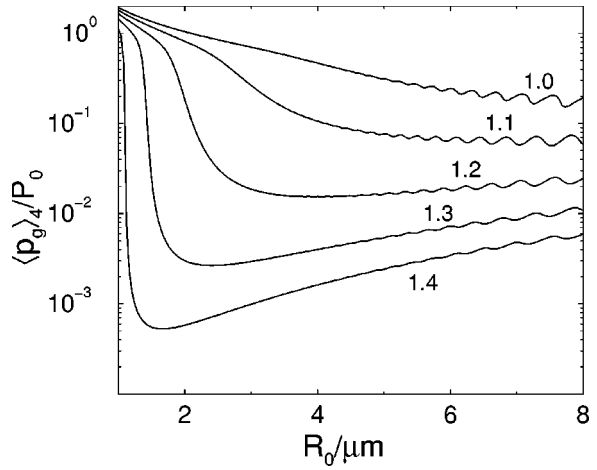

FIG. 30. $\langle p_g \rangle_4 / P_0$ as a function of the ambient radius R_0 for small forcing pressure amplitudes, $P_a = 1.0$ atm to $P_a = 1.4$ atm (top to bottom). From Hilgenfeldt *et al.* (1996).

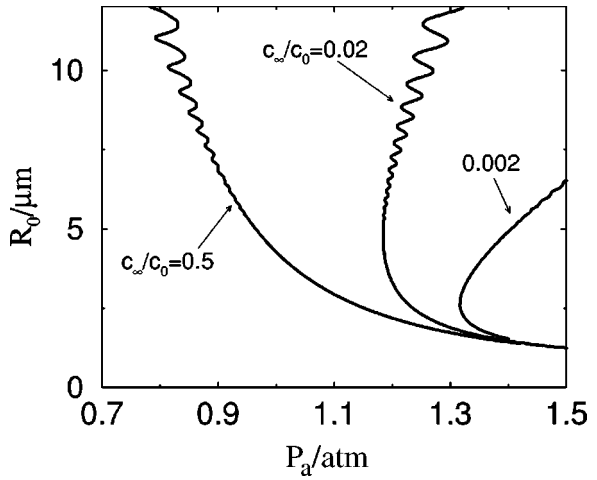

FIG. 31. Bifurcation diagrams in the R_0-P_a parameter space. The regimes with positive slope are stable. Gas concentrations are (right) $c_\infty/c_0 = 0.002$, (middle) $c_\infty/c_0 = 0.02$, and (left) $c_\infty/c_0 = 0.5$. To the left of the curves the bubbles shrink and finally dissolve, to the right of them they grow by rectified diffusion. From Hilgenfeldt *et al.* (1996).

The index 4 indicates that the average is weighted with R^4. The mass loss from the bubble over long periods of time can be calculated via

$$\dot{m} = -4\pi R_0^2 D \frac{\langle c \rangle_4 - c_\infty}{\delta}, \tag{53}$$

where δ is the boundary layer thickness, given by

$$\delta = R_0^2 \left(\int_0^\infty \frac{dh}{T_d^{-1} \int [3h + R^3(t)]^{4/3} dt} \right)^{-1}, \tag{54}$$

where the time integral spans one oscillation period T_d. Because of the dominance of the maximum radius in the integration (see also below), δ can be approximated as $\approx R_0^2/R_{max}$ (cf. Hilgenfeldt *et al.*, 1996). The time scale of mass diffusion is therefore approximately $R_0^3 \rho_g / R_{max} D c_0 \sim 0.1$ s, with the gas density ρ_g under standard conditions.

Fyrillas and Szeri (1994) applied the method of multiple scales (see, e.g., Hinch, 1991) to systematically derive the above formulas and demonstrate their accuracy to leading order in $D(\omega R_0^2)^{-1}$. As long as the diffusive time scale is much longer than the bubble oscillation cycle, the approximation is very reliable and can therefore be used instead of the more cumbersome direct solution of Eq. (45).

Equation (53) can be used to study the stability of the equilibrium ambient radius R_0^*: taking $R_0 = R_0^* + \epsilon$ and expanding $\langle c \rangle (R_0)$ around R_0^* implies that

$$\dot{\epsilon} = -\frac{D}{\rho_g \delta} \frac{d\langle c \rangle_4}{dR_0}\bigg|_{R_0^*} \epsilon.$$

The equilibrium point is therefore stable as long as $d\langle c \rangle_4 / dR_0 > 0$ or, equivalently, $d\langle p \rangle_4 / dR_0 > 0$.

Löfstedt *et al.* (1995) pointed out a useful approximate version of Eq. (52): Since the time average is weighted by R^4, and the bubble spends a large fraction of the cycle near the maximum radius, the equilibrium condition is approximately

$$\frac{p_g(R_{max})}{P_0} = \left(\frac{R_0}{R_{max}} \right)^3 = \frac{c_\infty}{c_0}. \tag{55}$$

What do these results imply for sonoluminescence? Figure 30 plots $\langle p_g \rangle_4$ as a function of R_0 for an argon bubble for various forcing pressure amplitudes P_a. We first examine small pressure, $P_a \approx 1.0$ atm, and gas concentrations of, say, $c_\infty/c_0 \approx 0.3$. There is an *unstable* equilibrium at $R_0^e \approx 6\ \mu$m. Smaller bubbles shrink and larger bubbles grow. The mechanism of growth is called rectified diffusion: when the bubble is large, the gas concentration in the bubble is small, and vice versa, so there is an influx or outflux of material. The net effect is not zero for a nonlinear oscillation because at maximum radius (i) the area for gas exchange is larger, and (ii) the diffusive boundary layer is stretched out (Brennen, 1995). Both effects favor net growth of the bubble. Note that an *undriven* bubble dissolves because its internal pressure exceeds that in the liquid. Sufficiently strong driving will overcome this tendency to shrink, and start rectified diffusion.

Turning our attention to higher forcing pressures (Fig. 30), we see that the average pressure is quite diminished, because R_{max} is very large now [see Eq. (55)]. This means very low gas concentrations (saturation levels c_∞/c_0) are needed to achieve diffusive equilibrium (around 0.005 for $P_a = 1.3$ atm). Moreover, under these conditions the equilibria become *stable*, as demonstrated by the positive slopes. In this example, the bubble reaches an equilibrium size of $R_0^* \approx 5\ \mu$m and will not gain or lose any further mass.

Figure 31 is a diagram showing the equilibrium bubble states in the R_0-P_a parameter space for three fixed concentrations ($c_\infty/c_0 = 0.5, 0.02, 0.002$). Stable equilibria have positive slope $\partial R_0 / \partial P_a|_{c_\infty}$; negative slope represents unstable equilibria. To the right of each line bubbles grow, and to the left they shrink.

Figure 31 shows that there are *no* diffusively stable sonoluminescence bubbles for *large* gas concentrations, where all equilibria are unstable.[5] For small concentrations c_∞/c_0 the situation is quite different. There are stable equilibria at large P_a and small R_0. Only in this region, and *for very low gas concentration* $c_\infty/c_0 \sim 0.001-0.02$ (depending on P_a,) is the bubble diffusively stable, and only then is stable SBSL possible. This is again easily appreciated using the approximation (55) of Löfstedt *et al.* (1995): when the bubble is small and strongly forced, the collapse ratio is $R_{\max}/R_0 \approx 10$. Hence Eq. (55) implies that $c_\infty/c_0 \sim 10^{-3}$ for the bubble to be in equilibrium, as observed in Fig. 31.

Löfstedt *et al.* (1995) realized that this requirement of diffusive equilibrium for strongly forced bubbles can only be fulfilled at very small gas concentrations, in agreement with experiments using argon or other inert gas bubbles. However, the finding blatantly disagrees with the results obtained for air bubbles, where stability is achieved at roughly 100 times larger gas concentrations. Recall that Gaitan (1990) needed to degas to only about 40% of saturation. If he had had to go to 100times lower concentrations, he might never have discovered SBSL. Löfstedt *et al.* (1995) postulated an "anomalous mass flow mechanism" to resolve this discrepancy. Indeed, in order to keep a constant R_0 in a liquid with such a high gas concentration, an air bubble would have to eject mass far above the usual diffusive transport rate in order to balance rectified diffusion.

C. Sonoluminescing bubbles rectify inert gases

1. The mechanism

The stabilizing mass ejection mechanism of sonoluminescing bubbles is now believed to be the consequence of chemical reactions that occur when the bubble is compressed. The maximum temperature of the bubble (larger than 10 000 K; see Sec. III) is large enough to destroy both molecular nitrogen and oxygen, so these molecules will be largely dissociated in the collapsed bubble. Moreover, as discussed in Sec. III, the high expansion ratio of the bubble results in a substantial amount of water vapor. Chemical reactions between water vapor and dissociated nitrogen and oxygen are well known to atmospheric chemists dealing with acid rain: the reaction products are NO, NH, and ultimately HNO_3 and NH_3. All of these substances (except NO) are very soluble in water. The idea of the argon rectification hypothesis (Lohse *et al.*, 1997) is that the reaction products are absorbed completely into the water, depleting the bubble of nitrogen and oxygen and thus establishing an efficient mass-loss mechanism. A sonoluminescing air bubble thus rectifies argon, the only substance inside the bubble that does not dissociate, which is contained in air with a concentration of 1%.

This argument immediately explains the discrepancies between the diffusive equilibria of air and argon: only the inert gas in the bubble is in diffusive equilibrium with the bulk liquid. Therefore the relevant parameter for the stability of sonoluminescing bubbles in equations like Eq. (52) is the partial pressure (or concentration) of the *inert gas* dissolved in the liquid, and not the partial pressure of air. Defining the argon fraction q as

$$\frac{c_\infty^{\mathrm{Ar}}}{c_0} = q\,\frac{c_\infty^{\mathrm{air}}}{c_0},$$

the stability criteria for air and argon should differ by a factor of $q \approx 0.01$, the fraction of argon in air. Indeed, experiments show stable sonoluminescence in air bubbles for $c_\infty/c_0 \sim 0.2-0.4$ (Gaitan *et al.*, 1992) and stable sonoluminescence in argon for $c_\infty/c_0 \sim 0.002-0.004$ (Barber *et al.*, 1995). The hundredfold difference is quantitatively consistent with the argon rectification theory. The earliest measurements confirming consequences of argon rectification were by Holt and Gaitan (1996), described in detail below.

As pointed out by Lohse and Hilgenfeldt (1997), another hint for the chemical activity inside the bubble is the isotope scrambling found by Hiller and Putterman (1995), who had analyzed sonoluminescence in H_2 and D_2 gas bubbles, in both normal and heavy water. The four respective spectra are grouped according to the liquid, *not* according to the dissolved gas. This suggests that water vapor invades the bubble and undergoes chemical reactions, ultimately leaving H_2 for normal water and D_2 for heavy water, independent of the type of hydrogen bubble with which one started. Hiller and Putterman's (1995) hydrogen bubbles were all diffusively unstable.

The most direct verification of argon rectification was accomplished in a clever experiment by Matula and Crum (1998). They were able to precisely measure the transition time over which the light intensity changed when the driving conditions were changed. They observed (see Fig. 32) that an air bubble that has not previously emitted light reaches maximum sonoluminescence intensity after a transition time of about 10^3 driving cycles. By contrast, if a bubble initially emits light, when the forcing pressure is dropped below the light-emitting threshold and then immediately raised back above it, sonoluminescence turns on immediately. As experimental controls, Matula and Crum used pure argon and pure nitrogen bubbles. The transition time for the nitrogen bubble matched the air bubble that initially did not emit light, and the argon bubble matched the air bubble which had sonoluminesced previously. This therefore provides direct evidence for the hysteresis that would be expected with argon rectification.

Other predictions from the rectification hypothesis have not been experimentally verified to our knowledge, e.g., the suggestion for making stable sonoluminescence

[5]Strictly speaking, stable equilibria do appear due to the "wiggles" in the curve of equilibria that result from resonance effects. Brenner, Lohse, *et al.* (1996) speculated that the wiggles could describe multiple stable equilibria. However, when introducing further damping mechanisms into the Rayleigh-Plesset dynamics as done by Hao and Prosperetti (1999a), the wiggles weaken and it is presently not clear whether there are multiple stable equilibria.

without degassing the liquid, preparing a percentage of argon in nitrogen so that $c_\infty^{\mathrm{Ar}}/c_0=0.003$, within the diffusive stability window. The ultimate proof of the argon rectification hypothesis would be the detection of the chemical species leaving the bubble. Lohse *et al.* (1997) suggested detecting a *p*H change due to the acidic reaction products. However, *p*H meters are probably not sensitive enough to detect an effect even if the experiment is run for a long time. Therefore Lepoint *et al.* (1999) exchanged the water in the experiment for Weissler's reagent. The oscillating bubble produced peroxide and chlorine radicals which oxidized iodide to iodine, giving the distinct blue color of the iodine-starch reaction. Thus chemical reactions in and around a single bubble were conclusively demonstrated. The bubble triggered the reaction even at driving pressures below the SBSL threshold, as the temperature there can already be sufficiently large. A thread of blue color was observed to emerge from the bubble, usually in either an upward or downward direction.

2. Bubble equilibria with chemical reactions

Chemical reactions modify the classical diffusive equilibria described above. The arguments outlined above can only make a quantitative prediction for the extreme cases of no chemistry or complete argon rectification. To describe the transition between these two stages (for example, as the driving pressure acting upon an air bubble is increased), the chemical reaction rates have to be modeled explicitly. As described in Sec. III, this modeling can be done to varying degrees of detail, trading accuracy for computational speed. Full simulations are still too expensive computationally to allow a mapping of the parameter space of SBSL. Therefore simple reaction models like those of Yasui (1997a), Toegel *et al.* (Toegel, Gompf, *et al.*, 2000; Toegel *et al.*, 2002), or Storey and Szeri (2001) are often employed.

In such a model, the changes in species numbers are given by diffusive transport [see Eq. (39) for water vapor], and by chemical reactions such as Eq. (41). Reaction rates under SBSL conditions must be either inferred from general principles (cf. Toegel *et al.*, 2002) or extrapolated from lower-temperature reaction data (cf. Kamath *et al.*, 1993; Bernstein *et al.*, 1996; Yasui, 1997b).

As an example, the change in the numbers N_{Ar} and $N_{\mathrm{N_2}}$ of argon and nitrogen particles in a mixture of these two gases can be written as

$$\dot{N}_{\mathrm{Ar}}=\frac{4\pi R^2 D_{\mathrm{Ar}}\partial_r c^{\mathrm{Ar}}|_{r=R}}{\mu_{\mathrm{Ar}}}, \tag{56}$$

$$\dot{N}_{\mathrm{N_2}}=\frac{4\pi R^2 D_{\mathrm{N_2}}\partial_r c^{\mathrm{N_2}}|_{r=R}}{\mu_{\mathrm{N_2}}}-A N_{\mathrm{N_2}}\exp\left(-\frac{T^*}{T(t)}\right), \tag{57}$$

where the first term in Eq. (57) represents diffusion and the second dissociation reactions, depending on the bubble temperature $T(t)$. D_{Ar}, $D_{\mathrm{N_2}}$, μ_{Ar}, and $\mu_{\mathrm{N_2}}$ are the respective diffusion coefficients and molar masses. For simplicity, Lohse *et al.* (1997) assumed

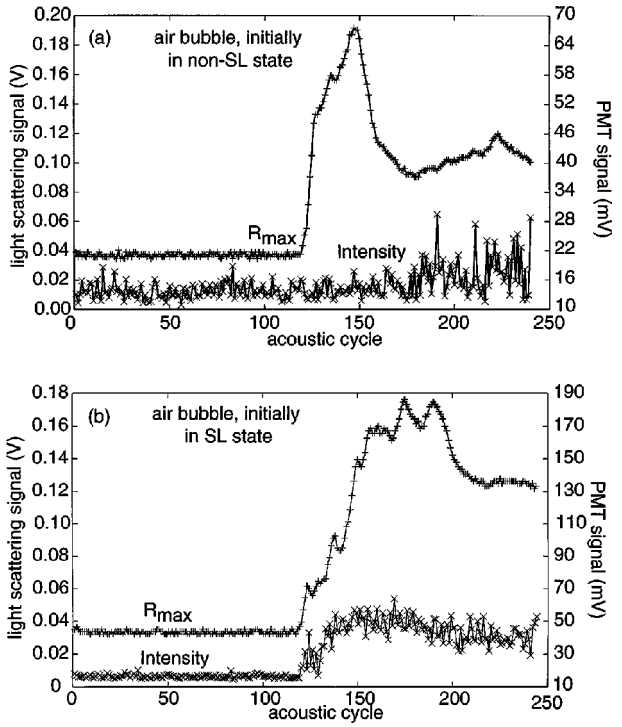

FIG. 32. (+) The maximum radius and (×) sonoluminescence intensity of an air bubble plotted over approximately 240 consecutive cycles. The "radius" is actually a signal level, proportional to the square of maximum radius (assuming a geometrical optics limit for Mie scattering from a sphere). (a) The bubble is initially below the light-emission threshold (the photomultiplier tube signal level corresponds to noise). At approximately the 120th acoustic cycle, the drive pressure is rapidly increased to a value above the SBSL threshold. (b) For this case, the bubble is initially in a stable sonoluminescing state. The drive pressure is then rapidly reduced to a value below the light-emission threshold, and then quickly increased again after a time period of approximately 90 ms. In both (a) and (b), the drive amplitudes at the lower and upper values are the same. From Matula and Crum (1998).

that the reaction rates follow a modified Arrhenius law, using empirical parameters from Bernstein *et al.* (1996) appropriate for nitrogen dissociation: $A\approx 6\times 10^{19}(T_0/T)^{5/2}(\rho_0/\mu_{\mathrm{N_2}})(R_0/R)^3$ cm^3/(mol s) gives the time scale of the reaction; $T^*\approx 113\,000$ K is the activation temperature, T_0 is ambient temperature, and ρ_0 the equilibrium gas density. This reaction law is very crude—it neglects backward reactions as well as the kinetics of the expulsion of reaction products; however, it is sufficient for a demonstrative calculation.

The concentration fields $c^{\mathrm{Ar}}(r,t)$,$c^{\mathrm{N_2}}(r,t)$ in Eqs. (56) and (57) *separately* obey Henry's law at the bubble wall, using the saturation concentrations c_0^{Ar},$c_0^{\mathrm{N_2}}$ specific for the gases ($c_0^{\mathrm{Ar}}\approx 3c_0^{\mathrm{N_2}}$). For diffusive stability, *both* gas species must fulfill the equilibrium condition (52) separately, with concentrations far from the bubble c_∞^{Ar},$c_\infty^{\mathrm{N_2}}$ given by the percentage ξ_l of argon in the gas dissolved in the liquid.

Requiring the temporal averages of $\dot{N}_{\mathrm{Ar}}$ and $\dot{N}_{\mathrm{N_2}}$ to

vanish yields the number of gas particles in the bubble at equilibrium and thus the percentage ξ_b of argon inside the bubble, which is larger than ξ_l because of dissociation reactions removing N_2. Of course, the last term in Eq. (57) only contributes when $T(t)$ is large. The chemical reaction rate therefore depends on the detailed space and time dependence of the temperature in the bubble. The calculations below use a simple spatially uniform temperature model inspired by Prosperetti (1977c) as discussed in Sec. III.B.1.

The resulting equilibrium radii R_0^* in the R_0-P_a plane for air ($\xi_l=0.01$) at $p_\infty/P_0=0.20$ are shown in Fig. 10. For small forcing, the temperatures are not high enough to initiate chemical reactions, so that the curve A of (unstable) equilibria corresponds to those described above for diffusion alone. These bubbles either shrink or grow by rectified diffusion, and for them $\xi_b=\xi_l$ to a good approximation. At high forcing (curve C), the reactions burn off all the N_2, so that the bubble contains pure argon ($\xi_b\approx 1$); this equilibrium corresponds to the (stable) equilibrium at the argon partial pressure $p_\infty^{\mathrm{Ar}}/P_0=0.01p_\infty/P_0=0.002$.

Note that curves A and C belong to the same experimental system now, and that bubbles of low P_a and large R_0 grow by rectified diffusion, while those with high P_a and large R_0 shrink due to the mass loss through chemical reactions (arrows in Fig. 10). There necessarily must be a region of intermediate forcing pressures where both processes cancel, and an *additional* equilibrium exists. These equilibria, which prove to be stable, are shown as curve B in Fig. 10. The onset of appreciable nitrogen dissociation ($T\approx 9000$ K) is depicted as a thin line in the figure and is quite close to line B. Note that this temperature is much smaller than T^*. The argon fraction ξ_b along curve B varies with P_a, but stays considerably smaller than 1.

This picture predicts the following sequence of events as the forcing pressure is increased. At low P_a, the bubble starts near the unstable equilibrium curve A, where the bubble is growing through rectified diffusion and eventually undergoes shape instabilities (see Sec. IV.D below). If the forcing pressure is turned up fairly rapidly, the ambient radius will grow in this regime. At some point, the forcing P_a will be large enough so that the bubble is trapped by the stable equilibrium B. When P_a is now further increased, the ambient radius shrinks along the curve B. Upon increasing the driving even further, fluctuations throw the bubble onto the stable curve C, so the ambient radius grows again. This behavior had been observed previously by Barber *et al.* (1994); see Fig. 7. A direct measurement was made by Gaitan and Holt (1999), who measured both the maximum bubble radius and the ambient radius as a function of forcing pressure (see Fig. 33). The breakdown in R_0 and $R_{\max}$ caused by the onset of chemical reactions inside the bubble is clearly visible.

Holt and Gaitan (1996) showed that at $p_\infty/P_0=0.2$ there is a relatively large forcing pressure regime $P_a\approx 1.2$–1.3 atm where bubbles dissolve (cf. Fig. 10). Such dissolution islands do not exist with pure diffusion (as

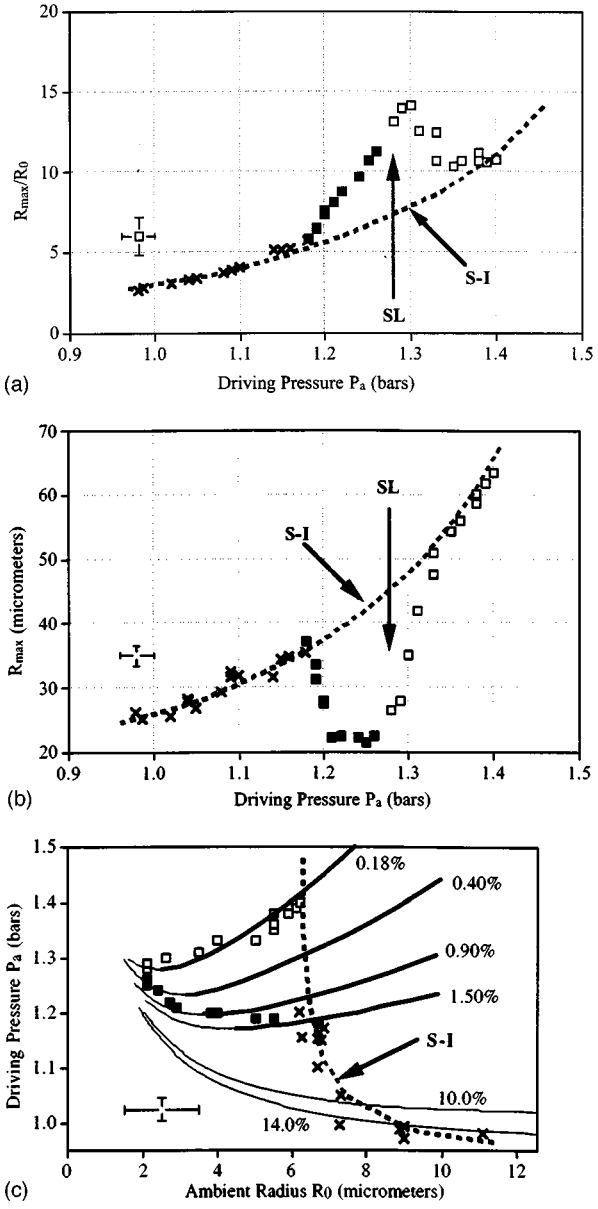

FIG. 33. Experimental maximal bubble radius and phase diagram for SBSL: (a) the ratio between maximum radius $R_{\max}$ and ambient radius R_0; (b) $R_{\max}$ as a function of the driving pressure P_a; (c) data points in the P_a vs R_0 phase space; □, stable glowing bubbles; ■, stable nonglowing bubbles; +, unstable, nonglowing bubbles; dashed line, the experimentally found shape instability; solid lines, theoretical diffusive equilibria for various argon concentrations. To compare this figure with theoretical phase diagrams such as Fig. 10 or other experimental results such as Fig. 12, one should exchange abscissa and ordinate. From Gaitan and Holt (1999).

shown above; see Fig. 31). Gaitan and Holt (1999) demonstrated that the stable equilibria of sonoluminescing bubbles were in excellent agreement with the shape predicted when assuming a much lower gas concentration. These observations agree with the theoretical results taking both diffusion and molecular dissociation into account.

In their comprehensive experimental study of bubble stability diagrams, Ketterling and Apfel (1998, 2000a)

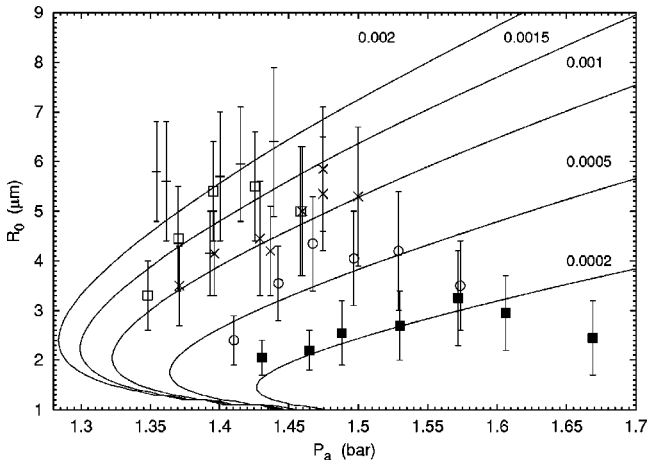

FIG. 34. Experimental data in the phase diagram in the P_a-R_0 plane: +, with an air concentration of $c_\infty^{\mathrm{air}}/c_0=0.2$; □, 0.15; +, 0.1; ■, 0.02. The data lie on the stable diffusive equilibria curves (solid lines) for argon concentrations of $c_\infty^{\mathrm{Ar}}/c_0=0.002$, 0.0015, 0.001, and 0.0002, confirming the argon rectification theory. Experimental data are taken for as large a P_a as possible, to probe the shape instability threshold. From Simon *et al.* (2001).

demonstrated that all stable and light-emitting bubbles indeed lie on a positively sloped equilibrium curve in the R_0-P_a plane, corresponding to the partial concentration of argon in the mixture. This is true regardless of how much nitrogen is present. A representative phase diagram is shown in Fig. 12 for air in water at $c_\infty/c_0=0.2$. The solid line represents the (unstable) diffusive equilibrium for the mixture, and the dashed line is the (stable) diffusive equilibrium for $c_\infty/c_0=0.002$ (the argon in the mixture). As the forcing pressure is increased, the bubble follows a stable equilibrium line above the unstable diffusive equilibrium (corresponding to line B in Fig. 10) and then transitions to the lower-concentration stable equilibrium (where it starts emitting light.) A pure argon bubble at $c_\infty/c_0=0.0026$ follows its stable diffusive equilibrium (see Fig. 5 of Ketterling and Apfel, 1998). No other stable configurations are possible. On the other hand, Fig. 4 of Ketterling and Apfel (1998) shows that a pure nitrogen bubble at $c_\infty/c_0=0.1$ follows a stable equilibrium much like curve B of the air mixture, but cannot reach a stable sonoluminescing state at higher P_a. Taken together, these two types of behavior synthesize the results in Fig. 12, strongly implying that the air bubble is composed mainly of nitrogen along curve B, and mainly argon along curve C, in agreement with the predictions of argon rectification.

Very recently, Simon *et al.* (2001) confirmed that light-emitting bubbles follow the stable diffusive equilibrium curves based on argon concentration alone (see Fig. 34). They employ a new experimental technique for measuring the parameters of the bubble dynamics (P_a and R_0) based on the timing of the light flash in the acoustic period. They also find that the attainable conditions inside a sonoluminescing bubble are more extreme at a low partial air pressure of 15 mm Hg as compared to 150 mm Hg, because then the bubbles are closer to the Blake threshold (where the most extreme conditions are achieved) and can be driven with larger P_a. This is due to the bubble shape instabilities treated in the next subsection.

D. Shape stability

The theoretical diffusive equilibrium curves stretch to far larger ambient radii R_0 than those observed for SBSL bubbles. There must be another requirement limiting the ambient size (or the total mass content) of the bubble. This limit is set by the onset of instabilities in the shape of the oscillating bubble. The analysis of shape stability is a classical problem in bubble dynamics, pioneered by Plesset (1949), Birkhoff (1954), Plesset and Mitchell (1956), Strube (1971), and Prosperetti (1977d). In this section we present the application of these ideas to single-bubble sonoluminescence.

1. Dynamical equations

To analyze the linear stability of the radial solution $R(t)$, consider a small distortion of the spherical interface $R(t)$,

$$r=R(t)+a_n(t)Y_n(\theta,\phi), \tag{58}$$

where Y_n is a spherical harmonic of degree n. The goal is to determine the dynamics $a_n(t)$ for each mode. The derivation of Plesset (1954) follows along the same lines as the derivation of the Rayleigh-Plesset equation, which it recovers to zeroth order in a_n. A potential flow outside the bubble is constructed to satisfy the boundary condition that the velocity at the bubble wall be $\dot{R}+\dot{a}_nY_n$. This potential is then used in Bernoulli's law to determine the pressure in the liquid at the bubble wall. If viscous effects are neglected, applying the pressure jump condition across the interface yields a dynamical equation for the distortion amplitude $a_n(t)$,

$$\ddot{a}_n+B_n(t)\dot{a}_n-A_n(t)a_n=0, \tag{59}$$

where $\beta_n=(n-1)(n+1)(n+2)$ and

$$B_n(t)=3\dot{R}/R, \tag{60}$$

$$A_n(t)=\left[(n-1)\frac{\ddot{R}}{R}-\frac{\beta_n\sigma}{\rho R^3}\right]. \tag{61}$$

The stability of the spherical bubble then depends on whether solutions to Eq. (59) grow or shrink with time. It is already apparent here that Eq. (59) has the form of a parametrically driven oscillator equation (Hill equation), with the radial dynamics $R(t)$ governing the periodic driving.

A more accurate stability analysis requires taking account of viscosity and other dissipative processes. Viscosity, treated by Prosperetti (1977d), poses difficulties because viscous stresses produce vorticity in the neighborhood of the bubble wall, which spreads convectively through the fluid. Once created, the vorticity acts back on the dynamics of $a_n(t)$. This interaction is nonlocal in time, and so the problem requires solving integrodiffer-

ential equations for the vorticity in the liquid, coupled with the shape oscillations. Details can be found in the literature (Prosperetti, 1977d; Hilgenfeldt *et al.*, 1996; Hao and Prosperetti, 1999b). Here we simply summarize the results of a simple "boundary layer" approximation, which assumes that the vorticity is localized in a thin region around the bubble. It was again Prosperetti (1977b) who first realized the usefulness of this approximation. If δ is the boundary layer thickness, the prefactors of Eq. (59) are modified to

$$A_n(t)=(n-1)\frac{\ddot{R}}{R}-\frac{\beta_n\sigma}{\rho R^3}+\frac{2\nu\dot{R}}{R^3}\left[-\beta_n+n(n-1)(n+2)\frac{1}{1+2\frac{\delta}{R}}\right], \tag{62}$$

$$B_n(t)=\frac{3\dot{R}}{R}+\frac{2\nu}{R^2}\left[-\beta_n+\frac{n(n+2)^2}{1+2\frac{\delta}{R}}\right], \tag{63}$$

with the kinematic viscosity ν of the liquid. The viscous contribution to $A_n(t)$ is not important since the ratio between the third and the second terms of the right-hand side in Eq. (62) is typically $\nu\rho R_0\omega/\sigma\lesssim 10^{-2}$. However, in the second term of the right-hand side of Eq. (63) it introduces a damping rate which causes exponential damping of shape modulations. The amount of damping strongly depends on both the boundary layer thickness δ and on n. Brenner *et al.* (1995) and Hilgenfeldt *et al.* (1996) choose δ to be the minimum of the oscillatory boundary layer thickness $\sqrt{\nu/\omega}$ and the wavelength of the shape oscillation $R/(2n)$.

The Hill equation (59) is driven by the strongly nonlinear Rayleigh-Plesset dynamics $R(t)$. Therefore, in contrast to the monofrequent driving of the prototypical Mathieu equation, instabilities in a_n can be excited on the many different time scales of the bubble oscillation discussed in Sec. II. In particular, three types of instabilities can be distinguished: the parametric instability (over time scales of the oscillation period), the afterbounce instability (over time scales of the bubble afterbounces), and the Rayleigh-Taylor instability (over time scales of the Rayleigh collapse).

2. Parametric instability

The parametric shape instability acts over the relatively long time scale $T_d=2\pi/\omega$ (period of the driving). If the nonspherical perturbations of bubble shape show net growth over one oscillation period, they will overwhelm the bubble after many periods. This argument neglects possible (nonlinear) saturation effects not contained in the linear approximation (59), which could inhibit further growth of the perturbations.

In the relevant parameter regime for the parametric instability, $R(t)$ and thus also $A_n(t)$ and $B_n(t)$ are strictly periodic in time with period T_d. Thus the stability of the Hill equation (59) can be rigorously analyzed (Nayfeh and Mook, 1979). Instability occurs whenever the magnitude of the maximum eigenvalue of the Floquet transition matrix $F_n(T_d)$ of Eq. (59) is larger than 1. The Floquet transition matrix is defined as the propagator of the perturbation vector over one period,

$$\begin{pmatrix} a_n(T_d) \\ \dot{a}_n(T_d)\end{pmatrix}=F_n(T)\begin{pmatrix} a_n(0) \\ \dot{a}_n(0)\end{pmatrix}. \tag{64}$$

By numerically computing the eigenvalues of the Floquet transition matrix, one can map out the phase diagram of parametric stability, i.e., identify parametrically stable and unstable regions.

In the sonoluminescence parameter range of $P_a\approx 1.2$–1.5 atm and a typical frequency $f=26.5$ kHz, calculations with the boundary layer approximation suggest that parametric instability sets in for ambient radii in excess of $R_0^{PI}\approx 4$–$5\ \mu$m, with only a weak dependence on P_a. Refined boundary layer models like those of Prosperetti and Hao (1999) or Augsdörfer *et al.* (2000) take into account higher-order terms in $\dot{R}/c$, heat losses, or the varying gas density in the bubble upon collapse. These models find upper stability bounds for R_0 about half a micron larger, because the additional effects result in less violent oscillation dynamics and smaller values of the (destabilizing) bubble acceleration.

For nonsonoluminescing bubbles, stability diagrams of a similar type were first measured by Eller and Crum (1970) and later by Horsburgh (1990). These experimental and theoretical studies examine larger bubble sizes with smaller forcing pressures for which sonoluminescence cannot occur. Applying the above shape stability analysis in the regime $P_a\sim 0.5$–1 atm (Brenner, Hilgenfeldt, and Lohse, 1998; Brenner *et al.*, 1999; Hao and Prosperetti, 1999b; Augsdörfer *et al.*, 2000) gives similar thresholds to those found in experiment by Eller and Crum (1970), Horsburgh (1990), and Gaitan and Holt (1998). For $P_a\lesssim 0.9$ atm, the $n=3$ mode takes over as the most unstable surface mode from the $n=2$ mode (Brenner, Hilgenfeldt, and Lohse, 1998; Brenner *et al.*, 1999; Augsdörfer *et al.*, 2000), just as was found in the experiments by Gaitan and Holt (1998). Overall, larger bubbles can be stabilized at small P_a, and the threshold in R_0 becomes strongly dependent on the driving pressure in this regime.

Holt and Gaitan (1996; Gaitan and Holt, 1999) also measured shape instabilities in the sonoluminescence regime and close to it. Their experimental results were compared with theory in the work of Brenner, Dupont, *et al.* (1998) and Hao and Prosperetti (1999b), with good agreement in evidence [see Fig. 35(a)]. Similar results are found for the higher n modes (see Hao and Prosperetti, 1999b).

The boundary layer approximation has been criticized by Putterman and Roberts (1998) as underestimating the amount of dissipation. These authors claim that there is insufficient evidence for the role of shape instabilities in limiting sonoluminescence, although Brenner, Dupont, *et al.* (1998) found that the approximation gives

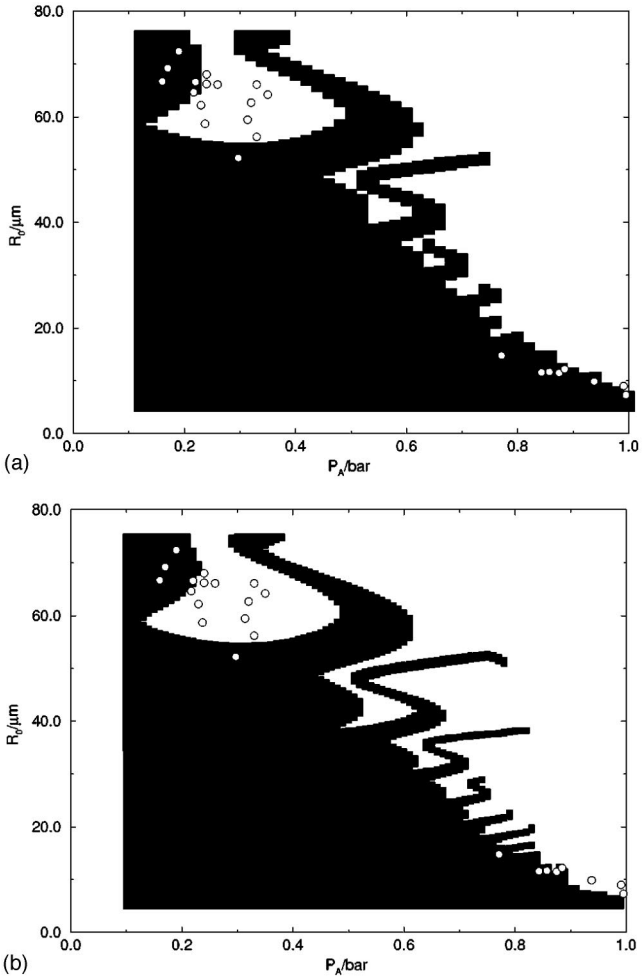

FIG. 35. Comparison of boundary layer approximation and full integrodifferential equation: (a) The dark area is the calculated stability region for the $n=2$ mode for an air bubble in water at $f=20.6$ kHz. The open circles are the data of Holt and Gaitan (1996; Gaitan and Holt, 1999). The calculation employed the boundary layer approximation. (b) Same calculation as above, but based on the full integrodifferential equations, rather than the boundary layer approximation: Hardly any difference as compared to (a) can be observed. From Hao and Prosperetti (1999).

results in good agreement with experiments. It is therefore important to ask how the shape stability results change when the boundary layer approximation is *not* made, and the full integrodifferential equations are solved. Such a comparison was carried out by Wu and Roberts (1998) and Hao and Prosperetti (1999b). A typical result for forcing pressure around $P_a \sim 1$ atm is shown in Figs. 35(a) and 35(b), taken from Hao and Prosperetti (1999b): Hardly any difference between the exact result and the boundary layer approximation can be seen. Wu and Roberts (1998) found similar agreement even for larger P_a in the regime of SBSL. These results indicate that the boundary layer approximation of Prosperetti (1997c), Brenner *et al.* (1995), and Hilgenfeldt *et al.* (1996) is appropriate for sonoluminescence experiments.

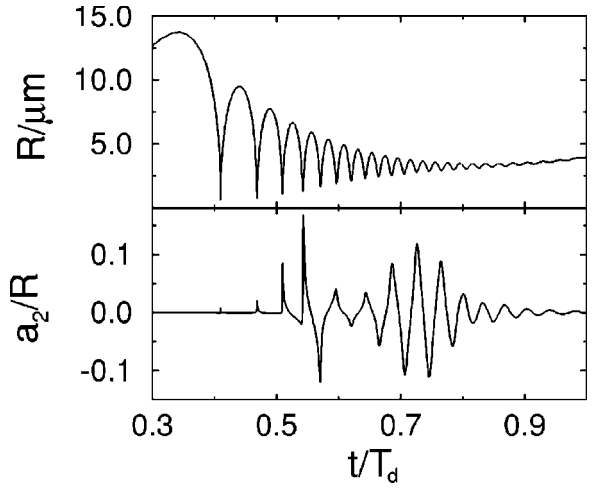

FIG. 36. Shape distortion of a bubble. (Upper part): Time development of the bubble radius $R(t)$ (lower part) and distortion amplitude $a_2(t)$ for a $R_0=4.4$ μm bubble driven at $P_a=1.1$ atm. Note the transition from Rayleigh-Taylor (time scale ns) to afterbounce perturbations (time scale μs) during the afterbounce part of the bubble dynamics. It can also be seen that the dynamics of the distortion $a_2(t)$ has half the frequency of the forcing radial dynamics $R(t)$, as is typical for an instability of the Mathieu type. From Hilgenfeldt *et al.* (1996).

3. Afterbounce instability

During the afterbounces, the bubble oscillates close to its resonance frequency (see Sec. II) on a time scale $\tau_0 = 1/f_0 \sim \sqrt{\rho R_0^2/3P_0} \sim 0.3$ μs. It turns out that the characteristic period of shape oscillations about the spherical bubble is very close to this resonant time scale, namely, $\sqrt{\rho R_0^3/(\gamma\beta_n)} \approx 1\ \mu\text{s}/\sqrt{\beta_n}$ (for the $n=2$ mode, $\sqrt{\beta_n} \approx 3$). This coincidence of time scales is the root cause of the parametric instability (which exhibits maximal growth when the time scale of the forcing is of the order of the

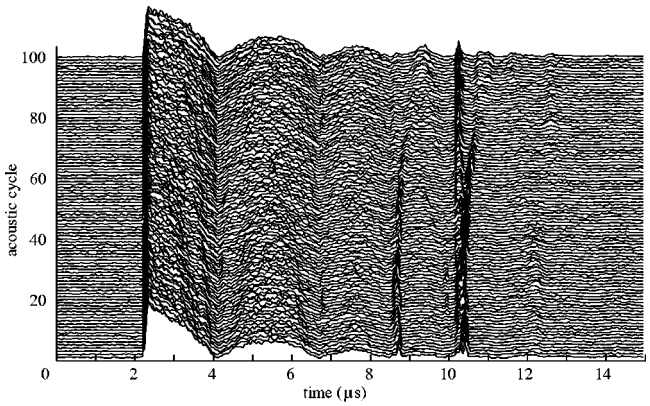

FIG. 37. Mie scattering data of the afterbounce dynamics of a bubble driven below the luminescence threshold. Parametric instabilities can be inferred from the occurrence of large scattering spikes (near 9 and 10.5 μs in this figure), a consequence of the strong shape distortions of the bubble. Direct imaging of the bubble (Matula, 1999) shows nonspherical bubble shapes. From Matula (1999).

time scale of the natural oscillation frequency). Under the right circumstances this instability can be so violent that the bubble is destroyed during the afterbounces of a single cycle. Examples for which the bubble "survived" considerable distortions during the afterbounces are shown in Fig. 36 (theory) and Fig. 37 (experiment), the latter taken from Matula (1999). The distortion can grow so much that the bubble breaks apart during the afterbounce period. The growth of instabilities during the afterbounce phase has been directly observed by Gaitan and Holt (1999).

The afterbounce instabilities must be triggered by noise. A good way to analyze this dependence is to model the thermal noise through coupling a Langevin-type force to the dynamical Eq. (59) for the shape distortion (Augsdörfer *et al.*, 2000), with a magnitude adjusted to satisfy the fluctuation-dissipation theorem.

4. Rayleigh-Taylor instability

The Rayleigh-Taylor shape instability occurs when a lighter fluid is accelerated into a heavier fluid (the classical example is the interface between two layers of liquid, the lower one being lighter and with buoyancy as the accelerating force). For sonoluminescing bubbles, this shape instability acts over the extremely short time scales of the final stages of Rayleigh cavitation collapse. Here the bubble interface *decelerates* in preparation for the reexpansion, leading to an extremely large relative acceleration of the gas with respect to the water in excess of 10^{12} g. This deceleration occurs for only a short time (nanoseconds); it is roughly the time a sound wave of speed c_g needs to cross a fully collapsed SBSL bubble of radius $R \sim h$. For the Rayleigh-Taylor instability to be effective, it must destroy the bubble during this time period. The competition between large magnitude and short duration of the accelerating force determines the stability threshold. A shock-front-driven variant of the Rayleigh-Taylor instability is the Richtmeyer-Meshkov instability, whose occurrence does not seem likely, since no evidence for shock-wave passage through the bubble wall was found (Wang *et al.*, 1999).

It should be emphasized that, in contrast to the parametric and afterbounce instabilities, the Rayleigh-Taylor instability acts on such a short time scale that the bubble dynamical approximations cannot be expected to be quantitatively correct. A proper calculation requires a full simulation of the gas-liquid interface dynamics down to the latest stages of the Rayleigh collapse.

The thresholds for the Rayleigh-Taylor shape instability do not depend on whether the boundary layer approximation is used or not, but instead on the chosen dynamics for the bubble radius $R(t)$. Hilgenfeldt *et al.* (1996) used the modified Rayleigh-Plesset dynamics (20), i.e., without the $\dot{R}/c$ corrections of the kinetic term [cf. Eq. (18)], and without thermal damping. Those terms were included by Prosperetti and Hao (1999), who found the Rayleigh-Taylor instability greatly suppressed due to the smaller bubble-wall acceleration $\ddot{R}$ resulting from higher-order equations (see Prosperetti and Hao, 1999). The uncertainties in modeling the bubble dynamics—and in particular in the second derivative $\ddot{R}$—are substantial enough to make a quantitative description of the Rayleigh-Taylor instability a difficult task. Another factor that changes the location of the Rayleigh-Taylor instability line in the phase diagrams is the diminishing density contrast between the liquid and the extremely compressed gas at collapse. Taking this effect into account in Eq. (62), Augsdörfer *et al.* (2000) and Yuan *et al.* (2001) found further suppression of the Rayleigh-Taylor instability.

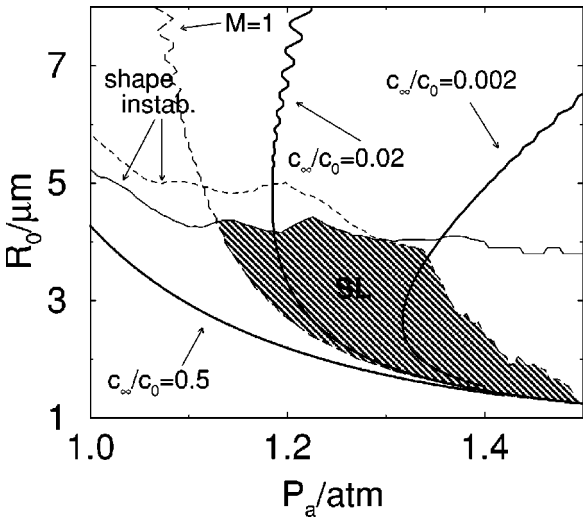

FIG. 38. Parameter space restrictions for sonoluminescing argon bubbles: The $M=1$ curve (long-dashed) characterizes the onset of strong bubble collapse and heating. The bubble grows thanks to rectified diffusion to the right of the diffusive stability curves (heavy lines, shown for $c_\infty/c_0=0.5$, 0.02, and 0.002, left to right). The thin solid line marks the onset of the parametric instability and the short-dashed line combines the threshold of Rayleigh-Taylor instability and afterbounce instabilities. These lines are calculated within the simplified theory of Hilgenfeldt *et al.* (1996), which slightly underestimates the shape stability, as discussed in the text.

In conclusion, though experimental results and theory give many hints that the Rayleigh-Taylor instability sets the upper threshold of the SBSL regime towards large forcing pressures P_a, the matter is not yet fully settled. As discussed in Sec. II, the Bjerknes force instability may also play a role. The parametric and afterbounce instabilities, on the other hand, set well-established limits for the parameter space of SBSL towards large R_0. Figure 36 shows that instabilities such as Rayleigh-Taylor and afterbounce can occur simultaneously in the same bubble, with the perturbation $a_2(t)$ growing over both nanosecond and microsecond time scales.

5. Parameter dependence of the shape instabilities

All calculations up to this point have been described for the material parameters of water at 20 °C and driving frequencies around $f=20$ kHz. The shape stability thresholds strongly depend on changes in the radial dynamics brought about, for example, by different liquid

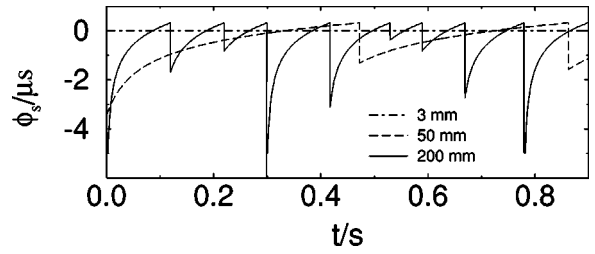

FIG. 39. Theoretical result from Hilgenfeldt *et al.* (1996) on the drift of the phase of light emission $\phi_s(\bar{t})$ for three different argon concentrations, $c_\infty/c_0=0.003\,95$, $c_\infty/c_0=0.0658$, and $c_\infty/c_0=0.26$, corresponding to gas pressures overhead of $p_\infty=3$ mm Hg, 50 mm Hg, and 200 mm Hg, respectively. According to the theory of Hilgenfeldt *et al.* (1996), the drift in the phase of light emission is a result of bubble growth through rectified diffusion, which is followed by a pinch-off of a microbubble when the bubble is running into the shape instability. The figure resembles the corresponding experimental result, Fig. 4 of Barber *et al.* (1995). Note that for air bubbles stable sonoluminescence (corresponding to a constant phase of the light pulse) is achieved for much higher gas concentration, $c_\infty^{\text{air}}/c_0=0.2$, corresponding to 150 mm Hg [see also Fig. 4 of Barber *et al.* (1995)].

viscosities or driving frequencies. The dependencies may act differently for different stabilities: if f is decreased, the parametric instability is suppressed as the stabilizing influence of viscosity can act for a longer time to suppress perturbations. The more violent collapses of low-frequency-driven bubbles, however, favor an earlier onset of the Rayleigh-Taylor instability. Nevertheless, for not too high forcing pressures, larger bubbles can be stabilized to show sonoluminescence, possibly emitting brighter light pulses ("upscaled" SBSL). However, as described in Sec. III.A.3, water vapor becomes increasingly important at low frequencies and counteracts the upscaling (Yasui, 1997b; Moss *et al.*, 1999; Storey and Szeri, 2000; Toegel, Gompf, *et al.*, 2000).

The water temperature also has an effect on the phase space of SBSL. As pointed out by Hilgenfeldt, Lohse, and Moss (1998) and Vuong *et al.* (1998), the increased viscosity at lower water temperature means that bubbles can be stabilized by cooling the fluid, allowing for much stronger acoustical driving and thus more light, as indeed experimentally observed by Barber *et al.* (1994).

E. Interplay of diffusive equilibria and shape instabilities

The conditions for diffusive equilibrium and shape stability must be fulfilled simultaneously for stable SBSL (Hilgenfeldt *et al.*, 1996). Outside this parameter regime, bubbles do not necessarily perish, but can undergo dynamical processes like rectified diffusion that can allow for unsteady sonoluminescence at a weaker level ("unstable sonoluminescence").

When at low forcing pressure $P_a\approx1.1$ atm the gas concentration is sufficiently large (e.g., $c_\infty/c_0=50\%$), rectified diffusion can overcome the tendency for dissolution, and growing bubbles are possible if R_0 lies above the unstable equilibrium line. Rectification then continues until shape instabilities limit the growth (see Fig. 38). When R_0 reaches the boundary for shape instability, a microbubble pinches off, decreasing R_0. If the remaining bubble is still large enough, i.e., above the unstable equilibrium line in Fig. 38, the process will repeat. For these low forcing pressures, the allowed size of the bubble after the pinch-off is very restricted. If the pinched-off microbubble is too large, the remaining bubble dissolves.

For relatively large forcing pressure ($P_a\approx1.3$ atm) the situation is quite different. For low enough gas concentration (e.g., $c_\infty/c_0=0.2\%$ in Fig. 31), bubbles can grow (or shrink) and approach a *stable* diffusive equilibrium. Since Rayleigh collapse occurs at large P_a, stable SBSL occurs here, with a well-defined, stable R_0 following from P_a and the gas concentration. For larger gas concentrations, large enough bubbles will again grow up to the threshold of parametric shape instability where microbubbles pinch off. Here, in contrast to the smaller P_a regime, the remaining bubble is very likely to end up in a regime where it can grow again.

The characteristically slow growth of R_0 (over the time scales of rectified diffusion) and sudden breakdown (at microbubble pinch-off) are reflected in other experimentally observable parameters as well, such as the phase of light emission (with respect to the driving). Experimental measurements of the phase are presented in Fig. 4 of Barber *et al.* (1995), showing the pinch-off/growth dynamics. From the diffusive theory outlined in Sec. IV.B, Hilgenfeldt *et al.* (1996) simulated this behavior (see Fig. 39), finding good agreement with the experimental result.

The momentum of pinched-off microbubbles also gives the remaining bubble a recoil. As this repeats again and again on the diffusive time scale of ~0.1 s, the bubble seems to "dance," as originally observed by Gaitan (1990) and later by Barber *et al.* (1995). The regime of dancing bubbles is indicated in the experimental phase diagram Fig. 12. If the bubbles in this regime are large enough (close to the instability line), they will also emit sonoluminescence light even as they undergo rectified diffusion, leading to the same pattern of slow increase and sudden breakdown in the light signal. This is known as (diffusively) unstable SBSL and is generally fainter than stable SBSL.

For very large driving pressures, the Rayleigh-Taylor shape instability (and possibly the Bjerknes instability) make stable bubble oscillations impossible for small R_0. This sets the upper limit in P_a for the observation of SBSL bubbles.

After computing phase diagrams like Fig. 38 with many different dissolved gas concentrations, the results can be summarized in a new plot whose variables are the experimentally controllable parameters c_∞ and P_a. This phase diagram in c_∞-P_a phase space is shown in Fig. 9. The notation in that diagram is as follows: stable SL or unstable SL means that there are glowing bubbles of certain ambient radii which are diffusively stable or undergoing rectified diffusion, respectively; other, smaller bubbles dissolve. Only a small, crescent-shaped region in

this phase space allows for stable SBSL. Luckily, the narrow range of extremely small argon concentrations necessary for stable SBSL is easily achievable by working with gas mixtures such as air, because the molecular constituents of air dissociate (Sec. IV.C). Experimental phase diagrams in the c_∞ and P_a phase space can be found in Simon *et al.* (2001).

F. Other liquids and contaminated liquids

Other parameter dependencies of SBSL involve changes in the material parameters of the liquid. It was already mentioned in Sec. IV.D.5 that increasing liquid viscosity allows for stable bubbles at larger R_0. Likewise, a change in surface tension can influence the location of the shape instability line in the phase diagrams (see Hilgenfeldt, Brenner, *et al.*, 1998). For nonsonoluminescing bubbles, Asaki and Marston (1997) have experimentally examined the effect of surfactants on both shape oscillations and dissolution rates; Fyrillas and Szeri (1995, 1996) supply theoretical understanding of the surfactant effect.

A change of the liquid in which a bubble oscillates has profound consequences on possible SBSL light emission, largely because of the chemical reactions occurring inside the bubble. In Secs. III.A.3 and III.B.2, we discussed the influence of water vapor invading the bubble on the bubble temperature and the resulting light emission, finding that more water vapor leads to less light. Moreover, dissociation products of the liquid (water) are crucial for the radical reactions that remove molecular gases from the bubble (Sec. IV.C).

For quite some time, it was thought that stable SBSL could be achieved in water only, and even today water is still considered the most "friendly" liquid for SBSL experiments. While dissolved salts (Matula *et al.*, 1995) or mixtures of water and freely miscible liquids (Gaitan *et al.*, 1996) do not prohibit stable SBSL, for years it could not be observed in other liquids, even though multibubble sonoluminescence in nonaqueous liquids had been known for a long time (see, for example, Suslick and Flint, 1987).

Weninger *et al.* (1995) showed that weakly emitting, unstable single sonoluminescing bubbles could be observed in pure alcohols, while the light of a stable SBSL bubble in water could be turned off by just adding a few drops of alcohol to the solution. The latter effect can be understood by recognizing that alcohols are surface active and tend to accumulate at the bubble surface. At collapse, they enter the bubble and reduce the heating because of their smaller polytropic exponent and endothermic chemical reaction. Alcohols act much like water vapor in this respect, but are much more efficient in reducing the temperatures. Evidence for this kind of model has been gathered experimentally and theoretically for both MBSL and SBSL (Ashokkumar *et al.*, 2000; Toegel, Hilgenfeldt, and Lohse, 2000; Grieser and Ashokkumar, 2001).

While alcohol contaminations quench the light emission quickly, the bubbles still oscillate in a stable fashion, indicating that the general mass balance of the diffusive/chemical equilibrium is not severely disrupted. The difference with the Weninger *et al.* (1995) experiment in pure alcohols thus lies in the solubility of the chemical reaction products in the surrounding liquid, which is still almost pure water in the case of alcohol contamination experiments. Didenko *et al.* (2000b) therefore sought ideal nonaqueous liquids for SBSL, requiring (i) a low vapor pressure to limit vapor invasion of the bubble and (ii) a high content of O or N heteroatoms to facilitate the chemical formation of species upon collapse that will readily dissolve in or react with the liquid phase. Using liquids such as formamide or adiponitrile, Didenko *et al.* (2000b) did produce bright SBSL and were the first to observe molecular spectral lines (see Introduction and Sec. V.G). Their bubbles were, however, unstable, in the sense that they were moving on circular or elliptic trajectories around the pressure antinode that held them trapped. Didenko *et al.* (2000b) call this state *moving* SBSL. Possibly the chemical reactions (of which the line emission gives direct evidence) still produce too much "waste" unable to dissolve fast enough in the surrounding liquid, sending the bubble into an unstable state of rectified diffusion and microbubble pinch-off. Revealing the mechanism of moving SBSL is an interesting open problem for future research.

V. SONOLUMINESCENCE LIGHT EMISSION

The previous sections have described how a micrometer-sized bubble in a water-filled flask can undergo oscillations of incredible violence, collapse at supersonic speeds, burn molecular gases, and still—under the right experimental conditions—maintain the stability of its spherical shape, showing precise repetitions of this highly nonlinear dynamics for millions and billions of driving cycles. These remarkable properties might not have been studied in detail without the phenomenon that gives sonoluminescence its name: the emission of visible light induced by insonation with an acoustic wave.

In order to release a photon of visible wavelength, an atom, ion, or molecule must be excited a few eV above its ground state. A sound wave of 1-atm amplitude, by contrast, carries an energy density of typically 10^{-11} eV per particle. The required tremendous energy concentration of almost 12 orders of magnitude (Barber and Putterman, 1991) is precipitated by the rapid collapse of the sonoluminescent bubble, where the layers of water surrounding the bubble act as a radial piston compressing its interior. But is this the whole story? Is the heating of the gas inside the bubble resulting from the rapid collapse sufficient to explain the light? Is the light emission completely of thermal origin, or is it necessary to invoke other physical processes? While researchers have come up with a plethora of creative ideas concerning light-emission processes, the results of a number of crucial experiments favor the thermal light-emission approaches over others, and rule out some other theories outright.

A. Theories of MBSL: discharge vs hot spot theories

When multibubble sonoluminescence was discovered in the 1930s by Marinesco and Trillat (1933) and Frenzel and Schultes (1934), different theories for its occurrence were soon put forth. Almost all light-emission mechanisms discussed since then can be classified under one of two headings: thermal or electrical processes.

The first attempts at explaining the mechanism behind the light emission favored electric discharges. Levshin and Rzhevkin (1937) initially brought up the subject of charge separation in cavitation bubbles; Harvey (1939) thought of the bubble as a spherical capacitor with charges at the center and the wall. Upon collapse, the capacitance decreases and voltage increases until electric breakdown takes place. Frenkel' (1940) suggested charge separation by enhancing charge fluctuations on the bubble wall. In this latter theory, however, breakdown should occur during the expansion phase of the bubble dynamics (Leighton, 1994), whereas the close proximity of bubble *collapse* and light pulse has been firmly established by the work of Meyer and Kuttruff (1959).

Since a symmetric charge distribution cannot radiate light, discharge theories in general have to assume that the emitting bubble undergoes an asymmetric collapse, and would predict increasing intensity of light emission as the asymmetry increases (Margulis, 2000). This contradicts recent systematic studies of single-bubble cavitation luminescence (Ohl *et al.*, 1998; Baghdassarian *et al.*, 1999, 2000, 2001; Ohl, 2000), in which the bubbles are created with strong, focused laser pulses, and in which, above a certain collapse asymmetry, light emission ceases altogether. It is also in contradiction with the observation that single sonoluminescing bubbles, which collapse under controlled conditions with high symmetry, emit light of much higher intensity than MBSL bubbles of comparable size driven at comparable levels, with the light of a single bubble easily visible to the naked eye (Gaitan *et al.*, 1992). Another example in which an increase in symmetry leads to (slightly) *more* light rather than less is given by the SBSL experiments under microgravity performed by Matula (2000).

The other large group of MBSL theories have been characterized as "hot spot" models, in which the energy for the light emission is supplied by *thermal* energy resulting from an adiabatic bubble collapse. Noltingk and Neppiras (1950) were the first to use Rayleigh-Plesset bubble dynamics to deduce bubble internal temperatures as high as 10 000 K at collapse of a spherically symmetric bubble. Within the hot spot models, which process of light emission will dominate depends on the actual maximum temperatures reached, e.g., recombination of dissociated molecules at lower temperatures (Saksena and Nyborg, 1970), or characteristic molecular radiation due to electronic excitation, in particular of the OH radical (Sehgal *et al.*, 1980). The latter was referred to as chemiluminescence by Suslick (1990) and must not be confused with secondary chemiluminescence, which may occur in the liquid as a result of chemical reactions of the radical molecules generated in the bubble collapse. One example of this is luminol, which emits light as it reacts with OH. While chemicals such as luminol are useful in detecting cavitation (Negishi, 1961), their emission is not directly related to sonoluminescence.

In the past decade, Kenneth Suslick and his group have amassed impressive evidence in favor of thermal molecular-emission luminescence in multibubble cavitation fields in the context of sonochemistry. From the presence of clearly identifiable molecular bands and the absence of other lines associated with discharges, Suslick (1990) deduces the thermal origin of the emission. Identifying line emissions by their location in the spectrum, Suslick *et al.* (1986) used comparative rate thermometry to evaluate the temperature from the intensity of the different lines. The temperatures obtained are very consistent and have been confirmed by different methods of spectral analysis by Flint and Suslick (1991a) and McNamara *et al.* (1999). Typical maximum temperatures of MBSL bubbles are thus determined to vary between $\sim$3000 and 6000 K, depending on experimental parameters (McNamara *et al.*, 1999). Another convincing feature of thermal hot spot theories is that they naturally predict higher temperatures for collapses of higher spherical symmetry, which is confirmed by studies such as those of Ohl *et al.* (1998) and Matula (2000), as mentioned above.

B. SBSL: A multitude of theories

With the advent of single-bubble sonoluminescence, a simple case study for cavitation and the resulting light emission was found. It was hoped that all open questions could be answered by studying this "hydrogen atom of cavitation physics." Initially, the discovery of single-bubble sonoluminescence actually increased the confusion about sonoluminescence light-emission mechanisms. The main reason for the multitude of speculative models was the uncertainty whether SBSL was similar to MBSL. SBSL led to more light than a single MBSL bubble, while the spectra did not reveal any structures such as lines or bands (Fig. 6). Both of these facts (as well as the apparently short duration of the light pulse) suggested more extreme temperatures and pressures.

Thus, early theoretical research tried to invent mechanisms that occur for more extreme conditions than MBSL. Some of these theories were quite exotic. For example, Schwinger (1992) hinted at the dynamical Casimir effect as a potential photon-emission process at the noninertially moving bubble interface. When a corresponding model was developed by Eberlein (1996a, 1996b), it soon became clear that, in order to match the observed light intensities, the bubble-wall speed would not just have to be comparable to the speed of sound, but exceed the speed of light (Unnikrishnan *et al.*, 1996; Lambrecht *et al.*, 1997; Milton and Ng, 1998; Brevik *et al.*, 1999). This particular line of research was thus abandoned.

A number of theories placed the location of light emission in the liquid, rather than inside the bubble. In

this vein, another attempt at an electrical breakdown model was made by Garcia *et al.* (1999). Earlier, Lepoint *et al.* (1997) speculated on sparklike discharges around water jets invading a bubble.

Prosperetti (1997) also invoked an electrical mechanism for light emission (fractoluminescence) as a by-product of a fluid-mechanical picture of sonoluminescence light emission that requires asymmetric collapse of the bubble. His idea was based on the fact that Bjerknes forces cause a sonoluminescing bubble to oscillate vertically during a bubble cycle, and that such oscillations are well known to cause asymmetric collapse (jets). The collision of the jet with the bubble wall would initiate fractoluminescence, an effect documented in solid-state materials. Prosperetti argued that, over the small time scales of collapse and jetting, water could "break" as well. The model made various predictions, but it fell out of favor when it became clear that they do not hold. First, it had predicted that less light should be emitted under microgravity, where a weaker jet is expected. Yet Matula (2000) found the opposite. Second, the details of Prosperetti's (1997) model specifically rely on the properties of water, while Didenko *et al.* (2000b) found bright SBSL in nonaqueous liquids. Finally, it had meanwhile become clear that models based on a spherically symmetric collapse were able to give a more quantitative explanation for the experimental data.

Other SBSL theories focused on a more ordinary explanation, the emission of photons due to the high temperatures in the bubble, akin to the hot spot theory of MBSL. In fact, all nonthermal models have to explain why their mechanism of emission would not be swamped by thermal radiation. Requiring spherical symmetry of collapse for intense light emission, thermal models of SBSL are favored even by proponents of discharge models for MBSL (Margulis, 2000). In an interesting twist, Xu *et al.* (1999) have suggested that electric fields do not directly lead to light emission, but suppress the Rayleigh-Taylor instability (see Sec. IV) and thus stabilize the bubble. However, the existence of large enough fields for such stabilization is a subject of debate (Moss, 2000).

Depending on the actual temperatures achieved during collapse, different excitations become dominant in the compressed gas, so that "thermal emission" can refer to a large variety of different processes. As temperatures increase from several hundred to many thousand kelvin, those processes can be, among others, molecular recombination (Saksena and Nyborg, 1970), collision-induced emission (Frommhold and Atchley, 1994), molecular emission (Didenko *et al.*, 2000b), excimers (Hammer and Frommhold, 2001), atomic recombination (Hilgenfeldt *et al.*, 1999b), radiative attachment of ions (Hammer and Frommhold, 2001), neutral and ion bremsstrahlung (Moss *et al.*, 1997; Xu *et al.*, 1998; Hilgenfeldt *et al.*, 1999b), or emission from confined electrons in voids (Bernstein and Zakin, 1995). The uncertainty about the precise temperatures of SBSL bubbles (see Sec. III) would allow for most of these mechanisms. Generally speaking, however, very-low-energy excitations are unlikely to produce a spectrum with enough visible photons to account for SBSL. On the other hand, the bubble collapse cannot generate arbitrarily high temperatures, so that very-high-energy excitations are rare and do not produce a large photon flux either.

Which of these mechanisms actually dominates depends critically on accurate measurements and calculations of the temperature inside the bubble. For example, at temperatures above several thousand kelvin, processes like collision-induced emission lose importance as higher-energy emission processes such as bremsstrahlung take over (Frommhold, 1998; Hammer and Frommhold, 2000a, 2000b, 2001). Calculations have shown that the emission intensity from a body at a temperature of $\sim 10^4$ K is not inconsistent with SBSL observations; although radiative enhancement effects (e.g., collective emission as proposed by Mohanty and Khare, 1998) have not been strictly ruled out, they are not necessary to explain the experimental data. It should be emphasized here that although all thermal processes can contribute to blackbody radiation, thermal emission does not necessarily result in a blackbody spectrum (as elaborated upon in Secs. V.D and V.E).

For many years, the most serious argument against thermal processes was the sonoluminescence pulse width. As measured, it was much shorter than the time for which the bubble is maximally collapsed (~ 1 ns, see Fig. 27). The need for ultrashort pulses fueled the popularity of "shock-wave" models, in which a focusing shock causes the light-producing region to be much smaller than the bubble size (see the Introduction). This shock picture (referred to as the mechanochemical mechanism in Leighton, 1994) was the most popular view of SBSL for quite some time.

C. Narrowing down the field

The critical event that narrowed the field was the experimental resolution of the light pulse, showing its width to be much longer than previously anticipated. Gompf *et al.* (1997) used time-correlated single-photon counting, a powerful method from solid-state physics and biophysics (O'Connor and Phillips, 1984), where it is used to register fluorescence lifetimes of sometimes only a few picoseconds. Using a modification of the classical setup, Gompf *et al.* (1997) employed two photomultiplier tubes to record the arrival times of single photons from the same SBSL light pulse in both detectors. From the autocorrelation function of the time differences between the registered events, they could reconstruct the shape (the temporal variation of intensity) of the light pulse and thus measure its duration. Gompf and coworkers confirmed these results using a direct streak camera measurement (Pecha *et al.*, 1998). Furthermore, both publications demonstrate that higher driving pressures lead to light pulses of both higher intensity and longer width. Their results were confirmed by Moran and Sweider (1998) and Hiller *et al.* (1998), the latter noting that xenon bubbles, long known to be the brightest SBSL emitters, also yield the longest pulses, with

widths up to 350 ps and more. Only for bubbles in highly degassed water can very faint flashes of about 40–60 ps duration be found.

We have seen before that the bubble dynamics near minimum radius occurs on a time scale ("turnaround time") of ~1 ns (Fig. 27). While the typical pulse width of 100–200 ps is still much smaller than this value, the gap between the light-emission time scale and the radial dynamics time scale is not nearly as wide as once thought. Gompf *et al.* (1997) demonstrate that a simple thermal model can result in a light pulse with the essential characteristics they measured. This made more credible all thermal models with heating processes directly connected to bubble dynamics. Conversely, exotic processes (yielding ultrashort pulses) were no longer necessary. It was then that shock-wave theories underwent a closer scrutiny with respect to their consequences for light emission. In Sec. III, we discussed how calculations showed that shock waves for noble gases would be far less intense than for molecular gases (Moss *et al.*, 1997) or might be altogether absent (Vuong *et al.*, 1999). The nonrobustness of the shock-wave phenomenon makes it an unlikely candidate for the heating necessary to generate thermal SBSL emission. In the work of Bourne and Field (1991), a shock wave was detected in an asymmetrically collapsing, mm-sized air bubble. However, the light emission detected at collapse did not originate from the shock wave, but from the compressed gas. All this evidence indicates that, while shock waves may be present in collapsing bubbles under certain circumstances, they do not substantially contribute to SBSL light emission. This can be because either (i) they are too weak, so that they do not focus energy to a scale much smaller than the bubble size, or (ii) they can only heat a tiny volume near the very center of the bubble to very high temperatures, and the ensuing light emission is much less intense than the thermal radiation from the bulk volume of the bubble.

D. The blackbody model and its failure

The seminal publication of Gompf *et al.* (1997) provided more valuable information: using wavelength filters, they determined the widths of the light pulse in different parts of the optical spectrum. The results showed (Fig. 13) that there was hardly any detectable difference between the pulse width in the ultraviolet part of the spectrum (300–400-nm wavelength) and in the red part (590–650 nm). This contradicted thermal models favoring blackbody emission. These predict that, since the bubble heats during collapse and cools during expansion, it maintains somewhat lower temperatures for a longer time than higher temperatures. It is therefore capable of emission at long optical wavelengths for a longer time than at short wavelengths (the latter requiring higher temperatures). Translating typical temperatures achieved in models of collapsing bubbles into blackbody emission shows that the "red pulse" should be about twice as long as the "ultraviolet pulse" (see below). Again, Hiller *et al.* (1998) and Moran and Sweider (1998) confirmed these findings, although the latter group did find a slightly longer pulse in the red than in the UV if cooled water was used.

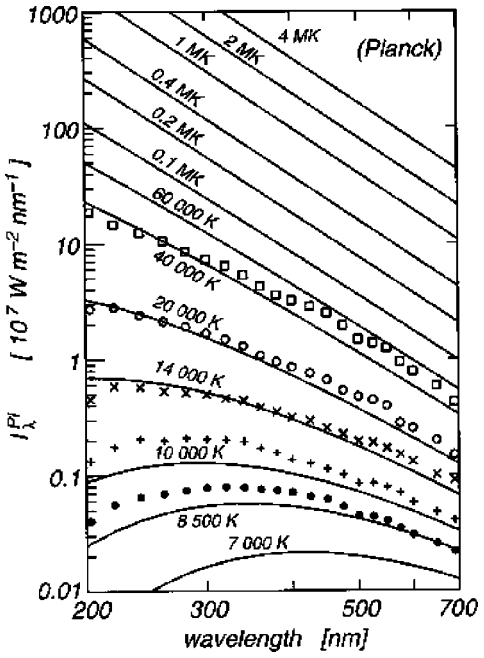

FIG. 40. Blackbody spectra with the indicated temperatures fitted to the data from Barber *et al.* (1997) for the noble gases: □, helium; ○, neon; ×, argon; +, krypton; and ●, xenon. The best-fit temperatures decrease dramatically with increasing molecular weight of the gas. From Hammer and Frommhold (2001).

Adiabatic heating does not necessarily result in blackbody radiation. Even though a model of pure blackbody emission cannot account for the experiments, it is helpful to outline this simplest of all thermal light-emission theories in the context of SBSL to introduce basic concepts and to point out where it fails. A blackbody calculation is of unrivaled simplicity because there is no need to specify the thermal emission as resulting from one of the many excitation processes listed Sec. V.B—only the *temperature* matters.

A blackbody of a given temperature emits a spectral light intensity (energy per unit time, wavelength interval, solid angle, and projected surface area) at wavelength λ of

$$I_\lambda^{Pl}[T]=\frac{2hc^2}{\lambda^5[\exp(hc/\lambda k_B T)-1]}, \tag{65}$$

the *Planck intensity*, with the Planck and Boltzmann constants h and k_B, and the speed of light in vacuum c. Experiments measure the spectral radiance (emitted energy per time and wavelength interval), for which we must integrate over the projected bubble surface and all solid angles:

$$P_\lambda^{Pl}(t)=4\pi^2 R(t)^2 I_\lambda^{Pl}[T(t)]. \tag{66}$$

This formula reflects the fact that a blackbody is a *surface emitter*, i.e., its radiation comes from its surface alone, as photons originating in deeper layers are ab-

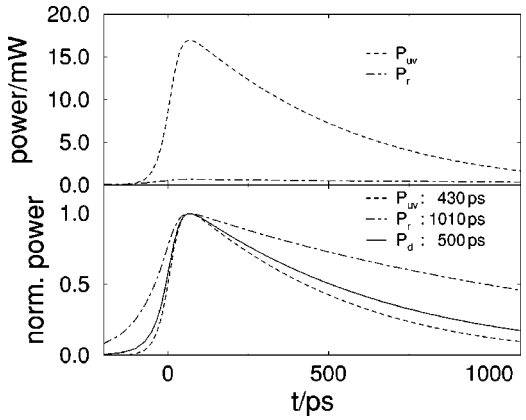

FIG. 41. Theoretically calculated light emission from a $R_0 = 5\ \mu$m SBSL bubble driven at $P_a = 1.3$ atm and $f = 20$ kHz under the assumption of blackbody radiation, using the temperature dynamics $T(t)$ from Fig. 27 and Eq. (66): dashed lines, pulses in the ultraviolet (P_{uv}); dotted lines, pulses in the red (P_r) wavelength range; (a) absolute instantaneous powers; (b) pulses normalized to a peak value of 1 for better comparison of their widths; solid line, pulse integrated over the entire range of detectable wavelengths (P_d). From Hilgenfeldt *et al.* (1999b).

sorbed within the blackbody. It can be compared directly with the measured spectra of sonoluminescence, as the only quantities that matter are the bubble temperature $T(t)$ and radius $R(t)$. Figure 40 shows a comparison (Hammer and Frommhold, 2001) of data from Barber *et al.* (1997) with blackbody calculations. The spectra match the blackbody law well, as the temperature varies from 8000 K to 30 000 K, depending on the inert gas.

The curves in Fig. 40 result from Eqs. (65) or (66) with both intensity and temperature as free fit parameters. To put SBSL models to the test, these parameters have to be linked to the dynamics of bubble radius and temperature resulting from the model. Indeed, since there is no direct method for measuring the temperature, this is the only way to correctly deduce it. Unfortunately, we shall see that small differences in modeling can lead to large differences in light intensity.

As outlined in previous sections, there are various approaches to obtaining bubble dynamics and temperature, with varying degrees of sophistication and accuracy. A simple starting point is to assume a spatially homogeneous temperature $T(t)$ (see Sec. III.B). Specifically, we choose Eq. (38) to supplement the radius dynamics $R(t)$ derived from the modified Rayleigh-Plesset Eq. (20). The time dependence of R,T results, via Eq. (66), in a dynamics of the emitted power $P_\lambda^{Pl} d\lambda$ in the wavelength interval $[\lambda, \lambda + d\lambda]$, i.e., the temporal shape of the SBSL pulse as viewed through filters of different color.

Experiments observe wavelengths in the detectable range $\lambda_{uv} < \lambda < \lambda_r$, where $\lambda_{uv} \approx 200$ nm is the ultraviolet cutoff of the visible spectrum (due to the strong absorption of smaller-wavelength light in water or other liquids), and $\lambda_r \approx 800$ nm marks the red end of the visible spectrum, where the spectral radiance is already quite small and experimental noise begins to obscure the spectrum. In experiment, filters of a certain bandwidth $\Delta\lambda$ are used, e.g., $\Delta\lambda \approx 100$ nm by Gompf *et al.* (1997) and $\Delta\lambda \approx 40$ nm by Moran and Sweider (1998), or replaced by spectrographic means for higher resolution (Hiller *et al.*, 1998). It is easy to integrate Eq. (66) over the corresponding wavelength ranges and compare the prediction with light pulse measurements such as those in Fig. 13.

Figure 41 shows the result of this calculation for the argon bubble whose dynamics and transport behavior we have discussed previously (driven at $P_a = 1.3$ atm, ambient radius $R_0 = 5\ \mu$m). Using $R(t), T(t)$ from Fig. 27, the emission intensities are calculated for the ultraviolet wavelength regime ($200\ \text{nm} < \lambda < 300\ \text{nm}$), for the red part of the spectrum ($700\ \text{nm} < \lambda < 800\ \text{nm}$), and for the complete detectable spectral range ($200\ \text{nm} < \lambda < 800\ \text{nm}$). Figure 41(a) shows the predominance of ultraviolet emission.

A calculation like this allows for comparison of at least three characteristic quantities with experimental data:

(a) The intensity of the pulse. In this model, it is about two orders-of-magnitude larger than the experimental values for these driving parameters.
(b) The duration of the pulses. These are comparable to the turnaround time of bubble dynamics [not surprisingly, as $R(t)$ is directly translated into $P_\lambda^{Pl}(t)$], and is thus at least a factor of 2 longer than experiments.
(c) The wavelength dependence of the pulse width. The length of the pulse varies dramatically with wavelength, in direct contradiction to the experiments of Gompf *et al.* (1997). The "red" pulse duration is over 1000 ps, and thus more than twice that of the UV pulse.

Because of the considerable modeling uncertainties in bubble temperature (see Sec. III), the absolute values of pulse intensity and width produced by this model should not be considered quantitative predictions. Even though the discrepancies with experiment are very large, one could still imagine that they could be due to defects in the temperature modeling $T(t)$ or a change in the size of the light-emitting region (as in some shock models). However, the large wavelength dependence is an intrinsic problem with the blackbody model that is independent of the temperature law or the absolute value of temperature. Therefore experiments conclusively show that it is necessary to seek a modification of the blackbody model.

E. The SBSL bubble as thermal volume emitter

Which of the assumptions of the blackbody model fails? One basic prerequisite is that the radiation be of thermal origin, with $T(t)$ a well-defined temperature, i.e., local thermodynamic equilibrium must hold even over the short time scales of the bubble dynamics at collapse, which seems doubtful at first sight. However,

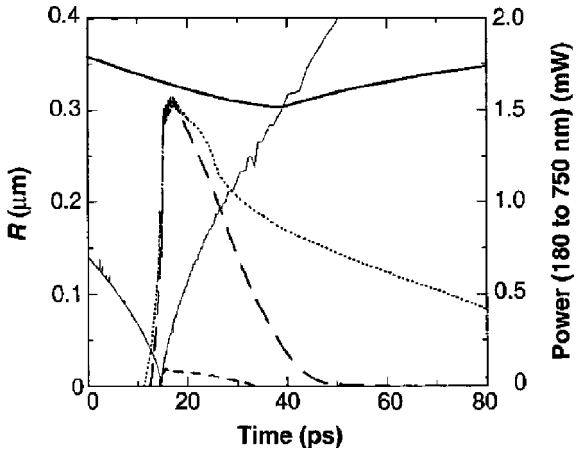

FIG. 42. Calculated power of light emission: dashed line, with plasma thermal conduction; dotted line, without plasma thermal conduction; short-dashed line, boundary line of the optically thick region of a nitrogen bubble; heavy solid line, the bubble radius; thin line, the shock front in the model. From Moss *et al.* (1997).

the immense particle densities ($n \sim 10^{28}$ m^{-3}) and high temperatures ($T \sim 10^4$ K) at bubble collapse create an environment in which collisions between particles are very frequent: a simple estimate suggests collision times well below a picosecond, so that local thermodynamic equilibrium is still well obeyed during SBSL light emission.

The other crucial assumption of the blackbody picture is that the bubble is *black*, i.e., it perfectly absorbs all wavelengths of electromagnetic radiation. This requires that the mean free path of photons (κ_λ^{-1}) be much smaller than the size of the object. Here κ_λ is the absorption coefficient for photons of wavelength λ (when divided by the gas density, κ_λ is often referred to as the opacity; see Unsöld and Baschek, 1991). A blackbody of extent (radius) R has $\kappa_\lambda R \gg 1$. The product $\tau_\lambda \equiv 2\kappa_\lambda R$ is the (dimensionless) *optical thickness* of the object at λ.

That opacity may play a role for sonoluminescence light emission had first been noted by Kamath *et al.* (1993), who speculated that radicals in the outer layers of the bubble "could resonantly absorb and scatter the radiation coming from the center thus shutting off the observed light. This effectiveness of resonant scattering in rendering gases effectively opaque is well known." Wu and Roberts (1993) also speculated that the compressed bubble might be a thermal volume emitter. Independently, Moss *et al.* (1994, 1997) discussed the possibility that the SBSL bubble might be transparent to its own photons. Using tabulated absorption coefficients of different gas species, they concluded that there was only a small region of opaque gas in the very center of the bubble (induced in their model by a converging shock wave), but that the rest of the bubble volume was characterized by $\tau_\lambda < 1$, and was thus *optically thin* (transparent). Figure 42 shows the line of demarcation between the optically thick and optically thin parts of the bubble. The emission volume of the optically thin shell is much larger than that of the optically thick core.

Moss *et al.* (1997) did not explicitly calculate pulses of emitted light at different wavelengths, and other features of their model lead to pulses that are much shorter than observed. However, the idea of a transparent bubble is the only proposition put forth to date that explains the wavelength independence of sonoluminescence radiation, and it is now widely accepted as a key ingredient to a consistent view of SBSL light emission. Models built on bubble transparency are sometimes referred to as "weakly ionized gas models" (Hammer and Frommhold, 2001), because a low degree of ionization of the gas is crucial (see below). We prefer the term *thermal volume emission*, as the radiation from the whole *volume* of a transparent body reaches the detector, rather than only the surface emission of a blackbody.

To illustrate that such a model leads to wavelength-independent emission spectra, we revert to the simple model discussed below, drawing $R(t)$ and $T(t)$ from Eqs. (20) and (38), respectively. For a volume emitter, the light intensity from a volume element of the bubble is dependent on the location inside the body (the depth s along the ray of vision to the element). Using the laws of absorption and emission in a medium (see, for example, Zel'dovich and Raizer, 1966, or Siegel and Howell, 1972),

$$I_\lambda(s,t) = I_\lambda^{Pl}[T(t)](1-\exp\{-\kappa_\lambda[T(t)]s\}),$$
$$0 < s < 2R \tag{67}$$

is the intensity at wavelength λ from a depth s, provided the temperature of the body is spatially uniform. Note that the source function of the emission is still I_λ^{Pl}, because local thermodynamic equilibrium is obeyed, and that for infinite absorption coefficient κ_λ, the Planck emissivity is recovered.

To obtain the spectral radiance, one must first integrate the intensity per surface area and per solid angle from Eq. (67) over the projected cross section of the bubble, the thickness s of the medium varying as $s = 2R\cos(\theta)$ with the angle θ from the line of view. The result is the emitted power from the whole bubble cross section per unit solid angle. Assuming isotropy of SBSL radiation, the spectral radiance is then

$$P_\lambda(t)d\lambda = 4\pi^2 R^2 I_\lambda^{Pl}[T(t)]\left(1+\frac{\exp(-2\kappa_\lambda R)}{\kappa_\lambda R} + \frac{\exp(-2\kappa_\lambda R)-1}{2\kappa_\lambda^2 R^2}\right)d\lambda. \tag{68}$$

Note that the Planck radiance (66) is now multiplied by a factor whose magnitude varies between 0 and 1, depending on the optical thickness $\tau_\lambda = 2\kappa_\lambda R$. As $\tau_\lambda \to \infty$, the Planck spectrum is recovered. In the transparent limit ($\tau_\lambda \ll 1$) the radiance reduces to

$$P_\lambda^{thin}(t)d\lambda = \frac{2}{3}\tau_\lambda P_\lambda^{Pl}[T(t)]d\lambda, \tag{69}$$

a spectral power that is much smaller than that for blackbody emission.

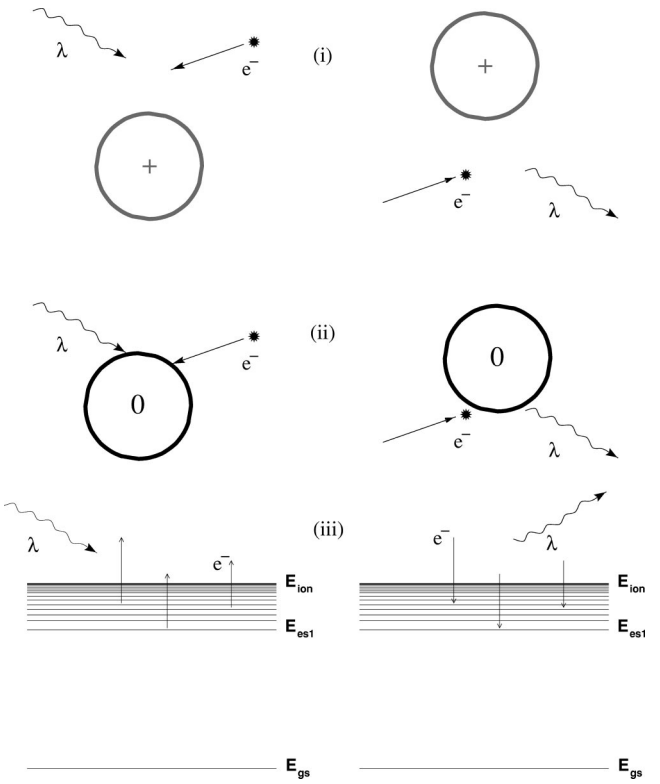

FIG. 43. Dominant photon absorption and emission processes at the typical temperatures and densities in a sonoluminescing bubble: left, absorption; right, emission. The three pairs of processes are (i) electron-ion (inverse) bremsstrahlung, (ii) electron-atom (inverse) bremsstrahlung, and (iii) photoionization/radiative recombination. Note the large gap between the ground-state energy (E_{gs}) and the first excited state (E_{es1}) in the term scheme of (iii).

1. Simple model for bubble opacity

To proceed further, we need to know how the absorption coefficients κ_λ depend on parameters. In contrast to the blackbody calculation, this requires identification of the most significant physical processes that contribute to photon absorption in the gas inside a sonoluminescing bubble. Now not only the temperature is relevant, but also the physics of photon-matter interaction. The original work of Moss *et al.* (1997) extrapolated tabulated values for κ_λ to the regime of the sonoluminescence experiments. Moss *et al.* (1999) used a full opacity model to extend these calculations. Here we summarize a simple model for κ_λ (Hilgenfeldt *et al.*, 1999a, 1999b; Hammer and Frommhold, 2001).

The model assumes that light emission predominantly stems from the ionization of a noble gas, and that neither molecular gases nor liquid vapor play a substantial role. If it is further assumed that the peak temperature is of order $\sim 10\,000$ K, the literature on absorption and emission of radiation (e.g., Zel'dovich and Raizer, 1966) suggests that there are three important processes, illustrated on the left-hand side of Fig. 43: the absorption of photons by (i) free electrons near ions (inverse bremsstrahlung), (ii) free electrons near neutral atoms (inverse neutral bremsstrahlung), and (iii) bound excited electrons that reach continuum energies after photon absorption (i.e., photoionization).

All three processes depend critically on the density of free electrons in the gas, which can be obtained from the Saha equation (Zel'dovich and Raizer, 1966; Unsöld and Baschek, 1991). At a temperature of $T \sim 10^4$ K, a noble gas such as argon is only weakly ionized. This is because $k_B T \ll E_{ion}$, the ionization energy of argon being $E_{ion} \approx 15.8$ eV. Zel'dovich and Raizer (1966) show that the degree of ionization $\alpha = n_e/n$ is then

$$\alpha[T] = \left(\frac{2\pi m_e k_B T}{h^2}\right)^{3/4} \left(\frac{2u_+}{n u_0}\right)^{1/2} \exp\left(-\frac{E_{ion}}{2k_B T}\right), \quad (70)$$

where m_e is the electron mass and u_+, u_0 are the statistical weights for the ionic and the neutral ground states, respectively. For argon SBSL bubbles α typically does not exceed 1%.

Note that, for the three processes mentioned above, the frequency of the electron-ion reaction (i) is proportional to α^2, while the two others are proportional to α alone. A small α thus seems to favor (ii) and (iii) as dominant, but the interaction cross section of electrons and ions is much larger than that for electrons and neutral atoms, which makes (i) an important factor for photon absorption.

Given α, the absorption coefficients for the processes (i)–(iii) can be calculated (Zel'dovich and Raizer, 1966) for ionized noble gas atoms. The evaluation of κ_λ for (iii) in principle requires knowledge of the complete atomic levels of the noble gas atom. Since the energy required for excitation to the first excited level is already a large fraction of the ionization energy (Fig. 43), the higher levels can be roughly approximated as part of a continuum of a hydrogenlike atom. In this limit, the only important parameter is the energy E_2 of the first excited level or, equivalently, the corresponding photon wavelength $\lambda_2 = hc/E_2$. Following Zel'dovich and Raizer (1966), one can show that the sum κ_λ^{ion} of the contributions to κ_λ from (i) and (iii) is

$$\kappa_\lambda^{ion}[T] = \frac{16\pi^2}{3\sqrt{3}} \frac{e^6 k_B T n}{(4\pi\varepsilon_0)^3 h^4 c^4} \lambda^3 \times \exp\left(-\frac{E_{ion} - hc/\max\{\lambda, \lambda_2\}}{k_B T}\right). \quad (71)$$

The contribution of electron-neutral atom inverse bremsstrahlung (ii) is rarely important in conventional plasma physics, where the degree of ionization is often high. For a weakly ionized SBSL gas, with the assumptions made above, it is often the dominant factor in κ_λ and can be written as (Zel'dovich and Raizer, 1966; Hilgenfeldt *et al.*, 1999b)

$$\kappa_\lambda^0[T] = 4 \frac{e^2}{4\pi\varepsilon_0} \frac{(2k_B T)^{9/4} n^{3/2}}{h^{3/2} c^3 m_e^{3/4} \pi^{3/4}} \lambda^2 \times \left(c_{tr} + \frac{d_{tr}}{3k_B T}\right) \exp\left(-\frac{E_{ion}}{2k_B T}\right). \quad (72)$$

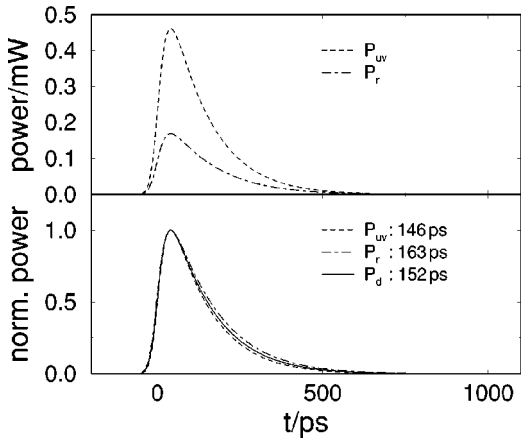

FIG. 44. Theoretically calculated light emission from a $R_0 = 5\ \mu$m SBSL bubble driven at $P_a = 1.3$ atm and $f = 20$ kHz under the assumption of thermal volume emission. We use $T(t)$ from Fig. 27, and Eq. (68) to evaluate the emission. (a) Absolute power; (b) relative power; line styles as in Fig. 41. The strong dependence of the pulse width on wavelength displayed in that figure is not present here, in agreement with experiments. The total power in the pulse is now much smaller. From Hilgenfeldt *et al.* (1999b).

Here, c_{tr} and d_{tr} are coefficients describing the electron-atom transport scattering cross section, extracted from Brown (1966). The accuracy of Eq. (72) is limited by its assumptions. Hammer and Frommhold (2000b, 2001) have evaluated the electron-neutral contribution using an *ab initio* quantum-mechanical calculation of the electron-atom scattering problem. At long wavelengths these calculations agree with the simple theory presented above, but at short wavelengths the quantum calculations are significantly more intense. The two approaches will be compared below.

2. Light emission and comparison with experiment

From Eqs. (71) and (72), the total absorption coefficient $\kappa_\lambda = \kappa_\lambda^0 + \kappa_\lambda^{ion}$ is obtained. The dimensionless optical thickness satisfies $\tau_\lambda < 1$ throughout the collapse for all wavelengths, and $\tau_\lambda \ll 1$ for the dominant ultraviolet part of the emission. Figure 44 presents the emission from such a bubble according to Eq. (68), using the same parameters that resulted in the blackbody emission displayed in Fig. 41.

Comparing with the blackbody calculation, it is seen, first, that the total intensity is reduced dramatically (to a few 10^5 photons per pulse). This is because the small optical thickness, by Eq. (69), leads to a drastic reduction of radiance compared to an opaque bubble. Second, the light pulses are now considerably shorter, and finally, the dependence of pulse width on wavelength has almost disappeared. All of these properties of the light pulse are now in much better agreement with those of experimentally observed SBSL pulses. Both the shorter pulse width and the wavelength independence are consequences of the exponential dependence of the degree of ionization on T in Eq. (70), which carries over to the SBSL radiance. Since $k_B T \ll E_{ion}$, this exponential "switch" is extremely sensitive to changes in T. Once the temperature has dropped only slightly as the bubble starts to reexpand, α and κ_λ are reduced severely. Consequently, the emission (69) is quenched rapidly (producing shorter pulse widths), *independent of wavelength*.

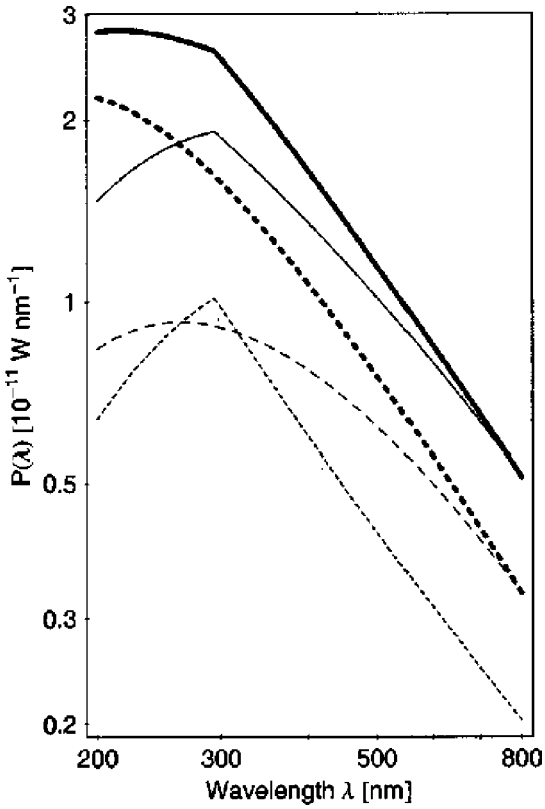

FIG. 45. Theoretical SBSL spectra for a $R_0 = 5\ \mu$m argon bubble driven at $P_a = 1.3$ atm and $f = 20$ kHz: heavy solid line, total spectrum calculated from first principles; thin solid line, spectrum calculated from the semiclassical model outlined in Sec. V.E; heavy and light dashed line, contribution of electron-neutral bremsstrahlung in the two models (more intense in the *ab initio* theory); dotted lines, electron-ion interaction contribution, the same for both approaches. From Hammer and Frommhold (2000a).

Equation (68) also yields reasonable results for the spectrum of the emission, although the spectra have a "kink" due to modeling assumptions of the atomic energy levels. Hammer and Frommhold (2000a) have extended the above calculations, using *ab initio* quantum mechanics. These calculations give a spectral shape more like the experiments for many parameter combinations (Fig. 45), with generally more intense radiation at the UV end of the spectrum, due to more intense electron-neutral bremsstrahlung.

It is also useful to examine the predictions of this model when the gas is changed from argon to, say, xenon. The spectrum is now much more intense (in agreement with observation) and has a maximum at $\lambda_2(\mathrm{Xe}) \approx 336$ nm, quite close to what is measured (Barber *et al.*, 1997). For xenon, with its lower ionization energy $E_{ion}(\mathrm{Xe}) \approx 12.1$ eV, the degree of ionization α can be as large as 10% (the temperatures obtained in argon and

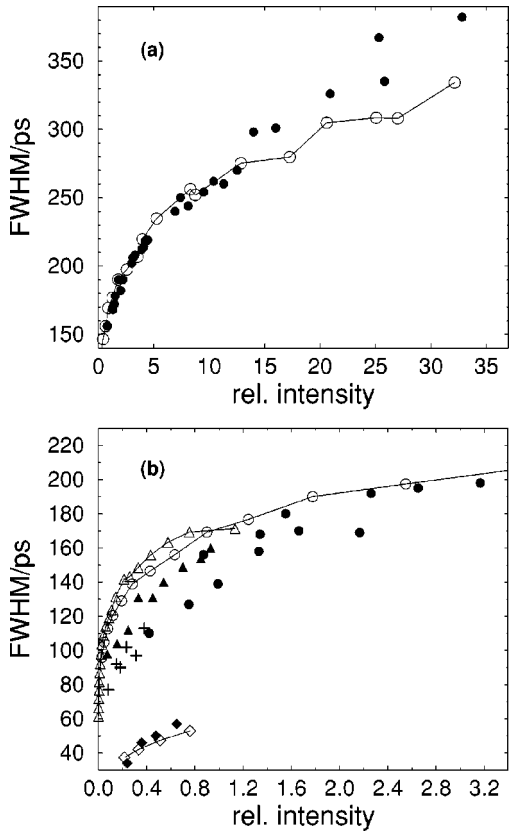

FIG. 46. Comparison of the theoretical results from the thermal volume emitter model of Hilgenfeldt *et al.* (1999b) to the experimental results of Hiller *et al.* (1998). The figure was modified from Hilgenfeldt *et al.* (1999a) to include the experimental results for helium (+). Filled symbols represent experiments using xenon (●), argon (▲), and air (◆) at the saturation concentrations displayed in the figure. Open symbols are theoretical results of the parameter-free theory of Hilgenfeldt *et al.* (1999b). (a) Higher light intensities and pulse widths of xenon bubbles; (b) lower-intensity data.

xenon bubbles are comparable). Consequently, the bubble is less transparent and its light emission more intense and more similar to those of a blackbody. As quantitatively shown by Hammer and Frommhold (2000b), xenon spectra display the characteristic kinked maximum at λ_2 in the quantum-mechanical version of the theory. This typical shape of the xenon spectrum was first understood by Moss *et al.* (1999).

Identifying the major contributions to the absorption coefficient automatically identifies the main light-emission mechanisms of SBSL. This follows from Kirchhoff's law, which states that every absorption process must balance a corresponding emission process—this is why P_λ in Eq. (68) grows with increasing absorption. Inverting the absorption events (i)–(iii) identifies SBSL light emission as a combination of (i) electron-ion bremsstrahlung, (ii) electron-neutral bremsstrahlung, and (iii) radiative recombination (see the right-hand side of Fig. 43). None of the three processes seems to be dominant over the whole range of the SBSL parameter space.

One possible absorption/emission process not discussed here is line emission (bound-bound-state transitions of electrons). Two sets of recent experiments have demonstrated that, in certain parameter regimes, line emission is important. We discuss these very recent results below in Sec. V.G (see also the Introduction).

We shall now use Eqs. (68), (71), and (72) to try a direct comparison with experimental results. To this end, a calculation for a single-parameter combination of P_a, R_0 is not useful, as the emission depends sensitively on these parameters, and their accuracy from experiment is not very high. However, a promising set of data was presented by Hiller *et al.* (1998), graphing the width of the light pulses vs their intensity. Both of these quantities can be measured reliably and with good accuracy. The experiments are conducted at a given relative concentration c_∞/c_0 of gas in the liquid, and the data points shown in Fig. 46 are a result of changing P_a through the whole range of stable SBSL under these conditions. The simple character of the light-emission model of Hilgenfeldt *et al.* (1999a, 1999b) allows one to first calculate the P_a, R_0 values for all stable SBSL bubbles at the given c_∞/c_0 (see, for example, Fig. 31) and then use these to calculate the light-emission intensities and pulse widths. Like the experimental data, the calculated light intensities were normalized by the intensities for a standard argon bubble. As P_a is increased in experiment, we follow the prescribed increase of R_0 for stable bubbles and consequently obtain larger, more strongly driven bubbles whose light pulses become longer and more intense. Without adjusting any fit parameters, the theoretical results are in close agreement with the data (Fig. 46) for both xenon and argon gases. Note that the observed close proximity of the width vs intensity curves for Xe and Ar [Fig. 46(b)] is reproduced, even though the P_a and R_0 are quite different for the two gases.

The data of Hiller *et al.* (1998) provide another check of the dissociation hypothesis discussed in Sec. IV.C. One of the data sets was obtained with strongly degassed air, which results in very small pulse widths and intensities [diamonds in Fig. 46(b)]. If the dissociation hypothesis is correct, these bubbles should not be air bubbles at $c_\infty/c_0 = 3\%$, but argon bubbles at $c_\infty/c_0 = 0.03\%$. The corresponding calculation indeed reproduces the experimental results.

The simple theory outlined above cannot reproduce the absolute light-emission intensities for every parameter combination. This should not be expected, since important factors such as the influence of water vapor on the bubble temperature are absent from this model. However, this kind of model does yield the correct relative intensities and their dependence on pulse width (Fig. 46), reasonable spectra (Fig. 45), and wavelength-independent pulse widths (Fig. 44). This agreement with experiment suggests that the essential physics is adequately represented and the concept of a bubble as a thermal volume emitter is probably correct (cf. also the extensive review of light-emission mechanisms by Hammer and Frommhold, 2001).

Even so, it should be emphasized that the good agreement between the model and experiment does not definitively settle the issue because a number of significant effects have not been included, in particular (i) the presence of water vapor and chemical reactions inside the bubble and (ii) the additional possibility of light emission from the molecular components of the gas (Didenko *et al.*, 2000b; Young *et al.*, 2001); again, water vapor may play an important role here. These and other processes could act to suppress or enhance the light emission, and to our knowledge no quantitative theory has incorporated all of these influences. In the theory formulated above, the number of photons is in reasonable agreement with the experiments, but it is entirely possible that this is because several neglected effects cancel each other out. The following section outlines some additions to the model that could affect the outcome of a light-emission calculation, and could lead to a more comprehensive model of SBSL radiation.

F. Modeling uncertainties: additional effects

The number of photons per oscillation cycle of sonoluminescence is the most conspicuous experimental observable; however, it is also the hardest to predict, in particular within a thermal volume emitter theory. The reason is that the light intensity depends exponentially on the temperature in the bubble [see Eq. (70)], which in turn depends strongly on modeling assumptions. The situation is illustrated in Fig. 23. What can be measured with good accuracy are the radius $R(t)$ and the radiance $P_\lambda(t)$ of SBSL light. Those two quantities are connected via the temperature $T(t)$ of the SBSL bubble, which up to now could not be experimentally measured. Therefore modeling is required both for obtaining $T(t)$ from $R(t)$ and for obtaining $P_\lambda(t)$ from $T(t)$. Both modeling steps depend on the assumptions entering the respective theories, and often the dependence is sensitive. We now review some of the most relevant sources of modeling uncertainties.

1. Bubble hydrodynamics

As discussed in Sec. III, any uncertainty in modeling the hydrodynamics and thus the temperature inside the bubble will be directly reflected in some uncertainty about the light emission. Since the work of Plesset and Prosperetti (1977), it has been popular to state that the temperature law is initially isothermal and then switches abruptly to adiabatic once the bubble accelerates sufficiently. There are slightly more sophisticated versions of this, e.g., the approximation used by Hilgenfeldt *et al.* (1999b) in which the polytropic exponent changes continuously. Precisely where the temperature law changes from isothermal to adiabatic strongly affects both the width of the pulse (since heating commences when this transition occurs) and the total number of photons emitted (since the transition controls the total amount of time for which heating occurs).

Storey and Szeri (2000) have performed full numerical simulations showing that these approximations are reasonably reliable for typical parameter combinations. However, to date there has not been a complete study of the full parameter space, documenting quantitatively the error in the simple models for the temperature. Without such an error estimate (as a function of parameters), it is difficult to assess how much of the current uncertainty about light-emission intensities comes from simple hydrodynamics.

2. Water vapor as emitter and quencher of light

As an example for the above-mentioned possibility of canceling errors of approximations connected with the two modeling steps in Fig. 23, we mention the role of water vapor in argon bubbles: In Sec. III we have shown how the consideration of vapor can drastically reduce the temperatures achieved inside the bubble, both because of the reduced polytropic exponent and because of the endothermic water dissociation. Because of the lower temperatures, less light should result. On the other hand, the reaction products of water (O and H) have an ionization potential ($\approx$13.6 eV for both species) very similar to that of argon, and therefore will also contribute to the light emission, increasing the photon output again.

SBSL experiments with helium bubbles illustrate the latter effect: The large ionization energy $E_{ion}^{\mathrm{He}} \approx 24.6$ eV, together with the exponential dependence of the photon absorption coefficient on the ratio of $E_{ion}/k_B T$, predicts negligible light emission from He, about four orders-of-magnitude dimmer than for Xe. Yet Barber *et al.* (1997) observed He bubbles to be only about a factor of 10 less bright than Xe (see data in Fig. 46). To a lesser degree, this discrepancy occurs for neon as well. The data of Barber *et al.* (1997) demonstrate that there is a pronounced decrease in SBSL intensity from the heavier to the lighter noble gas species in the order Xe$\rightarrow$Kr$\rightarrow$Ar, but Ne and He are not much different (in fact, He spectra are sometimes more intense than Ne spectra).

Moss (1998) pointed out that these observations can be accounted for when light emission from O and H radicals generated from dissociated water is considered. These species emit light much more readily than neon and helium, whose ionization energies are considerably higher. In a Ne or He bubble, the emission intensity of the dissociation products of water vapor overcomes the tiny contribution of the light noble gases and does not vary much between these two gases. Thus, as pointed out by Hilgenfeldt *et al.* (1999b), the light from Ne and He bubbles could originate from the vapor in the bubble rather than from the noble gas. The measurement of OH lines in the spectrum of a sonoluminescing bubble by Young *et al.* (2001) (see Sec. V.G below) supports this view, directly demonstrating light emission from water dissociation products.

Section III.A.3 detailed the important role of water vapor as a quencher for SBSL light. Through changes in polytropic exponent and endothermic chemical reactions, it can reduce the bubble temperature considerably,

as demonstrated by Yasui (1997a), Storey and Szeri (2000), and others. In bubbles consisting of heavier noble gases, this effect more than outweighs the role of water vapor as an emitter of light. Vazquez and Putterman (2000) have found a nice demonstration of this effect, in which two SBSL bubbles display almost indistinguishable $R(t)$ dynamics (very similar R_0 and P_a), but differ in light intensity by a factor of about 5 due to the different water-vapor pressures at different ambient temperatures.

3. Further difficulties in modeling the temperature

Temperature calculations that take into account chemical reactions suffer from considerable uncertainty, because the reaction rates of water-vapor chemistry are not well known under the extremely high densities and pressures achieved in the bubble. For example, as discussed in Sec. III.B.2 above, Toegel *et al.* (2002) took the reduction of the water dissociation rate caused by the high densities inside the bubble into consideration and got about 50% higher temperatures than Storey and Szeri (2000).

Another relevant effect may be the segregation of different species inside the bubble, which had been suggested by Storey and Szeri (1999). Yasui (2001) put forth this mechanism to account for the relative brightness of helium bubbles compared to what would be expected in a thermal volume emitter model with homogeneous distribution of all species. In a bubble with helium and water vapor, the lighter noble gas is driven towards the bubble center. A higher temperature could then be expected inside the bubble: First, the diffusive equilibrium condition changes, allowing for higher driving pressures; second, the water vapor accumulates near the (cool) wall of the bubble and therefore does not consume so much of the collapse energy by its endothermic dissociation; third, the condensation of water out of the bubble is also facilitated by this mass segregation (in a helium bubble), further helping to keep temperatures high.

4. Modifications of photon-emission processes

All the effects listed above concern modeling uncertainties on the $R(t) \rightarrow T(t)$ side of Fig. 23. On the other side, less work has been done to evaluate how much quantitative errors affect the simplifying assumptions introduced by the light-emission formulas (70), (71), and (72). The *ab initio* calculations of Hammer and Frommhold (2000a, 2000b) show encouraging agreement with this simpler model, but other effects could still play a role, in particular those associated with the extremely high densities in the compressed bubble.

The Saha equation may require corrections due to many-body effects (Chihara *et al.*, 1999), leading to different degrees of ionization and different absorption coefficients. Also, the term schemes and ionization potentials of the noble gas atoms could shift under a high density of electrons (Zel'dovich and Raizer, 1966). Hammer and Frommhold (2001) pointed out that the latter effect tends to enhance the light emission, because electron-electron interactions decrease the ionization potential. Thus more atoms get ionized, resulting in more light.

A quantitative modeling of the magnitude of these effects for the case of a sonoluminescing bubble has not yet been attempted. It would be valuable in order to assess where, in the two-step scheme of Fig. 23, the most important modeling errors are introduced.

5. Towards a more comprehensive model of SBSL light emission

How can we overcome the various modeling uncertainties? From our point of view the only way is to test the models through detailed experiments in a large parameter domain, varying not only the forcing pressure and the gas type and concentration (and therefore also the ambient radius), but also the water temperature and driving frequencies. Indeed, the experiments along these lines by Vazquez and Putterman (2000) at low temperature and those by Toegel, Gompf, *et al.* (2000) at low frequencies have demonstrated the relevance of liquid vapor.

Many more experiments of this type will be necessary to improve the models connecting $R(t)$ and $T(t)$, on the one hand, and $T(t)$ and $P_\lambda(t)$ on the other hand. Given the unusual conditions inside the bubble (in particular, the high pressure at low degree of ionization), this is a research direction whose benefits lie not only in explaining SBSL, but in elucidating the physical makeup of matter in a state that has not been studied in any detail before. Understood this way, the SBSL bubble is an ideal microlab for high-pressure/high-density hydrodynamics, chemistry, and plasma physics. The focus of the questions asked should perhaps shift from the nature of light-emission mechanisms (which, from our point of view, is now understood quite well) to more application-oriented problems.

If this model is able to capture the essential features of SBSL, no exotic "new physics" is necessary to explain the phenomenon. With classical hydrodynamics, dissociation chemistry, thermodynamics, and the theory of light absorption and emission in hot gases, well-known results from diverse fields now seem to be fitting into a consistent whole.

G. Line emission in SBSL

Line emission in multibubble sonoluminescence has long been known (Suslick, 1990; Flint and Suslick, 1991b); typically it originates from neutral hydroxyl radicals, or other molecular species present in the liquid. Until very recently, molecular lines had never been observed in single-bubble sonoluminescence. Two explanations were typically given for the absence of lines in single-bubble sonoluminescence: either the lines are broadened by the immense pressure inside the bubble and smeared over the whole visible spectrum, or the

continuum radiation is just much more intense than the lines, which are consequently "swamped" by the continuum spectrum.

Very recently, the groups of Suslick (Didenko *et al.*, 2000b) and Kang (Young *et al.*, 2001) have discovered parameter regimes in which there is line emission from single sonoluminescing bubbles. These were measured in situations where the bubble tended (i) to be unstable ("moving SBSL," in which the bubble gyrates around a pressure antinode of the ultrasound field) and (ii) to emit light rather weakly, close to the sonoluminescence threshold.

Didenko *et al.* (2000b) generated SBSL in various organic liquids such as adiponitrile, a liquid with very low vapor pressure (to keep the effective polytropic exponent high) and a chemical structure that results in dissociation products easily soluble in the liquid. In these respects, adiponitrile and other polar aprotic liquids resemble water. The choice of liquids by Didenko *et al.* (2000b) was guided by the theoretical findings that liquid vapor can be responsible for quenching SBSL (see Sec. III.A.3) and that the chemistry of dissociation products plays an important role in bubble stability (see Sec. IV.C).

Figure 19 shows the observed spectra from moving SBSL bubbles in adiponitrile. Didenko *et al.* (2000b) attribute the observed lines to excited species of CN, one of the groups that make up adiponitrile. It can be seen that the line-emission component of the spectra is very prominent at lower driving pressure amplitudes (and lower total emission intensities) and becomes undetectable as the driving pressure and the light intensity increase, until only the continuum part of the emission remains. This observation favors the idea of "swamped" spectral lines: at lower forcing, with lower temperatures in the bubble, the thermal bremsstrahlung processes (generating a continuum spectrum) are still weak, and the easily excited characteristic molecular emission from CN is strong enough to outshine the continuum. Higher driving generates higher temperatures and more ionization in the bubble, leading to bremsstrahlung emission much brighter than the contributions from lines, yielding the appearance of a pure continuum as observed for stable SBSL bubbles. While it is not clear to what extent the instability of the moving SBSL bubble in this experiment influences the relative intensity of the spectral lines (as compared to stable SBSL), this work is extremely important because it conclusively demonstrates that liquid-vapor chemistry occurs inside a single luminescing bubble.

Working independently, Young *et al.* (2001) found spectral lines for pure noble gases dissolved in water. The lines were present at low driving pressures, right at the onset pressure for sonoluminescence. The dissolved gas concentration was about 20%, which corresponds to unstable sonoluminescence for a pure noble gas, with "dancing" bubbles ejecting microbubbles (see Sec. IV.B). For pure argon dissolved in water, stable SBSL is not possible at the very low light intensities that are of interest here. To collect enough photons, Young *et al.* (2001) needed to develop methods for collecting reliable data from single bubbles for up to 5 days; the dimmest bubble they studied had an intensity more than three orders-of-magnitude smaller than a typical sonoluminescing bubble.

For bubbles with very low light intensity, spectral peaks were seen at both 310 nm and 337 nm (see Fig. 18). The 310-nm line is a clear signature of the vibrational/rotational bands in excited OH radicals. This experiment therefore provides the first direct experimental indication that there is water vapor in the bubble. The origin of the line at 337 nm is unclear; Young *et al.* (2001) conjecture that it could be due to another molecular excitation of OH.

When Young *et al.* (2001) increased the driving pressure, they observed, just as had Didenko *et al.* (2000b), that the continuum part of the spectrum became stronger relative to the line emission. They determined that, although the relative intensity of the lines decreases with increasing driving, the absolute line intensity still increases, again indicating that the reason spectral lines are not typically seen in single-bubble sonoluminescence is that they are overwhelmed by the continuum. Young *et al.* (2001) also used different noble gases and showed that the intensity of the 310-nm line increased with the molecular weight of the noble gas (Fig. 2 of that work), so that xenon had a more intense 310-nm emission than argon (the 337-nm line, however, seemed to be unaffected by the gas species). By lowering the temperature of the water, Young *et al.* (2001) observed that the intensity of the spectral lines increased. At 5 °C, additional lines appeared.

Another crucial issue was to determine precisely why the spectral lines were only observed in unstable or moving single-bubble sonoluminescence. Young *et al.* (2001) tried to find spectral lines in stable sonoluminescing bubbles, but did not succeed at the high driving pressures needed for stable SBSL, where the continuum part of the spectrum is always overwhelming. On the other hand, growth by rectified diffusion, followed by the ejection of microbubbles due to shape instabilities (Hilgenfeldt *et al.*, 1996) could lead to quantitatively different water-vapor content and different chemistry inside an unstable bubble as compared to a stable one. Again, a quantitative model of line emission would settle this question, predicting the range of parameters for which line emission can outshine the SBSL continuum.

Recent experimental results of Baghdassarian *et al.* (2001) on the spectra of single-cavitation bubble luminescence may help in developing such a model: Beyond a certain laser energy threshold, OH lines show up in the emitted spectra. The interpretation is that for large enough bubbles the collapse is aspherical, so that some fluid can enter the bubble. This interpretation of the single-cavitation bubbles thus provides a connection to the moving SBSL (Didenko *et al.*, 2000b), unstable SBSL (Young *et al.*, 2001), and MBSL (Matula *et al.*, 1995) spectra, which can also show lines.

VI. SUMMARY AND OUTLOOK

This review has presented current ideas about single-bubble sonoluminescence, emphasizing the most important physical processes that govern bubble behavior and light emission. A combination of different physical effects are important for the dynamics and thermodynamics that act over different time scales and, therefore, at different times during the bubble's oscillation. To summarize these effects, the beginning of this section follows an SBSL bubble through one oscillation cycle, indicating the most important phenomena at work. The second part of this section deals with unanswered questions in SBSL and possible applications of the new insights sonoluminescence research has allowed.

A. An SBSL bubble through its oscillation cycle

In Fig. 4, we have numbered the various parts of the oscillation cycle of a typical SBSL bubble containing argon in water [for definiteness, we use an example from Storey and Szeri (2000, 2001), with $R_0=4.5$ μm, driven at $f=26.5$ kHz and $P_a=1.2$ atm]. The cycle begins, by definition, when the driving pressure begins to dip into the negative half of its cycle, and the bubble is therefore allowed to expand. The surrounding liquid far from the bubble is degassed to some level and maintained at room temperature. Consequently, the bubble contains about 10^{10} argon atoms and about 2×10^8 water molecules at the outset.

(1) *Expansion*. The bubble expansion is comparatively slow and the growth is sustained for almost half a cycle (~15 μs). In this phase, the bubble is in both thermal and mass transfer equilibrium with the liquid. Because of the falling pressure inside the bubble, it gains large numbers of water-vapor molecules (evaporating from the wall) and also some gas molecules from the liquid.

(2) *Turnaround at maximum radius*. The driving pressure begins to increase again, and the expansion comes to a halt. At maximum radius ($R_{\max}\approx7R_0$), the bubble contains little more than the initial 10^{10} argon atoms, but has collected up to 10^{11} water molecules.

(3) *Rayleigh collapse*. As the external pressure increases, the inertial collapse of the liquid layers around the bubble begins. Even with the increased number of molecules, the internal pressure is still very low, and the collapse proceeds almost exactly like the classical collapse of an empty cavity treated by Lord Rayleigh (1917). The radius decreases quickly (over about 4 μs) from $R_{\max}$ to a value comparable to R_0. During this collapse, water vapor recondenses at the wall and the argon atoms again become the dominant species inside the bubble.

(4) *Decoupling of water vapor*. About 50 ns before the minimum radius is reached, the time scale of the bubble collapse ($\sim R/|\dot{R}|$) becomes smaller than the time scale for the diffusion of water vapor. The water vapor still left inside the bubble is now trapped until the reexpansion. Calculations show that about 20% water vapor should be mixed with the argon. Up to this moment, the polytropic exponent of the gas mixture has not increased significantly above 1, and the temperature has only risen to about 500 K.

(5) *Thermal decoupling*. Only ≈30 ns later, the accelerating bubble wall becomes fast enough that heat can no longer escape the bubble. Until reexpansion, the bubble is now thermally isolated from the liquid as well, and the polytropic exponent γ rises quickly to its adiabatic value. The latter is determined by the mixture of 80% Ar and 20% H_2O to $\gamma\approx1.6$. From now on, the temperature increases rapidly.

(6) *Onset of dissociation reactions*. Once the temperature exceeds roughly 4000 K, water-vapor molecules start dissociating into OH and H radicals. While the dissociation products have lower adiabatic exponents than H_2O, this endothermic reaction also consumes much energy and curbs the temperature rise. At this stage, faint molecular band light emission is a possibility.

(7) *Onset of light emission*. Despite the temperature-limiting influence of water vapor, about 10 000 K are finally reached in the bubble about 100 ps before maximum compression. At this temperature, a small fraction of the Ar as well as of the O and H atoms now present undergo ionization and release free electrons. The electrons interact with the ions and neutral atoms, and emission of electromagnetic radiation (thermal bremsstrahlung and radiative recombination) begins, which spans the spectrum of visible and ultraviolet wavelengths. Sonoluminescence is observed.

(8) *Maximum compression*. At this point, the gas density reaches (almost) solid-state values. The deceleration of the bubble wall down to zero speed has begun to enhance random shape perturbations (Rayleigh-Taylor instability) and leads to massive energy loss through acoustic wave emission. The temperature and light emission peak, helped by the high densities that prevent further endothermic dissociation reactions.

(9) *Reexpansion*. The bubble loses about 90% of its energy in the collapse, mostly due to acoustic emission. The reexpansion is much slower than the collapse. The Rayleigh-Taylor instability grows and may overwhelm a strongly driven bubble during this stage. Only a small increase in radius and decrease in temperature are sufficient to dramatically reduce the photon absorption coefficient and quench the light emission uniformly for all wavelengths, about 100–200 ps after it has begun. Subsequently, reaction chemistry stops and thermal as well as diffusive equilibria are reestablished.

(10) *Afterbounces*. The bubble rebounds to a much smaller size than the maximum radius before the main collapse, and for no parameter combination realized so far is there enough energy left to induce sonoluminescence during the afterbounces. The afterbounces provide a parametric excitation that can accumulate and render the bubble shape unstable. The radial motion is, however, damped rapidly until the driving pressure dips into its negative cycle once again, and the oscillation starts anew. Over the whole cycle, shape perturbations may have been enhanced (then the bubble is parametrically unstable), or a net gain or loss of gas may have

resulted (diffusive instability). In the correct parameter range, the bubble is stable with respect to both processes and continues to oscillate and emit light in exactly the same fashion.

The above 10 steps hold for SBSL bubbles in water with only argon (or any other noble gas) dissolved. If in addition molecular gases such as nitrogen and oxygen are dissolved, not only water dissociates at step 6, but also these gases (at around 7000 K for N_2 and O_2). The reaction products subsequently dissolve in water. "Cleaning" the bubble from molecular gases in this fashion can take thousands of cycles, as shown by Matula and Crum (1998).

B. Unanswered questions

Possible refinements of this simple picture abound. Detailed simulations of the bubble interior have been carried out (Moss *et al.*, 1997, 1999; Cheng *et al.*, 1998; Storey and Szeri, 1999), indicating that many effects could in principle play a role that were not mentioned in the above summary. Moss *et al.* (1997) include the possible existence of two temperatures for ions and electrons, as the collision rate of the atoms may not be sufficient to thermalize the electrons. They emphasize the importance of this effect for a proper modeling of heat exchange between the ionized gas and the exterior of the bubble. In the same work, shock waves have been computed, although Vuong and Szeri (1996) and Lin and Szeri (2001) showed that their formation is much delayed due to the entropy profiles inside the bubble. While it seems clear that shock waves are not necessary to explain SBSL light emission, they could lead to higher temperatures in an extremely small central region of the bubble.

Detailed models of the water-vapor chemistry in the bubble (Yasui, 1997a; Storey and Szeri, 2000) suffer from uncertainties in the reaction rates for even fundamental processes, as the peculiar conditions inside the bubble have not been probed in other experimental setups. Therefore, bubble temperature predictions from these reactions carry considerable uncertainty. More fundamental work is necessary here. A similar uncertainty concerns a more quantitative modeling of the bound-free contributions to the light emission, as the term schemes of the atoms involved could be substantially altered by the extreme densities.

Current models of sonoluminescence use simplified notions about the final stages of the bubble collapse. There are two classes of results for heat transfer: simple models, which extrapolate the point where the heat transfer transitions from isothermal to adiabatic from linear theory, and full simulations, which solve for the complete heat transfer numerically. The drawback of the latter approach is that it is not possible to span the entire SBSL parameter space with large numerical simulations, while the drawback of the former is that more approximations have to be made.

The quest for the ideal liquid for SBSL continues. Didenko *et al.* (2000b) showed that the peculiar combination of low vapor pressure and benign dissociation chemistry favors certain organic liquids. Attempts by Baghdassarian *et al.* (2000) to achieve SBSL in liquid noble gases (e.g., for a helium bubble in liquid argon) have not achieved higher levels of light intensity than those for the conventional case. One reason for this is the necessarily much lower temperature at which the bubble starts. If the compressive heating at comparable expansion ratios starts at, say, 10 K instead of 300 K, the peak temperature is automatically penalized by a factor of 30, even though the collapse heating itself may be more efficient.

Perhaps other liquids or environments can also be used to probe spectral ranges of the light emission outside the optical regime—the exact shape of the ultraviolet spectrum for light noble gases is still unknown, due to the strong absorption of those wavelengths in water (and most other liquids). Matula *et al.* (2001) have recently measured the near-infrared part of the spectra of SBSL and MBSL, confirming the thermal nature of the radiation.

One of the persistent puzzles in the research on MBSL is the origin of spectral lines from metal ions dissolved in the water (see Fig. 6). Do the metal ions get into the bubble at its asymmetric collapse? Or is the water around the bubble somehow playing a role in the light-emission process? At present, there are no answers to these questions.

We might also briefly mention here the possible effect of a strong magnetic field on sonoluminescing bubbles. While preliminary work by Young *et al.* (1996) suggested that this effect would be very pronounced, later findings by the same group revealed that the observed magnetic-field effect was mainly on the flask, and not on the bubble itself.

C. Scientific uses and spinoffs

One question arises naturally whenever SBSL is discussed: Is there an application for sonoluminescence? A commercial use of the light itself seems unlikely, given that only a fraction of $\sim 10^{-4}$ of the energy in a collapsing bubble ends up as visual photons. Sonoluminescence might provide illumination for certain photographs, e.g., in dentistry where ultrasound-driven devices are used (Leighton, 1994). But in most situations, illumination can easily be achieved by other means.

Grieser and Ashokkumar (2001) have recently shown that sonoluminescence can be used to excite fluorescent molecules to emit light themselves, often at much higher intensity, a process which those authors dubbed sonophotoluminescence. This form of emission due to external photoexcitation changes in the same fashion as the sonoluminescence signal, with changes in solution contents and solution concentration, and thus provides a true, amplified representation of the sonoluminescence intensity. Being closely associated with chemical reactions due to cavitation, sonoluminescence light can also serve as an indicator for sonochemistry (see below)

when light intensities and chemical reaction yields are correlated (Beckett and Hua, 2001).

D. Other applications of bubble dynamics and cavitation

With the consistent and rather simple picture that has now emerged, SBSL could well fulfill its promise as an exemplary, well-controlled system of cavitation physics. Sonochemistry, in particular, will profit from it. In sonochemistry, ultrasound (usually of low frequency) is used to enhance, assist, or induce chemical reactions that would not occur spontaneously—the ultrasound works like a catalyst (Mason and Lorimer, 1988; Suslick, 1990; Reisse *et al.*, 1999). Collapsing bubbles generate temperatures and pressures not easily achieved otherwise, and do so repeatedly over very short time scales. It is thus possible to induce unique reactions.

While it has been demonstrated that the presence of bubbles and cavitation is essential for sonochemistry, it is not clear at all where exactly the chemical reactions take place: in the interior of a collapsing bubble, at their surface, in a liquid layer around the bubble, or even at greater distances, mediated by the diffusion of primary reaction products from the bubble interior (Suslick, 1990). The situation is complicated by the presence of many bubbles, inhomogeneities in the sound field, and the proximity of vessel walls, which all favor asymmetric bubble collapses. The ensuing strong shape deformation and/or fragmentation of the bubbles enhance mixing between bubble exterior and interior, which makes the question of the reaction locus even more difficult to decide.

On the other hand, even if a large number of bubbles partake in the reaction catalysis, the yields of many sonochemical reactions are still woefully low (Reisse *et al.*, 1999). Some selected ultrasound-assisted processes of chemical technology are now approaching application on an industrial scale, e.g., waste water treatment (Russel, 1999). Nevertheless, the reaction efficiency will have to be enhanced before a more widespread use of sonochemistry is feasible. One approach to achieving higher yields is the search for an optimal frequency of the driving ultrasound (Beckett and Hua, 2001).

Just like sonochemistry, a great number of other fields rely crucially on the energy-focusing powers of collapsing bubbles: Materials science makes use not only of the high temperatures and pressures, but also of the tremendous cooling rate of reexpanding bubbles far in excess of 10^{10} K/s (see Suslick, 1995). These cooling rates are unmatched by any other technique, and allow for the fabrication of amorphous metal nanoclusters that prove to be highly effective catalysts, as shown by Suslick and Casadonte (1987).

In ultrasonic cleaning, the shear and pressure forces around collapsing bubbles are used to rid material surfaces of contaminations (see Leighton, 1994). If this surface erosion goes too far and affects the material properties, we speak of cavitation damage (Leighton, 1994; Brennen, 1995). Weninger, Cho, *et al.* (1997) observed that an isolated bubble sitting on a solid surface can even emit light. Ever since Lord Rayleigh's (1917) first study of cavitation was motivated by the study of cavitation damage on ship propellers, this has been a major driving force behind research on bubbles. A large industry is thus concerned with *avoiding* violent bubble collapses that can do damage by shear as well as with the shock waves they emit, or the thin, fast liquid jets ejected from asymmetrically collapsing bubbles (Blake *et al.*, 1997; Ohl *et al.*, 1998). Even when the forces are not too large, cavitation can simply disrupt laminar fluid flow, with serious consequences for applications such as fuel transport through valves and tubes or inkjet printing (Dijksman, 1999).

In biology, cavitation can occur spontaneously in water-transporting vessels in plants, which are often under high tension (Holbrook *et al.*, 2001). Another nice application of collapsing bubbles occurs for various species of "snapping shrimp" (*alpheus heterochaelis* and others), a shrimp whose most distinctive feature is one giant claw opposite a normal-sized one. This animal lives in large colonies that generate noise so loud that it disturbs submarine communication. It was believed that the noise is emitted when the giant claw rapidly closes and its two sides hit each other. However, Versluis *et al.* (2000) showed with the help of high-speed video and parallel sound detection that the origin of the noise in fact is a collapsing cavitation bubble: When rapidly closing the pair of scissors, the shrimp emits a thin water jet at such high speeds that a cavitation bubble develops. When the bubble collapses, sound is emitted in the form of a shock wave that stuns or even kills small prey. Very recently Lohse *et al.* (2001) showed that, at bubble collapse, not only sound but also a short light pulse (about 10^4 photons) gets emitted. They called the phenomenon "shrimpoluminescence."

Another example in which high water velocities lead to bubble cavitation is the converging fluid flow in a Venturi tube analyzed by Peterson and Anderson (1967) and later by Weininger *et al.* (1999). The bubbles cavitate as they flow through the device, and the resulting light emission from this device has many features in common with SBSL, for example, enhancement of emission using xenon instead of argon gas.

Some of the most promising applications lie in the field of medicine. More than 30 years ago, Gramiak and Shah (1968) had already suggested using micrometer-sized bubbles as contrast agents for ultrasound diagnostics. The bubbles are of resonant size for the MHz frequencies of diagnostic ultrasound, and therefore are extremely potent scatterers with cross sections several thousand times larger than their geometrical cross section (see Nishi, 1975). When injected intravenously, the bubbles allow for brighter images and higher contrast. The nonlinearity of bubble dynamics and the violent collapses help to increase the bubble response and imprint a distinctive signature onto the emitted sound, making it easier to distinguish bubble echoes from unwanted tissue reflections (de Jong and Hoff, 1993; Hilgenfeldt, Lohse, and Zomack, 1998; Frinking *et al.*, 1999). Yet even here the potential for various kinds of "cavitation

damage" has to be carefully assessed: mechanical damage to living tissue (Barnett, 1986), thermal hazard from the absorption of high-frequency sound in tissue and blood (Wu, 1998; Hilgenfeldt *et al.*, 2000), or chemical hazard from the sonochemical production of radicals inside the body (Barnett, 1986).

Medicine is also beginning to discover the benefits of cavitation damage, using bubbles as vehicles for *therapeutic* applications as well. It has recently been demonstrated by Tachibana *et al.* (1999) and others that the directed delivery of drugs as well as the transfection of genes through the wall of living cells is dramatically enhanced in the presence of ultrasound and microbubbles. Doubtless, one or several of the above-mentioned processes of cavitation damage are at work here to render the cell wall permeable for drugs and genes, but without permanently damaging the cell (in experiment, many cells appear healthy after treatment, as drugs are effective and genes are expressed). The exact mechanism remains to be uncovered.

E. Multibubble fields: in search of a theory

All of the applications mentioned in previous paragraphs will be feasible only if *many* bubbles undergo the described processes to focus the energy of the cavitation collapse where it is needed. Thus a theoretical description of sonochemistry or ultrasound diagnostics cannot rely entirely on what we have learned about single bubbles studying SBSL. Interactions between bubbles and their emitted sound fields will be very important above a certain volume fraction of gas, which may be as low as 10^{-5} (Marsh *et al.*, 1998). These interactions take on a plethora of different shapes, such as secondary Bjerknes forces (Brennen, 1995; Mettin *et al.*, 1997), bubble shadowing (Marsh *et al.*, 1998), collective bubble collapses (Brennen, 1995), or collective bubble translation (streamers; Akhatov *et al.*, 1996). In addition, multibubble applications always have to deal with the interaction of bubbles with boundaries, be they hard (as in materials science) or soft (as in biological and medical contexts). With the experimental observation and numerical simulation of jet cavitation in bubble collapses near a wall by Vogel and Lauterborn (1988a, 1988b), Vogel *et al.* (1989), Tomita and Shima (1990), Blake *et al.* (1997), Philipp and Lauterborn (1997), Lauterborn and Ohl (1998), Blake *et al.* (1998, 1999), Tong *et al.* (1999), Brujan *et al.* (2001a, 2001b), research in this complex area has only just begun.

Modeling the collapses of interacting bubbles in detail is very cumbersome, since the bubble motion is typically asymmetric, and the bubble interface can even change its topology. The liquid jet can penetrate the bubble that generated it, as seen in the famous photograph by Crum (1979). Clearly, a tractable theory cannot model each individual bubble in a cloud. The ultimate goal is a simple, effective-medium theory that describes the response of a bubble field hit by an intense sound wave (continuous or pulsed) in terms of field variables encoding the deposited energy density and its distribution. This goal still seems far ahead.

So for those with applications in mind, the original case of multibubble sonoluminescence from the 1930s (Frenzel and Schultes, 1934), deemed unimpressive and not very interesting, may in fact be the more challenging and rewarding task. Single-bubble sonoluminescence has taught us more about the astounding forces at work when a bubble collapses, and remains a beautiful and unique phenomenon. We now must show that we have learned enough to take this research program to the next, more general level.

ACKNOWLEDGMENTS

We thank all the colleagues with whom we had very fruitful collaborations and discussions over the years. Without them this work would not have been possible. We would like to name Robert Apfel, Bradley Barber, John Blake, Tom Chou, Lawrence Crum, Todd Dupont, Lothar Frommhold, Felipe Gaitan, Bruno Gompf, Franz Grieser, Siegfried Grossmann, Dominik Hammer, Glynn Holt, Joachim Holzfuss, Leo Kadanoff, Woowon Kang, Jeffrey Ketterling, Lou Kondic, Werner Lauterborn, Stefan Luther, Philip Marston, Thomas Matula, William McNamara, Michael Moran, William Moss, Claus-Dieter Ohl, David Oxtoby, Rainer Pecha, Andrea Prosperetti, Ruediger Toegel, Gabor Simon, Brian Storey, Kenneth Suslick, Andrew Szeri, Keith Weninger, Kyuichi Yasui, and Joseph Young.

M.B. acknowledges support from the National Science Foundation (NSF) Division of Mathematical Sciences and also from an NSF International Travel grant supporting this collaboration. The work is part of the research program of the Stichting voor Fundamenteel Onderzoek der Materie (FOM), which is financially supported by the Nederlandse Organisatie voor Wetenschappelijk Onderzoek (NWO).

REFERENCES

Akhatov, I., R. Mettin, C. D. Ohl, U. Parlitz, and W. Lauterborn, 1997, "Bjerknes force threshold for stable single bubble sonoluminescence," Phys. Rev. E **55**, 3747–3750.

Akhatov, I., U. Parlitz, and W. Lauterborn, 1996, "Towards a theory of self-organization phenomena in bubble-liquid mixtures," Phys. Rev. E **54**, 4990–5003.

Asaki, T. J., and P. L. Marston, 1997, "The effects of a soluble surfactant on quadrupole shape oscillations and dissolution of air bubbles in water," J. Acoust. Soc. Am. **102**, 3372–3377.

Ashokkumar, M., L. A. Crum, C. A. Frensley, F. Grieser, T. J. Matula, W. B. McNamara, and K. S. Suslick, 2000, "Effects of solutes on single-bubble sonoluminescence in water," J. Phys. Chem. **104**, 8462–8465.

Augsdörfer, U. H., A. K. Evans, and D. P. Oxley, 2000, "Thermal noise and the stability of single sonoluminescing bubbles," Phys. Rev. E **61**, 5278–5286.

Baghdassarian, O., H. C. Chu, B. Tabbert, and G. A. Williams, 2001, "Spectrum of luminescence from laser-created bubbles in water," Phys. Rev. Lett. **86**, 4934–4937.

Baghdassarian, O., B. Tabbert, and G. A. Williams, 1999, "Luminescence characteristics of laser-induced bubbles in water," Phys. Rev. Lett. **83**, 2437–2440.

Baghdassarian, O., B. Tabbert, and G. A. Williams, 2000, "Luminescence from laser-created bubbles in cryogenic liquids," Physica B **284-288**, 393–394.

Barber, B. P., R. Hiller, K. Arisaka, H. Fetterman, and S. Putterman, 1992, "Resolving the picosecond characteristics of synchronous sonoluminescence," J. Acoust. Soc. Am. **91**, 3061–3063.

Barber, B. P., R. A. Hiller, R. Löfstedt, S. J. Putterman, and K. R. Weninger, 1997, "Defining the unknowns of sonoluminescence," Phys. Rep. **281**, 65–143.

Barber, B. P., and S. J. Putterman, 1991, "Observation of synchronous picosecond sonoluminescence," Nature (London) **352**, 318–320.

Barber, B. P., K. Weninger, R. Lofstedt, and S. Putterman, 1995, "Observation of a new phase of sonoluminescence at low partial pressures," Phys. Rev. Lett. **74**, 5276–5279.

Barber, B. P., C. C. Wu, R. Lofstedt, P. H. Roberts, and S. J. Putterman, 1994, "Sensitivity of sonoluminescence to experimental parameters," Phys. Rev. Lett. **72**, 1380–1383.

Barnett, S., 1986, Ed., *Proceedings of the WFUMB Symposia on Safety of Ultrasound in Medicine 1994 and 1996*, in Ultrasound Med. Biol. Suppl. **24**, S1–S55 (Elsevier, London).

Baulch, D. L., *et al.*, 1972–1976, *Evaluated Kinetic Data for High Temperature Reactions* (Butterworths, London), Vols. 1–3.

Beckett, M. A., and I. Hua, 2001, "Impact of ultrasonic frequency on aqueous sonoluminescence and sonochemistry," J. Phys. Chem. A **105**, 3796–3802.

Bernstein, L., and M. Zakin, 1995, "Confined electron model for single bubble sonoluminescence," J. Phys. Chem. **99**, 14 619–14 627.

Bernstein, L., M. Zakin, E. Flint, and K. Suslick, 1996, "Cavitation thermochemistry using molecular and continuum sonoluminescence," J. Phys. Chem. **100**, 6612.

Birkhoff, G., 1954, "Note on Taylor instability," Q. Appl. Math. **12**, 306.

Bjerknes, V., 1909, *Die Kraftfelder* (Vieweg, Braunschweig).

Blake, F. G., 1949, Ph.D. thesis (Harvard University).

Blake, J. R., M. C. Hooton, P. B. Robinson, and R. P. Tong, 1997, "Collapsing cavities, toroidal bubbles and jet impact," Philos. Trans. R. Soc. London, Ser. A **355**, 537–550.

Blake, J. R., G. S. Keen, R. P. Tong, and M. Wilson, 1999, "Acoustic cavitation: the fluid dynamics of non-spherical bubbles," Philos. Trans. R. Soc. London, Ser. A **357**, 251–267.

Blake, J. R., Y. Tomita, and R. P. Tong, 1998, "The art, craft and science of modelling jet impact in a collapsing cavitation bubble," Appl. Sci. Res. **58**, 77–90.

Bogoyavlenskiy, V. A., 1999, "Differential criterion of a bubble collapse in viscous liquids," Phys. Rev. E **60**, 504–508.

Bourne, N. K., and J. E. Field, 1991, "Bubble collapse and the initiation of explosion," Proc. R. Soc. London, Ser. A **435**, 423–435.

Bowman, C. T., R. K. Hanson, D. F. Davidson, W. C. Gardiner, V. Lissianski, G. P. Smith, D. M. Golden, M. Frenklach, and M. Goldenberg, 1999, "GRI-mech 3.0 reaction rate coefficients," e-print http://www.me.berkeley.edu/gri_mech

Brennen, C. E., 1995, *Cavitation and Bubble Dynamics* (Oxford University, Oxford).

Brenner, M. P., T. F. Dupont, S. Hilgenfeldt, and D. Lohse, 1998, "Reply to comment by Putterman and Roberts," Phys. Rev. Lett. **80**, 3666; **80**, 3668.

Brenner, M. P., S. Hilgenfeldt, and D. Lohse, 1998, in *NATO Advanced Studies Institute on Sonoluminescence and Sonochemistry*, edited by L. Crum (Kluwer Academic, Dordrecht), pp. 165–182.

Brenner, M. P., S. Hilgenfeldt, and D. Lohse, 1999, in *Sonochemistry and Sonoluminescence*, edited by L. A. Crum, T. J. Mason, J. L. Reisse, and K. S. Suslick (Kluwer Academic, Dordrecht), pp. 165–182.

Brenner, M. P., S. Hilgenfeldt, D. Lohse, and R. R. Rosales, 1996, "Acoustic energy storage in single-bubble sonoluminescence," Phys. Rev. Lett. **77**, 3467–3470.

Brenner, M. P., D. Lohse, and T. F. Dupont, 1995, "Bubble shape oscillations and the onset of sonoluminescence," Phys. Rev. Lett. **75**, 954–957.

Brenner, M. P., D. Lohse, D. Oxtoby, and T. F. Dupont, 1996, "Mechanisms for stable single-bubble sonoluminescence," Phys. Rev. Lett. **76**, 1158–1161.

Brevik, I., V. N. Marachevsky, and K. A. Milton, 1999, "Identity of the van der Waals force and the Casimir effect and the irrelevance of these phenomena to sonoluminescence," Phys. Rev. Lett. **82**, 3948–3951.

Brown, S. C., 1966, *Basic Data of Plasma Physics* (MIT, Cambridge, MA).

Brujan, E.-A., K. Nahen, P. Schmidt, and A. Vogel, 2001a, "Dynamics of laser-induced cavitation bubbles near an elastic boundary," J. Fluid Mech. **433**, 251–281.

Brujan, E.-A., K. Nahen, P. Schmidt, and A. Vogel, 2001b, "Dynamics of laser-induced cavitation bubbles near elastic boundaries: influence of the elastic modulus," J. Fluid Mech. **433**, 283–314.

Carey, V. P., 1992, Ed., *Liquid-Vapor Phase Change Phenomena* (Hemisphere, Washington, D.C.).

Cheng, H. Y., M.-C. Chu, P. T. Leung, and L. Yuan, 1998, "How important are shock waves to single-bubble sonoluminescence?," Phys. Rev. E **58**, 2705–2708.

Chihara, J., Y. Ueshima, and S. Kiyokawa, 1999, "Nucleus-electron model for states changing from a liquid metal to a plasma and the Saha equation," Phys. Rev. E **60**, 3262–3272.

Chu, M.-C., and D. Leung, 1997, "Effects of thermal conduction in sonoluminescence," J. Phys.: Condens. Matter **9**, 3387–3397.

Colussi, A. J., and M. R. Hoffmann, 1999, "Vapor supersaturation in collapsing bubbles. Relevance to the mechanisms of sonochemistry and sonoluminescence," J. Phys. Chem. A **103**, 11 336–11 339.

Colussi, A. J., L. K. Weavers, and M. R. Hoffmann, 1998, "Chemical bubble dynamics and quantitative sonochemistry," J. Phys. Chem. A **102**, 6927–6934.

Cordry, S. M., 1995, Ph.D. thesis (University of Mississippi).

Crum, L. A., 1979, "Surface oscillations and jet development in pulsating air bubbles," J. Phys. Colloq. **40**, 285–288.

Crum, L. A., 1994, "Sonoluminescence," Phys. Today **47**, 22–29.

Crum, L. A., and G. T. Reynolds, 1985, "Sonoluminescence produced by 'stable' cavitation," J. Acoust. Soc. Am. **78**, 137–139.

de Jong, N., and L. Hoff, 1993, "Ultrasound scattering properties of albunex microspheres," Ultrasonics **31**, 175–181.

Didenko, Y. T., W. B. McNamara III, and K. S. Suslick, 1999, "Temperature of multibubble sonoluminescence in water," J. Phys. Chem. A **103**, 10 783–10 788.

Didenko, Y. T., W. B. McNamara III, and K. S. Suslick, 2000a, "Effect of noble gases on sonoluminescence temperatures during multibubble cavitation," Phys. Rev. Lett. **84**, 777–780.

Didenko, Y. T., W. B. McNamara III, and K. S. Suslick, 2000b, "Molecular emission from single-bubble sonoluminescence," Nature (London) **407**, 877–879.

Dijksman, J., 1999, "Hydro-acoustics of piezoelectrically driven ink-jet print heads," Flow, Turbul. Combust. **61**, 211–237.

Eames, I. W., N. J. Marr, and H. Sabir, 1997, "The evaporation coefficient of water: a review," Int. J. Heat Mass Transf. **40**, 2963–2973.

Eberlein, C., 1996a, "Sonoluminescence as quantum vacuum radiation," Phys. Rev. Lett. **76**, 3842–3845.

Eberlein, C., 1996b, "Theory of quantum radiation observed as sonoluminescence," Phys. Rev. A **53**, 2772–2787.

Eller, A., 1969, "Growth of bubbles by rectified diffusion," J. Acoust. Soc. Am. **46**, 1246–1250.

Eller, A., and L. A. Crum, 1970, "Instability of motion of a pulsating bubble in a sound field," J. Acoust. Soc. Am. Suppl. **47**, 762.

Eller, A., and H. G. Flynn, 1964, "Rectified diffusion during nonlinear pulsations of cavitation bubbles," J. Acoust. Soc. Am. **37**, 493–503.

Epstein, P. S., and M. S. Plesset, 1950, "On the stability of gas bubbles in liquid-gas solutions," J. Chem. Phys. **18**, 1505.

Evans, A. K., 1996, "Instability of converging shock waves and sonoluminescence," Phys. Rev. E **54**, 5004–5011.

Flint, E. B., and K. S. Suslick, 1989, "Sonoluminescence from nonaqueous liquids: emission from small molecules," J. Am. Chem. Soc. **111**, 6987–6992.

Flint, E. B., and K. S. Suslick, 1991a, "Sonoluminescence from alkali-metal salt solutions," J. Phys. Chem. **95**, 1484–1488.

Flint, E. B., and K. S. Suslick, 1991b, "The temperature of cavitation," Science **253**, 1397–1399.

Flynn, H. G., 1975a, "Cavitation dynamics. I. A mathematical formulation (in sound field)," J. Acoust. Soc. Am. **57**, 1379–1396.

Flynn, H. G., 1975b, "Cavitation dynamics. II. Free pulsations and models for cavitation bubbles," J. Acoust. Soc. Am. **58**, 1160–1170.

Frenkel', Y. I., 1940, Zh. Fiz. Khim. **14**, 305.

Frenzel, H., and H. Schultes, 1934, "Lumineszenz im ultraschall-beschickten Wasser," Z. Phys. Chem. Abt. B **27B**, 421–424.

Frinking, P. J. A., N. de Jong, and E. I. Cespedes, 1999, "Scattering properties of encapsulated gas bubbles at high ultrasound pressures," J. Acoust. Soc. Am. **105**, 1989–1996.

Frommhold, L., 1997, "Collision-induced emission at high temperatures and densities: Modeling of sonoluminescence spectra," Proc. SPIE **3090**, 272–276.

Frommhold, L., 1998, "Electron-atom bremsstrahlung and the sonoluminescence of rare gas bubbles," Phys. Rev. E **58**, 1899–1905.

Frommhold, L., and A. A. Atchley, 1994, "Is sonoluminescence due to collision-induced emission?," Phys. Rev. E **73**, 2883–2886.

Frommhold, L., and W. Meyer, 1997, *Spectral Line Shapes*, edited by M. Zoppi and L. Ulivi, AIP Conf. Proc. No. 386 (AIP, Woodbury, NY), pp. 471–484.

Fyrillas, M. M., and A. J. Szeri, 1994, "Dissolution or growth of soluble spherical oscillating bubbles," J. Fluid Mech. **277**, 381–407.

Fyrillas, M. M., and A. J. Szeri, 1995, "Dissolution or growth of soluble spherical oscillating bubbles—the effect of surfactants," J. Fluid Mech. **289**, 295–314.

Fyrillas, M. M., and A. J. Szeri, 1996, "Surfactant dynamics and rectified diffusion of microbubbles," J. Fluid Mech. **311**, 361–378.

Gaitan, D. F., 1990, Ph.D. thesis (The University of Mississippi).

Gaitan, D. F., A. A. Atchley, S. D. Lewia, J. T. Carlson, X. K. Maruyama, M. Moran, and D. Sweider, 1996, "Spectra of single-bubble sonoluminescence in water and glycerin-water mixtures," Phys. Rev. E **54**, 525–528.

Gaitan, D. F., and L. A. Crum, 1990, in *Frontiers of Nonlinear Acoustics. 12th ISNA*, edited by M. F. Hamilton and D. T. Blackstock (Elsevier Appl. Sci, London), pp. 459–463.

Gaitan, D. F., L. A. Crum, C. C. Church, and R. A. Roy, 1992, "Sonoluminescence and bubble dynamics for a single, stable, cavitation bubble," J. Acoust. Soc. Am. **91**, 3166–3183.

Gaitan, D. F., and G. Holt, 1998, "Nonlinear bubble dynamics and light emission in single-bubble sonoluminescence," J. Acoust. Soc. Am. **103**, 3046.

Gaitan, D. F., and R. G. Holt, 1999, "Experimental observations of bubble response and light intensity near the threshold for single bubble sonoluminescence in an air-water system," Phys. Rev. E **59**, 5495–5502.

Garcia, N., and A. Hasmy, 1998, "Theory of sonoluminescence in single bubbles: flexoelectric energy contribution," Pis'ma Zh. Eksp. Teor. Fiz. **66**, 442–448 [JETP Lett. **66**, 472 (1998)].

Garcia, N., and A. P. Levanyuk, 1996, "Sonoluminescence: a new electrical breakdown hypothesis," Pis'ma Zh. Eksp. Teor. Fiz. **64**, 849–852 [JETP Lett. **64**, 907–910 (1996)].

Garcia, N., A. P. Levanyuk, and V. V. Osipov, 1999, "Scenario of the electric breakdown and uv radiation spectra in single-bubble sonoluminescence," Pis'ma Zh. Eksp. Teor. Fiz. **70**, 417–421 [JETP Lett. **70**, 431–437 (1999)].

Gardiner, W. C., 1984, Ed., *Combustion Chemistry* (Springer, New York).

Gilmore, F. R., 1952, "The growth or collapse of a spherical bubble in a viscous compressible liquid," Hydrodynamics Laboratory, California Institute Technology, Pasadena, report 26-4.

Gompf, B., R. Gunther, G. Nick, R. Pecha, and W. Eisenmenger, 1997, "Resolving sonoluminescence pulse width with time-correlated single photon counting," Phys. Rev. Lett. **79**, 1405–1408.

Gompf, B., and R. Pecha, 2000, "Mie scattering from a sonoluminescing bubble with high spatial and temporal resolution," Phys. Rev. E **61**, 5253–5256.

Gong, C., and D. P. Hart, 1998, "Ultrasound induced cavitation and sonochemical yields," J. Acoust. Soc. Am. **104**, 2675–2682.

Gramiak, R., and P. M. Shah, 1968, "Echocardiography of the aortic root," Invest. Radiol. **3**, 356–366.

Greenspan, H. P., and A. Nadim, 1993, "On sonoluminescence of an oscillating gas bubble," Phys. Fluids A **5**, 1065–1067.

Grieser, F., and M. Ashokkumar, 2001, "The effect of surface active solutes on bubbles exposed to ultrasound," Adv. Colloid Interface Sci. **89-90**, 423–438.

Guderley, G., 1942, "Starke kugelige und zylindrische verdichtungsstösse in der nähe des kugelmittelpunktes bzw. der zylinderachse," Luftfahrtforschung **19**, 302.

Hammer, D., and L. Frommhold, 2000a, "Comment on 'sonoluminescence light emission' [Phys. Fluids **11**, 1318 (1999)]," Phys. Fluids **12**, 472–473.

Hammer, D., and L. Frommhold, 2000b, "Spectra of sonoluminescent rare-gas bubbles," Phys. Rev. Lett. **85**, 1326–1329.

Hammer, D., and L. Frommhold, 2001, "Sonoluminescence: how bubbles glow," J. Mod. Opt. **48**, 239–277.

Hao, Y., and A. Prosperetti, 1999a, "The dynamics of vapor bubbles in acoustic pressure fields," Phys. Fluids **11**, 2008–2019.

Hao, Y., and A. Prosperetti, 1999b, "The effect of viscosity on the spherical stability of oscillating gas bubbles," Phys. Fluids **11**, 1309–1317.

Harvey, E. N., 1939, J. Am. Ceram. Soc. **61**, 2392.

Herring, C., 1941, "Theory of the pulsations of the gas bubble produced by an underwater explosion," OSRD report 236.

Hickling, R., 1963, "Effects of thermal conduction in sonoluminescence," J. Acoust. Soc. Am. **35**, 967.

Hickling, R., 1994, "Transient, high-pressure solidification associated with cavitation in water," Phys. Rev. Lett. **73**, 2853.

Hilgenfeldt, S., M. P. Brenner, S. Grossmann, and D. Lohse, 1998, "Analysis of Rayleigh-Plesset dynamics for sonoluminescing bubbles," J. Fluid Mech. **365**, 171–204.

Hilgenfeldt, S., S. Grossmann, and D. Lohse, 1999a, "A simple explanation of light emission in sonoluminescence," Nature (London) **398**, 402–405.

Hilgenfeldt, S., S. Grossmann, and D. Lohse, 1999b, "Sonoluminescence light emission," Phys. Fluids **11**, 1318–1330.

Hilgenfeldt, S., S. Grossmann, and D. Lohse, 2001, "Cavitation science—is there a simple theory on sonoluminescence?" Nature (London) **409**, 783.

Hilgenfeldt, S., and D. Lohse, 1999, "Predictions for upscaling sonoluminescence," Phys. Rev. Lett. **82**, 1036–1039.

Hilgenfeldt, S., D. Lohse, and M. P. Brenner, 1996, "Phase diagrams for sonoluminescing bubbles," Phys. Fluids **8**, 2808–2826; **9**, 2462(E). The erratum presents higher print-quality figures.

Hilgenfeldt, S., D. Lohse, and W. C. Moss, 1998, "Water temperature dependence of single-bubble sonoluminescence," Phys. Rev. Lett. **80**, 1332–1335; **80**, 3164(E).

Hilgenfeldt, S., D. Lohse, and M. Zomack, 1998, "Response of bubbles to diagnostic ultrasound: a unifying theoretical approach," Eur. Phys. J. B **4**, 247–255.

Hilgenfeldt, S., D. Lohse, and M. Zomack, 2000, "Sound scattering and localized heat deposition of pulse-driven microbubbles," J. Acoust. Soc. Am. **107**, 3530.

Hiller, R., S. J. Putterman, and B. P. Barber, 1992, "Spectrum of synchronous picosecond sonoluminescence," Phys. Rev. Lett. **69**, 1182–1184.

Hiller, R., K. Weninger, S. J. Putterman, and B. P. Barber, 1994, "Effect of noble gas doping in single-bubble sonoluminescence," Science **266**, 248–250.

Hiller, R. A., and S. J. Putterman, 1995, "Observation of isotope effects in sonoluminescence," Phys. Rev. Lett. **75**, 3549–3551.

Hiller, R. A., S. J. Putterman, and K. R. Weninger, 1998, "Time-resolved spectra of sonoluminescence," Phys. Rev. Lett. **80**, 1090–1093.

Hinch, E. J., 1991, *Perturbation Methods* (Cambridge University, Cambridge).

Hirschfelder, J. O., C. F. Curtiss, and R. B. Bird, 1954, *Molecular Theory of Gases and Liquids* (Wiley, New York).

Holbrook, N. M., E. T. Ahrens, M. J. Burns, and M. A. Zwieniecki, 2001, "In vivo observation of cavitation and embolism repair using magnetic resonance imaging," Plant Physiol. **126**, 27–31.

Holt, R. G., and D. F. Gaitan, 1996, "Observation of stability boundaries in the parameter space of single-bubble sonoluminescence," Phys. Rev. Lett. **77**, 3791–3794.

Holzfuss, J., M. Rüggeberg, and A. Billo, 1998, "Shock-wave emissions of a sonoluminescing bubble," Phys. Rev. Lett. **81**, 5434–5437.

Holzfuss, J., M. Rüggeberg, and R. Mettin, 1998, "Boosting sonoluminescence," Phys. Rev. Lett. **81**, 1961–1964.

Horsburgh, S., 1990, Ph.D. thesis (University of Mississippi).

Jarman, P., 1959, "Measurements of sonoluminescence from pure liquids and some aqueous solutions," Proc. Phys. Soc. London **73**, 628–640.

Jarman, P., 1960, "Sonoluminescence: a discussion," J. Acoust. Soc. Am. **32**, 1459.

Kamath, V., A. Prosperetti, and F. N. Egolfopoulos, 1993, "A theoretical study of sonoluminescence," J. Acoust. Soc. Am. **94**, 248–260.

Keller, J. B., and I. I. Kolodner, 1956, "Damping of underwater explosion bubble oscillations," J. Appl. Phys. **27**, 1152–1161.

Keller, J. B., and M. J. Miksis, 1980, "Bubble oscillations of large amplitude," J. Acoust. Soc. Am. **68**, 628.

Ketterling, J. A., and R. E. Apfel, 1998, "Experimental validation of the dissociation hypothesis for single bubble sonoluminescence," Phys. Rev. Lett. **81**, 4991–4994.

Ketterling, J. A., and R. E. Apfel, 2000a, "Extensive experimental mapping of sonoluminescence parameter space," Phys. Rev. E **61**, 3832–3837.

Ketterling, J. A., and R. E. Apfel, 2000b, "Using phase space diagrams to interpret multiple frequency drive sonoluminescence," J. Acoust. Soc. Am. **107**, 819–826.

Kirkwood, J. G., and H. A. Bethe, 1942, "The pressure wave produced by an underwater explosion," OSRD report 558.

Kondic, L., J. I. Gersten, and C. Yuan, 1995, "Theoretical studies of sonoluminescence radiation: radiative transfer and parametric dependence," Phys. Rev. E **52**, 4976–4990.

Kuttruff, H., 1962, "Uber den Zusammenhang Zwischen Sonolumineszenz und der Schwingungskavitation in Flüssigkeiten," Acustica **12**, 230–254.

Lambrecht, A., M.-T. Jaekel, S. Reynaud, N. Garcia, A. P. Levanyuk, and C. Eberlein, 1997, "Comments on sonoluminescence as quantum vacuum radiation [and reply]," Phys. Rev. Lett. **78**, 2267–2270.

Landau, L. D., and E. M. Lifshitz, 1987, *Fluid Mechanics* (Pergamon, Oxford).

Lastman, G. J., and R. A. Wentzell, 1981, "Comparison of five models of spherical bubble response in an inviscid compressible liquid," J. Acoust. Soc. Am. **69**, 638.

Lastman, G. J., and R. A. Wentzell, 1982, "On two equations of radial motion of a spherical gas-filled bubble in a compressible liquid," J. Acoust. Soc. Am. **71**, 835.

Lauterborn, W., 1976, "Numerical investigation of nonlinear oscillations of gas bubbles in liquids," J. Acoust. Soc. Am. **59**, 283.

Lauterborn, W., and C.-D. Ohl, 1998, "The peculiar dynamics of cavitation bubbles," Appl. Sci. Res. **58**, 63–76.

Lauterborn, W., and E. Suchla, 1984, "Bifurcation superstructure in a model of acoustic turbulence," Phys. Rev. Lett. **53**, 2304–2307.

Leighton, T. G., 1994, *The Acoustic Bubble* (Academic, London).

Lentz, W. J., A. A. Atchley, and D. F. Gaitan, 1995, "Mie scattering from a sonoluminescing air bubble in water," Appl. Opt. **34**, 2648–2654.

Lepoint, T., F. Lepoint-Mullie, and A. Henglein, 1999, in *Sonochemistry and Sonoluminescence*, edited by L. A. Crum, T. J. Mason, J. L. Reisse, and K. S. Suslick (Kluwer Academic, Dordrecht), pp. 285–290.

Lepoint, T., D. D. Pauw, F. Lepoint-Mullie, M. Goldman, and A. Goldman, 1997, "Sonoluminescence: an alternative electrohydrodynamic hypothesis," J. Acoust. Soc. Am. **101**, 2012–2030.

Levshin, V. N., and S. N. Rzhevkin, 1937, Dokl. Akad. Nauk SSSR **16**, 407.

Lezzi, A., and A. Prosperetti, 1987, "Bubble dynamics in a compressible liquid. 2. Second-order theory," J. Fluid Mech. **185**, 289–321.

Lin, H., B. D. Storey, and A. J. Szeri, 2001, "Inertially driven inhomogeneities in violently collapsing bubbles: the validity of the Rayleigh-Plesset equation," J. Fluid Mech. **452**, 145–162.

Lin, H., and A. J. Szeri, 2001, "Shock formation in the presence of entropy gradients," J. Fluid Mech. **431**, 161–188.

Löfstedt, R., B. P. Barber, and S. J. Putterman, 1993, "Toward a hydrodynamic theory of sonoluminescence," Phys. Fluids A **5**, 2911–2928.

Löfstedt, R., K. Weninger, S. Putterman, and B. P. Barber, 1995, "Sonoluminescing bubbles and mass diffusion," Phys. Rev. E **51**, 4400–4410.

Lohse, D., M. P. Brenner, T. F. Dupont, S. Hilgenfeldt, and B. Johnston, 1997, "Sonoluminescing air bubbles rectify argon," Phys. Rev. Lett. **78**, 1359–1362.

Lohse, D., and S. Hilgenfeldt, 1997, "Inert gas accumulation in sonoluminescing bubbles," J. Chem. Phys. **107**, 6986–6997.

Lohse, D., B. Schmitz, and M. Versluis, 2001, "Snapping shrimp make flashing bubbles," Nature (London) **413**, 477–478.

Maas, U., and J. Warnatz, 1988, "Ignition processes in hydrogen-oxygen mixtures," Combust. Flame **74**, 53–69.

Margulis, M. A., 2000, "Sonoluminescence," Usp. Fiz. Nauk **170**, 263–287 [Sov. Phys. Usp. **43**, 259–282 (2000)].

Marinesco, N., and J. J. Trillat, 1933, "Action des ultrasons sur les plaques photographiques," Proc. R. Acad. Sci. Amsterdam **196**, 858–860.

Marsh, J. N., M. S. Hughes, C. S. Hall, S. H. Lewis, R. L. Trousil, G. H. Brandenburger, H. Levene, and J. G. Miller, 1998, "Frequency and concentration dependence of the backscatter coefficient of the ultrasound contrast agent albunex," J. Acoust. Soc. Am. **104**, 1654–1666.

Mason, T. J., and J. P. Lorimer, 1988, *Sonochemistry: Theory, Applications and Uses of Ultrasound in Chemistry* (Ellis Horwood, Chichester, UK).

Matsumoto, M., K. Miyamoto, K. Ohguchi, and T. Kinjo, 2000, "Molecular dynamics simulation of a collapsing bubble," Prog. Theor. Phys. Suppl. **138**, 728–729.

Matula, T. J., 1999, "Inertial cavitation and single-bubble sonoluminescence," Philos. Trans. R. Soc. London, Ser. A **357**, 225–249.

Matula, T. J., 2000, "Single-bubble sonoluminescence in microgravity," Ultrasonics **38**, 559–565.

Matula, T. J., S. M. Cordry, R. A. Roy, and L. A. Crum, 1997, "Bjerknes force and bubble levitation under single-bubble sonoluminescence conditions," J. Acoust. Soc. Am. **102**, 1522–1527.

Matula, T. J., and L. A. Crum, 1998, "Evidence for gas exchange in single-bubble sonoluminescence," Phys. Rev. Lett. **80**, 865–868.

Matula, T. J., J. Guan, L. A. Crum, A. L. Robinson, and L. W. Burgess, 2001, "Near-infrared emissions in single and multibubble sonoluminescence" Phys. Rev. E **64**, 026310.

Matula, T. J., I. M. Hallaj, R. O. Cleveland, L. A. Crum, W. C. Moss, and R. A. Roy, 1998, "The acoustic emissions from single-bubble sonoluminescence," J. Acoust. Soc. Am. **103**, 1377–1382.

Matula, T. J., R. A. Roy, P. D. Mourad, W. B. McNamara III, and K. S. Suslick, 1995, "Comparison of multibubble and single-bubble sonoluminescence spectra," Phys. Rev. Lett. **75**, 2602–2605.

McNamara, W. B., III, Y. T. Didenko, and K. S. Suslick, 1999, "Sonoluminescence temperatures during multi-bubble cavitation," Nature (London) **401**, 772–775.

Metten, B., and W. Lauterborn, 2000, in *Nonlinear Acoustics at the Turn of the Millennium*, edited by Werner Lauterborn and Thomas Kurz, AIP Conf. Proc. No. 524 (AIP, Melville, NY), pp. 429–432.

Mettin, R., I. Akhatov, U. Parlitz, C. D. Ohl, and W. Lauterborn, 1997, "Bjerknes forces between small cavitation bubbles in a strong acoustic field," Phys. Rev. E **56**, 2924–2931.

Meyer, E., and H. Kuttruff, 1959, "On the phase relation between sonoluminescence and the cavitation process with periodic excitation," Z. Angew. Phys. **11**, 325–333.

Milton, K. A., and Y. J. Ng, 1998, "Observability of the bulk Casimir effect: Can the dynamical Casimir effect be relevant to sonoluminescence?," Phys. Rev. E **57**, 5504–5510.

Mohanty, P., and S. V. Khare, 1998, "Sonoluminescence as a cooperative many-body phenomenon," Phys. Rev. Lett. **80**, 189–192.

Moran, M. J., R. E. Haigh, M. E. Lowry, D. R. Sweider, G. R. Abel, J. T. Carlson, S. D. Lewia, A. A. Atchley, D. F. Gaitan, and X. K. Maruyama, 1995, "Direct observations of single sonoluminescence pulses," Nucl. Instrum. Methods Phys. Res. B **96**, 651–656.

Moran, M. J., and D. Sweider, 1998, "Measurements of sonoluminescence temporal pulse shape," Phys. Rev. Lett. **80**, 4987–4990.

Moss, W., 1998 (private communication).

Moss, W. C., 1997, "Understanding the periodic driving pressure in the Rayleigh-Plesset equation," J. Acoust. Soc. Am. **101**, 1187–1190.

Moss, W. C., 2000, "Comment on extreme electrostatic phenomena in a single sonoluminescing bubble," Phys. Rev. Lett. **85**, 4837 (C).

Moss, W. C., D. B. Clarke, J. W. White, and D. A. Young, 1994, "Hydrodynamic simulations of bubble collapse and picosecond sonoluminescence," Phys. Fluids **6**, 2979–2985.

Moss, W. C., D. B. Clarke, J. W. White, and D. A. Young, 1996, "Sonoluminescence and the prospects for table-top microthermonuclear fusion," Phys. Lett. A **211**, 69–74.

Moss, W. C., D. B. Clarke, and D. A. Young, 1997, "Calculated pulse widths and spectra of a single sonoluminescing bubble," Science **276**, 1398–1401.

Moss, W. C., D. A. Young, J. A. Harte, J. L. Levatin, B. F. Rozsnyai, G. B. Zimmerman, and I. H. Zimmerman, 1999, "Computed optical emissions from a sonoluminescing bubble," Phys. Rev. E **59**, 2986–2992.

Nayfeh, A. H., and D. T. Mook, 1979, *Nonlinear Oscillations* (Wiley, New York).

Negishi, K., 1961, "Experimental studies on sonoluminescence and ultrasonic cavitation," J. Phys. Soc. Jpn. **16**, 1450–1465.

Neppiras, E. A., 1980, "Acoustic cavitation," Phys. Rep. **61**, 159–251.

Nishi, R. Y., 1975, "The scattering and absorption of sound waves by a gas bubble in a viscous liquid," Acustica **33**, 65–74.

Noltingk, B. E., and E. A. Neppiras, 1950, "Cavitation produced by ultrasonics," Proc. Phys. Soc. London, Sect. B **63**, 674.

O'Connor, D. V., and D. Phillips, 1984, Eds., *Time-Correlated Single Photon Counting* (Academic, New York).

Ohl, C.-D., 2000, "Luminescence from acoustic-driven laser-induced cavitation bubbles," Phys. Rev. E **61**, 1497–1500.

Ohl, C. D., O. Lindau, and W. Lauterborn, 1998, "Luminescence from spherically and aspherically collapsing laser induced bubbles," Phys. Rev. Lett. **80**, 393–396.

Pecha, R., and B. Gompf, 2000, "Microimplosions: Cavitation collapse and shock wave emission on a nanosecond time scale," Phys. Rev. Lett. **84**, 1328–1330.

Pecha, R., B. Gompf, G. Nick, Z. Q. Wang, and W. Eisenmenger, 1998, "Resolving the sonoluminescence pulse shape with a streak camera," Phys. Rev. Lett. **81**, 717–720.

Peterson, F. B., and T. P. Anderson, 1967, "Light emission from hydrodynamic cavitation," Phys. Fluids **10**, 874–879.

Phillipp, A., and W. Lauterborn, 1997, "Damage of solid surfaces by single laser-produced cavitation bubbles," Acust. Acta Acust. **83**, 223–227.

Plesset, M., 1949, "The dynamics of cavitation bubbles," J. Appl. Mech. **16**, 277.

Plesset, M., 1954, "On the stability of fluid flows with spherical symmetry," J. Appl. Phys. **25**, 96.

Plesset, M. S., and T. P. Mitchell, 1956, "On the stability of the spherical shape of a vapor cavity in a liquid," Q. Appl. Math. **13**, 419–430.

Plesset, M. S., and A. Prosperetti, 1977, "Bubble dynamics and cavitation," Annu. Rev. Fluid Mech. **9**, 145–185.

Plesset, M. S., and S. A. Zwick, 1952, "The growth of vapor bubbles in superheated liquids," J. Appl. Phys. **23**, 95.

Prosperetti, A., 1974, "Nonlinear oscillations of gas bubbles in liquids: steady-state solutions," J. Acoust. Soc. Am. **56**, 878–885.

Prosperetti, A., 1975, "Nonlinear oscillations of gas bubbles in liquids: transient solutions and the connection between subharmonic signal and cavitation," J. Acoust. Soc. Am. **57**, 810–821.

Prosperetti, A., 1977a, "Current topics in the dynamics of gas and vapor bubbles," Meccanica **12**, 214–235.

Prosperetti, A., 1977b, "On the stability of spherically symmetric flows," Atti Accad. Naz. Lincei, Cl. Sci. Fis., Mat. Nat., Rend. **62**, 196.

Prosperetti, A., 1977c, "Thermal effects and damping mechanisms in the forced radial oscillations of gas bubbles in liquid," J. Acoust. Soc. Am. **61**, 17–27.

Prosperetti, A., 1977d, "Viscous effects on perturbed spherical flows," Q. Appl. Math. **34**, 339–350.

Prosperetti, A., 1991, "The thermal behavior of oscillating gas bubbles," J. Fluid Mech. **222**, 587.

Prosperetti, A., 1997, "A new mechanism for sonoluminescence," J. Acoust. Soc. Am. **101**, 2003–2007.

Prosperetti, A., 1998, in *NATO Advanced Studies Institute on Sonoluminescence and Sonochemistry*, edited by L. Crum (Kluwer Academic, Dordrecht), pp. 39–62.

Prosperetti, A., L. A. Crum, and K. W. Commander, 1988, "Nonlinear bubble dynamics," J. Acoust. Soc. Am. **83**, 502–514.

Prosperetti, A., and Y. Hao, 1999, "Modelling of spherical gas bubble oscillations and sonoluminescence," Philos. Trans. R. Soc. London, Ser. A **357**, 203–223.

Prosperetti, A., and A. Lezzi, 1986, "Bubble dynamics in a compressible liquid. I. First-order theory," J. Fluid Mech. **168**, 457–478.

Putterman, S., P. G. Evans, G. Vazquez, and K. Weninger, 2001, "Cavitation science—is there a simple theory on sonoluminescence?" Nature (London) **409**, 782.

Putterman, S. J., and P. H. Roberts, 1998, "Comment on 'bubble shape oscillations and the onset of sonoluminescence' [Phys. Rev. Lett. **75**, 954 (1995)]," Phys. Rev. Lett. **80**, 3666–3668.

Putterman, S. J., and K. R. Weninger, 2000, "Sonoluminescence: How bubbles turn sound into light," Annu. Rev. Fluid Mech. **32**, 445–476.

Rayleigh, L., 1917, "On the pressure developed in a liquid during the collapse of a spherical cavity," Philos. Mag. **34**, 94–98.

Reid, R. C., J. M. Prausnitz, and B. E. Poling, 1987, Eds., *Properties of Gases and Liquids* (McGraw-Hill, New York).

Reisse, J., T. Caulier, C. Deckerkheer, Y. Kegelaers, N. Segebarth, and K. Bartik, 1999, in *Sonochemistry and Sonoluminescence*, edited by L. A. Crum, T. J. Mason, J. L. Reisse, and K. S. Suslick (Kluwer Academic, Dordrecht), pp. 205–224.

Russell, J. P., 1999, in *Sonochemistry and Sonoluminescence,* edited by L. A. Crum, T. J. Mason, J. L. Reisse, and K. S. Suslick (Kluwer Academic, Dordrecht), pp. 372–376.

Saksena, T. K., and W. L. Nyborg, 1970, "Sonoluminescence from stable cavitation," J. Chem. Phys. **53**, 1722–1734.

Schwinger, J., 1992, "Casimir energy for dielectrics: spherical geometry," Proc. Natl. Acad. Sci. U.S.A. **89**, 11 118.

Sehgal, C., R. G. Sutherland, and R. E. Verrall, 1980, "Optical spectra of sonoluminescence from transient and stable cavitation in water saturated with various gases," J. Phys. Chem. **84**, 388–395.

Siegel, R., and J. R. Howell, 1972, *Thermal Radiation Heat Transfer* (McGraw-Hill, New York).

Simon, G., I. Csabai, A. Horvath, and F. Szalai, 2001, "Sonoluminescence and phase diagrams of single bubbles at low dissolved air concentration," Phys. Rev. E **63**, 026301.

Storey, B. D., and A. J. Szeri, 1999, "Mixture segregation within sonoluminescence bubbles," J. Fluid Mech. **396**, 203–221.

Storey, B. D., and A. J. Szeri, 2000, "Water vapour, sonoluminescence and sonochemistry," Proc. R. Soc. London, Ser. A **456**, 1685–1709.

Storey, B. D., and A. J. Szeri, 2001, "A reduced model of cavitation physics for use in sonochemistry," Proc. R. Soc. London, Ser. A **457**, 1685–1700.

Strube, H. W., 1971, "Numerical investigations on the stability of bubbles oscillating nonspherically," Acustica **25**, 289–303.

Suslick, K. S., 1990, "Sonochemistry," Science **247**, 1439–1445.
Suslick, K. S., 1995, "Applications of ultrasound to materials chemistry," MRS Bull. **20**, 29.
Suslick, K. S., and D. J. Casadonte, 1987, "Heterogeneous sonocatalysis with nickel powder," J. Am. Chem. Soc. **109**, 3459–3461.
Suslick, K. S., and E. B. Flint, 1987, "Sonoluminescence from non-aqueous liquids," Nature (London) **330**, 553–555.
Suslick, K. S., D. A. Hammerton, and R. E. Cline, Jr., 1986, "The sonochemical hot spot," J. Am. Chem. Soc. **108**, 5641–5642.
Tachibana, K., T. Uchida, N. Yamashita, and K. Tamura, 1999, "Induction of cell-membrane porosity by ultrasound," Lancet **353**, 1409.
Toegel, R., B. Gompf, R. Pecha, and D. Lohse, 2000, "Does water vapor prevent upscaling sonoluminescence?," Phys. Rev. Lett. **85**, 3165–3168.
Toegel, R., S. Hilgenfeldt, and D. Lohse, 2000, "The effect of surfactants on single bubble sonoluminescence," Phys. Rev. Lett. **84**, 2509–2512.
Toegel, R., S. Hilgenfeldt, and D. Lohse, 2002, "Suppressing dissociation in sonoluminescing bubbles: The effect of excluded volume," Phys. Rev. Lett. **88**, 034301.
Tomita, Y., and A. Shima, 1990, "High-speed photographic observations of laser-induced cavitation bubbles in water," Acustica **71**, 161–171.
Tong, R. R., W. P. Schiffers, S. J. Shaw, J. R. Blake, and D. C. Emmony, 1999, "The role of 'splashing' in the collapse of a laser-generated cavity near a rigid boundary," J. Fluid Mech. **380**, 339–361.
Trilling, L., 1952, "The collapse and rebound of a gas bubble," J. Appl. Phys. **23**, 14–17.
Unnikrishnan, C. S., S. Mukhopadhyay, and C. Eberlein, 1996, "Comment on 'sonoluminescence as quantum vacuum radiation' [and reply]," Phys. Rev. Lett. **77**, 4690–4691.
Unsöld, A., and B. Baschek, 1991, *The New Cosmos* (Springer, New York).
Vacca, G., R. D. Morgan, and R. B. Laughlin, 1999, "Differential light scattering: Probing the sonoluminescence collapse," Phys. Rev. E **60**, 6303–6306.
Vazquez, G. E., and S. J. Putterman, 2000, "Temperature and pressure dependence of sonoluminescence," Phys. Rev. Lett. **85**, 3037–3040.
Verral, R. E., and C. M. Sehgal, 1988, in *Sonoluminescence in Ultrasound: Its Chemical, Physical and Biological Effects*, edited by K. Suslick (VCH, Weinheim), p. 227.
Versluis, M., A. v. d. Heydt, B. Schmitz, and D. Lohse, 2000, "How snapping shrimp snap: through cavitating bubbles," Science **289**, 2114–2117.
Vogel, A., and W. Lauterborn, 1988a, "Time-resolved particle image velocimetry applied to the investigation of cavitation bubble dynamics," Proc. SPIE **814**, 711–719.
Vogel, A., and W. Lauterborn, 1988b, "Time-resolved particle image velocimetry used in the investigation of cavitation bubble dynamics," Appl. Opt. **27**, 1869–1876.
Vogel, A., W. Lauterborn, and R. Timm, 1989, "Optical and acoustic investigations of the dynamics of laser-produced cavitation bubbles near a solid boundary," J. Fluid Mech. **206**, 299–338.
Vuong, V. Q., M. M. Fyrillas, and A. J. Szeri, 1998, "The influence of liquid temperature on the sonoluminescence hot spot," J. Acoust. Soc. Am. **104**, 2073–2076.
Vuong, V. Q., and A. J. Szeri, 1996, "Sonoluminescence and diffusive transport," Phys. Fluids **8**, 2354–2364.
Vuong, V. Q., A. J. Szeri, and D. A. Young, 1999, "Shock formation within sonoluminescence bubbles," Phys. Fluids **11**, 10–17.
Walton, A. J., and G. T. Reynolds, 1984, "Sonoluminescence," Adv. Phys. **33**, 595–600.
Wang, Z. Q., R. Pecha, B. Gompf, and W. Eisenmenger, 1999, "Single bubble sonoluminescence: Investigations of the emitted pressure wave with a fiber optic probe hydrophone," Phys. Rev. E **59**, 1777–1780.
Weninger, K. R., B. P. Barber, and S. J. Putterman, 1997, "Pulsed Mie scattering measurements of the collapse of a sonoluminescing bubble," Phys. Rev. Lett. **78**, 1799–1802.
Weninger, K. R., C. G. Camara, and S. J. Putterman, 1999, "Energy focusing in a converging fluid flow: implications for sonoluminescence," Phys. Rev. Lett. **83**, 2081–2084.
Weninger, K. R., H. Cho, R. A. Hiller, S. J. Putterman, and G. A. Williams, 1997, "Sonoluminescence from an isolated bubble on a solid surface," Phys. Rev. E **56**, 6745–6749.
Weninger, K. R., P. G. Evans, and S. J. Putterman, 2000, "Time correlated single photon Mie scattering from a sonoluminescing bubble," Phys. Rev. E **61**, 1020–1023.
Weninger, K. R., R. A. Hiller, B. P. Barber, D. Lacoste, and S. J. Putterman, 1995, "Sonoluminescence from single bubbles in nonaqueous liquids—new parameter space for sonochemistry," J. Phys. Chem. **99**, 14 195.
Wu, C. C., and P. H. Roberts, 1993, "Shock-wave propagation in a sonoluminescing gas bubble," Phys. Rev. Lett. **70**, 3424–3427.
Wu, C. C., and P. H. Roberts, 1994, "A model of sonoluminescence," Proc. R. Soc. London, Ser. A **445**, 323–349.
Wu, C. C., and P. H. Roberts, 1998, "Bubble shape instability and sonoluminescence," Phys. Lett. A **250**, 131–136.
Wu, J., 1998, "Temperature rise generated by ultrasound in the presence of contrast agent," Ultrasound Med. Biol. **24**, 267–274.
Xu, N., L. Wang, and X. Hu, 1998, "Numerical study of electronic impact and radiation in sonoluminescence," Phys. Rev. E **57**, 1615–1620.
Xu, N., L. Wang, and X. Hu, 1999, "Extreme electrostatic phenomena in a single sonoluminescing bubble," Phys. Rev. Lett. **83**, 2441–2444.
Yasui, K., 1995, "Effects of thermal conduction on bubble dynamics near the sonoluminescence threshold," J. Acoust. Soc. Am. **98**, 2772–2782.
Yasui, K., 1997a, "Alternative model of single-bubble sonoluminescence," Phys. Rev. E **56**, 6750–6760.
Yasui, K., 1997b, "Chemical reactions in a sonoluminescing bubble," J. Phys. Soc. Jpn. **66**, 2911–2920.
Yasui, K., 2001, "Single-bubble sonoluminescence from noble gases," Phys. Rev. E **63**, 035301.
Young, D. A., and E. M. Corey, 1995, "A new global equation of state model for hot, dense matter," J. Appl. Phys. **78**, 3748–3755.
Young, J. B., J. A. Nelson, and W. Kang, 2001, "Line emission in single-bubble sonoluminescence," Phys. Rev. Lett. **86**, 2673–2676.
Young, J. B., T. Schmiedel, and W. Kang, 1996, "Sonoluminescence in high magnetic fields," Phys. Rev. Lett. **77**, 4816–4819.

Yuan, L., C. Y. Ho, M. C. Chu, and P. T. Leung, 2001, "Role of gas density in the stability of single-bubble sonoluminescence," Phys. Rev. E **64**, 016317.

Zel'dovich, Y. B., and Y. P. Raizer, 1966, *Physics of Shock Waves and High-Temperature Hydrodynamic Phenomena* (Academic, New York), Vols. I and II.